

**A Vehicle Design and Optimization Model for
On-Demand Aviation**

by

Arthur Brown

B.A.Sc., Engineering Science, University of Toronto (2016)

Submitted to the Department of Aeronautics and Astronautics
in partial fulfillment of the requirements for the degree of

Master of Science in Aeronautics and Astronautics

at the

MASSACHUSETTS INSTITUTE OF TECHNOLOGY

June 2018

© Massachusetts Institute of Technology 2018. All rights reserved.

Signature redacted

Author
.....

Department of Aeronautics and Astronautics
May 24, 2018

Signature redacted

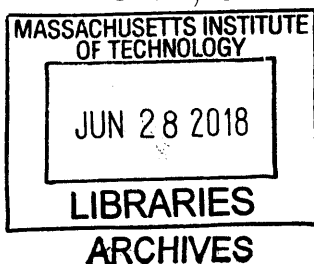
Certified by
.....

✓ Wesley L. Harris
Professor of Aeronautics and Astronautics
Thesis Supervisor

Signature redacted

Accepted by
.....

Hamsa Balakrishnan
Associate Professor of Aeronautics and Astronautics
Chair, Graduate Program Committee



A Vehicle Design and Optimization Model for On-Demand Aviation

by

Arthur Brown

Submitted to the Department of Aeronautics and Astronautics
on May 24, 2018, in partial fulfillment of the
requirements for the degree of
Master of Science in Aeronautics and Astronautics

Abstract

On-demand aviation refers to an envisaged air taxi service, using small, autonomous, vertical-takeoff-and-landing, battery-powered electric aircraft. A conceptual design and optimization tool for on-demand aviation is presented in this thesis. The tool uses Geometric Programming, a class of optimization problems with extremely fast solve times and for which global optimality is guaranteed. The optimization model consists of a vehicle, a sizing mission, a revenue-generating mission, and a deadhead (non-passenger-carrying) mission. Cost per trip, including the additional cost due to the deadhead mission, is used as the objective function. Vehicle noise is computed during post-processing using a semi-empirical method. The tool is used to conduct a study of on-demand aviation from a vehicle design perspective.

A trade study is conducted between several different on-demand aircraft configurations. Four configurations are viable: the lift + cruise configuration, the compound helicopter, the tilt wing, and the tilt rotor. Configurations with a higher lift-to-drag ratio, but a higher disk loading, generally weigh less and cost less to operate; configurations with a lower lift-to-drag ratio, but a lower disk loading, are quieter. Using New York City as an example market, it is shown that an on-demand air service will cost significantly less as compared to current helicopter air taxi operations. The two most important costs are pilot salary and battery amortization. If these two costs can be reduced (via vehicle automation and reduced battery manufacturing costs respectively), an on-demand air service becomes competitive with current car ridesharing on the basis of cost per seat mile. Therefore, on-demand aviation has the potential to become a system for everyday commutes.

Technological assumptions and vehicle requirements, especially mission range, battery energy density, vehicle autonomy level, battery manufacturing cost, and reserve requirements, have significant impacts on vehicle weight and cost. Vehicle noise can be reduced through the careful selection of key design parameters. However, envisaged noise requirements cannot easily be met, even with the most generous long-term

technological assumptions. Vehicle noise is therefore a critical issue for on-demand aviation; substantial engineering effort to reduce noise will be required.

Thesis Supervisor: Wesley L. Harris
Title: Professor of Aeronautics and Astronautics

Acknowledgments

The author wishes to thank all those who contributed their insights to this work. In particular, Parker Vascik, Edward “Ned” Burnell, Bjarni Kristinsson, Prof. Warren “Woody” Hoburg, Prof. John Hansman, and Prof. Mark Drela of MIT; Carl Dietrich of Terrafugia; Martin Kearney-Fischer, Brian Yutko, and Diana Siegel of Aurora Flight Sciences; Michael Duffy of Boeing; Michel Merluzeau of AirInsightResearch; Steve Rizzi of NASA Langley; Rodin Lyasoff of Airbus A³; and Thomas Sebastian of Lincoln Labs; are acknowledged. The author would also like to thank Ned and Prof. Hoburg for developing and maintaining GPkit, the open-source software package for solving geometric programs that was used throughout this research. Finally, the author would like to thank his advisor, Professor Wesley Harris, for his advice, encouragement, and support throughout this project, particularly with regards to funding.

This work was funded in part by the Arthur Gelb graduate fellowship, and also by the AIAA William T. Piper, Sr. General Aviation Systems Graduate Award.

Contents

1	Introduction	21
1.1	Electric Aircraft	21
1.1.1	Overview	21
1.1.2	Advantages: Cost	23
1.1.3	Advantages: Environmental Impact	24
1.1.4	Advantages: Scale Invariance	24
1.1.5	Disadvantages	26
1.1.6	Certification	27
1.2	On-Demand Aviation	28
1.2.1	Overview	28
1.2.2	Concept of Operations	29
1.2.3	Autonomy	31
1.3	Research Goals	33
2	Methodology	35
2.1	Geometric Programming	36
2.1.1	Definition	36
2.1.2	Discussion	37
2.2	Vehicle Model	38
2.2.1	Components	38
2.2.2	Cruise Performance	39
2.2.3	Hover Performance	39
2.3	Mission Model	43

2.4	Cost Model	46
2.4.1	Capital Expenses	46
2.4.2	Operating Expenses	47
2.4.3	Effect of Deadhead	48
2.4.4	Limitations	49
2.5	Noise Model	50
2.5.1	Importance of Noise	50
2.5.2	Noise Metrics	51
2.5.3	Sources of Noise	52
2.5.4	Blade Slap	53
2.5.5	Rotational Noise	53
2.5.6	Vortex Noise	55
2.5.7	A-Weighting Scheme	56
2.5.8	Limitations	59
3	Configurational Trade Study	61
3.1	Inputs	61
3.2	Results	66
3.3	Noise Analysis	72
4	Case Studies	75
4.1	New York City Airport Transfers	75
4.2	Technological Assumptions by Time Frame	80
4.3	Low-Noise Design	83
4.4	The Joby S4 Configuration Change	88
4.5	Sizing Plot	93
4.6	Boeing Study Comparison	95
5	Sensitivity Studies	101
5.1	Design Requirements	101
5.1.1	Mission Range	101

5.1.2	Number of Passengers	103
5.1.3	Reserve Requirement	105
5.1.4	Time in Hover	107
5.2	Vehicle Parameters	108
5.2.1	Battery Energy Density	108
5.2.2	Empty Weight Fraction	111
5.2.3	Rotor Solidity	112
5.2.4	Rotor Mean Lift Coefficient	114
5.2.5	Number of Rotors	116
5.2.6	Deadhead Ratio	118
6	Future Work	121
7	Conclusions	125
A	Noise Definitions	127
B	Decibel Arithmetic	129
C	Rotational Noise Derivation	131
D	Vortex Noise Derivation	133
D.1	Unweighted Sound Pressure Level	133
D.2	Frequency Spectrum	136
D.3	A-Weighting Procedure	138
E	Code API	141
E.1	Overview	141
E.2	Class Definitions	141
E.3	Inputs	142
E.4	Solutions	143
E.5	Tips & Tricks	144
Bibliography		145

List of Figures

1-1	The Pipistrel Alpha [3]	22
1-2	The X-57 Maxwell [8]	25
1-3	A screenshot of the proposed UberAIR app [17]	29
1-4	An artist's conception of a vertiport [15]	30
2-1	Validation of the rotor aerodynamic model.	42
2-2	Mission profiles. Segment 4 of the revenue and deadhead missions (time on ground) is not shown.	44
2-3	Azimuthal angle diagram.	54
2-4	The A-weighting response function.	56
2-5	Correlation between noise and annoyance, from Reference [49].	58
3-1	Configuration representative images. Note that the example conventional helicopter, coaxial helicopter, and autogyro are gasoline-powered; they do not represent eVTOL concepts.	63
3-2	Results of the configurational trade study. SPL values are from the sizing mission; the horizontal line represents the 62-dBA Uber noise requirement [15].	66
3-3	More results from the configurational trade study. All data presented is from the sizing mission. Energy use in hover is the sum from all four hover segments.	68
3-4	Cost breakdown. Cost per seat mile is given in terms of statute miles, instead of nautical miles.	70

3-5	Example noise spectra. Both rotational and vortex noise values are unweighted.	72
3-6	Noise as a function of observer location, for constant $z = 500$ ft.	74
4-1	New York City helicopter routes (black lines). Note that the direct route passes over Brooklyn. While this is in accordance with the established helicopter route [64], an overwater-only route is also included in case this route is shut down for noise reasons.	77
4-2	Results from the New York City study.	78
4-3	Time frame study results.	81
4-4	Cost breakdown from the time frame study. Capital and operating expenses are per trip; i.e. the effect of deadhead is included. Cost per seat mile is given in terms of statute miles.	82
4-5	First set of results from the low-noise design study.	86
4-6	Second set of results from the low-noise design study.	87
4-7	VSP sketches of the Joby S4.	89
4-8	First set of results from the Joby S4 configuration study.	91
4-9	Second set of results from the Joby S4 configuration study.	92
4-10	Sizing plot for the lift + cruise configuration. An intersection between any two lines on the plot represents an optimized vehicle design, for that combination of cruise lift-to-drag ratio and hover disk loading. . .	94
4-11	Comparison with the Boeing study.	99
5-1	Sensitivity to mission range. Cost per seat mile is plotted instead of cost per passenger.	102
5-2	Sensitivity to number of passengers carried on the sizing mission. . .	104
5-3	Sensitivity to reserve requirement.	106
5-4	Sensitivity to time in hover (sizing mission).	107
5-5	Sensitivity to battery energy density.	109
5-6	Sensitivity to empty weight fraction.	111
5-7	Sensitivity to rotor solidity.	112

5-8	Sensitivity to rotor mean lift coefficient.	114
5-9	Sensitivity to number of rotors.	116
5-10	Sensitivity to deadhead ratio. Capital expenses, operating expenses, and total costs are per trip; i.e. the effect of deadhead is included. . .	118
6-1	Example toroidal propellers, with conventional propellers shown for reference [75].	123
D-1	Validation of the rotor vortex noise model. Note that the experimental data was rounded to the nearest decibel in Reference [48].	135
D-2	Plot used to draw the vortex-noise frequency spectrum, obtained from Reference [45].	137

List of Tables

1.1	Comparison of performance data for the Pipistrel Alpha, from Reference [2].	22
1.2	Comparison of hourly operating costs for the Pipistrel Alpha, based on data from Reference [4].	23
2.1	Rotor model parameters.	42
2.2	Flight conditions for maximum range and endurance.	45
2.3	Parameters used by the cost model.	46
2.4	Empty weight (W_e) and cost estimates for several representative vehicles.	47
3.1	Generic vehicle input parameters.	61
3.2	Mission input parameters.	62
3.3	Input data for each configuration [26].	64
3.4	Power increase percentages for configurations with a tail rotor.	65
3.5	Charging times for the revenue mission.	69
4.1	Trip distance for the airport transfer routes, computed using Google Maps.	76
4.2	Input parameters for the different time frames.	80

4.3	Input parameters for the low-noise design study. While the Aircraft Redesign category uses all five parameter values, the Rotor Replacement category only uses the values for number of rotor blades and blade thickness-to-chord ratio. Number of rotors, rotor solidity, and maximum mean lift coefficient for Rotor Replacement are the same as those from the configurational trade study.	85
4.4	Input parameters for the Joby S4 configuration study.	90
4.5	Generic Boeing study input parameters.	96
4.6	Configuration-specific Boeing study inputs.	97
4.7	Takeoff gross weight percentages differences, relative to those from the Boeing study.	100
D.1	Frequency spectrum weights.	137

Nomenclature

A	Rotor disk area
A_b	Rotor blade area
$A(f)$	A-weighting frequency response function
AR	Aircraft wing aspect ratio
ATC	Air Traffic Control
a	Speed of sound
B	Number of rotor blades
BVI	Blade-Vortex Interaction
C	Battery energy used
C_1	Vortex-noise interpolation constant 1
C_2	Vortex-noise interpolation constant 2
C_{D_0}	Aircraft 3D zero-lift drag coefficient
C_{d_0}	Rotor blade 2D zero-lift drag coefficient
C_L	Aircraft wing 3D lift coefficient
C_l	Rotor local blade lift coefficient, referenced to $V_{0.7}$
\overline{C}_l	Rotor mean lift coefficient
C_P	Rotor power coefficient
C_{P_i}	Rotor induced power coefficient
C_{P_p}	Rotor profile power coefficient
C_Q	Rotor torque coefficient
C_T	Rotor thrust coefficient
c	Average rotor blade chord
c_d	Cost of flying 1 deadhead mission

c_r	Cost of flying 1 revenue-generating mission
dB	Decibel
dBA	A-weighted decibel
DEP	Distributed Electric Propulsion
DNL	Day Night Average Sound Level
DOC	Direct Operating Cost
DOE	Department of Energy
dr	Deadhead ratio
EASA	European Aviation Safety Administration
EPNL	Effective Perceived Noise Level (in dB)
e	Oswald efficiency
eVTOL	Electric VTOL
FAA	Federal Aeronautics Administration
<i>FOM</i>	Rotor figure of merit
f	Frequency
f_{peak}	Vortex-noise peak frequency
fr	Frequency ratio
GP	Geometric Program
h	Rotor blade projected thickness
INS	Inertial Navigation System
IOC	Indirect Operating Cost
J_{mB}	Bessel function of the first kind, of order mB
K	Noise constant ($6.1 \times 10^{-11} \frac{s^6}{ft^8}$)
K_2	Noise constant 2 ($1.206 \times 10^{-2} s^3/ft^3$)
k	Aircraft induced power factor
k_i	Rotor induced power factor
$L_{A_{eq}}$	A-weighted Equivalent Continuous Sound Level
L_{AE}	A-weighted decibels, sound exposure level
L_{dn}	Day Night Average Sound Level
L/D	Vehicle lift-to-drag ratio

LIDAR	Light Detection and Ranging
LSA	Light Sport Aircraft
M_{tip}	Rotor tip Mach number
MMH/FH	Maintenance man-hours per flight hour
MTOW	Maximum Takeoff Weight
m	Harmonic number
N	Number of rotors
N_d	Number of deadhead missions
N_r	Number of revenue-generating missions
NPV	Net Present Value
ODA	On-Demand Aviation
ODM	On-Demand Mobility
OEI	One Engine Inoperative
PNL	Perceived Noise Level (in dB)
p	Effective sound pressure
p_0	Static air pressure
p_{mL}	Root-mean-square loading pressure
p_{mT}	Root-mean-square thickness pressure
p_{ref}	Reference sound pressure (2×10^{-5} Pa)
p_{total}	Total air pressure
$p(t)$	Acoustic pressure
Q	Rotor torque
R	Rotor radius
R_e	Effective rotor radius ($0.8R$)
RMS	Root Mean Square
ROC	Remote Operations Center
r	Rotor blade radial location
SPL	Sound pressure level (in dB)
St	Strouhal number
s	Rotor solidity

T	Thrust generated by 1 rotor
T/A	Rotor disk loading
t	Rotor blade thickness
$t_{mission}$	Time to complete mission
t/c	Rotor blade thickness-to-chord ratio
UAV	Unmanned Aerial Vehicle
V	Cruising flight speed
$V_{0.7}$	Rotor blade velocity at a radial location $r/R = 0.7$ (i.e. $0.7V_T$)
V_T	Rotor tip speed
V_{cruise}	Cruising flight speed
V_{loiter}	Loiter flight speed
VFR	Visual Flight Rules
VTOL	Vertical Takeoff and Landing
W	Vehicle weight
W_e	Vehicle empty weight
W_0	Vehicle gross (total) weight
y	Observer ground location
z	Vehicle height above ground
α	Rotor blade angle of attack at a radial location $r/R = 0.7$
ΔS	Distance from noise source to observer
$(\Delta S)_{ref}$	Reference distance (500 ft)
η	System efficiency
θ	Observer azimuthal angle
ρ	Air density
Ω	Rotor angular velocity

Chapter 1

Introduction

This chapter begins with an overview of electric propulsion, as a technology to be applied to aircraft design. A discussion of on-demand aviation, a promising new application for electric aircraft, follows. The chapter concludes with the research goals addressed in this thesis.

1.1 Electric Aircraft

1.1.1 Overview

General-aviation aircraft are normally powered with either piston or turboprop engines, which burn fuel and drive propellers. One idea for improvement is to replace the system with electric motors and batteries. A number of advantages are hypothesized, including, but not limited to: lower operating costs, lower environmental impact, scale invariance, and integration benefits. A more complete list is given in Reference [1]. This section will delve into an overview of the hypothesized advantages, as well as disadvantages. Electric aircraft certification challenges are also discussed.

One interesting example of an electric aircraft is the Pipistrel Alpha, a two-seat, single-engine lightplane designed for the light-sport and trainer roles [2]. The Alpha is available in two versions. One version is powered by a piston engine (the Alpha), while the other (the Alpha Electro) is powered by an electric motor and battery. The

Alpha is depicted in Figure 1-1; key performance specifications for the two versions are given in Table 1.1.



Figure 1-1: The Pipistrel Alpha [3].

Table 1.1: Comparison of performance data for the Pipistrel Alpha, from Reference [2].

Version	Internal Combustion	Electric
Empty weight (lbf)	615	771
Maximum takeoff weight (lbf)	1,210	1,210
Sea-level rate of climb (fpm)	1,220	1,348
Takeoff distance (ft)	739	739
Landing distance (ft)	1,510	1,510
Range (nmi)	390	81
Endurance (with 30-minute reserve)	3 hr 36 min	1 hr

1.1.2 Advantages: Cost

The first hypothesized advantage of electric propulsion is energy cost. Energy for an electric aircraft should cost less than that of a piston-powered aircraft, because electricity costs significantly less than aviation fuel. Also, electric motors are more reliable than piston engines; they have fewer moving parts, and operate at lower temperatures. This should result in reduced maintenance costs.

The authors of Reference [4] perform cost analysis on the Alpha. Based on their analysis, the hourly operating cost estimates in Table 1.2 were obtained. Airframe cost is based on straight-line depreciation; i.e. the purchase price of the aircraft (given in Reference [4]) is divided by an assumed 4,000-hour airframe life.

Table 1.2: Comparison of hourly operating costs for the Pipistrel Alpha, based on data from Reference [4].

Version	Internal Combustion	Electric
Energy cost	\$20.40/hour	\$1.10/hour
Maintenance (overhaul) cost	\$8.67/hour	\$8.70/hour
Airframe cost	\$25.75/hour	\$29.25/hour
Total cost	\$54.82/hour	\$39.05/hour

Table 1.2 shows that energy costs for the Alpha Electric are significantly lower than those of the piston-powered Alpha (\$1.10/hour vs. \$20.40/hour). However, maintenance cost is slightly higher. It is hypothesized that this is due to battery replacement cost. While it does indeed cost less to maintain electric motors, batteries have a limited cycle life and are quite expensive to replace.

The total hourly operating cost of the Alpha Electric is \$39.05/hour, 29% less than the hourly cost of the piston-powered Alpha. Therefore, in the case of the Alpha, electric aircraft cost significantly less to operate, primarily due to lower energy costs.

1.1.3 Advantages: Environmental Impact

General-aviation aircraft are typically powered by either piston engines or turboprops. Both types of engines burn fuel, byproducts of which include greenhouse gases (which contribute to climate change) and NO_x (a pollutant). Electric aircraft do not suffer from this issue.

A second important environmental issue specific to piston-powered GA aircraft is lead emissions. While lead in automotive gasoline has been banned since 1986 due to its toxicity to humans, the fuel used by piston-powered aircraft (aviation gasoline, or avgas) still contains lead [5]. This is because, as of this writing, no operationally safe alternative is available. Switching to electric propulsion would eliminate harmful lead emissions.

A third potential environmental benefit from electric propulsion concerns community noise. A good example of the importance of community noise emerged in New York City in 2016. Under pressure from local residents and the City Council, the mayor ordered the city's helicopter tour operators to reduce their flight frequency by 50% and eliminate Sunday flights [6]. If the tour operators refused to comply, they would lose their right to operate from the (city-owned) Pier 6 helipad in downtown Manhattan.

Next to blade slap (when it occurs), the most significant source of noise for a piston-engine helicopter is the engine exhaust [7]. This source of noise can be eliminated by switching to electric motors, which are much quieter.

1.1.4 Advantages: Scale Invariance

Scale invariance, as applied to electric propulsion, means that motors and propellers can be scaled up or down in size without significantly changing the efficiency or power-to-weight ratio [1]. For example, a system of 12 small electric motors and propellers, each producing 1 hp, are about as efficient and weigh approximately the same as one large electric motor and propeller system producing 12 hp.

Fuel-burning engines are not scale-invariant. Instead, larger engines tend to be

more efficient. The first reason is the square-cube law: power output scales with engine volume, while losses tend to scale with surface area. Reynolds effects and manufacturing tolerance limitations also mean that larger engines are more efficient than smaller ones [1].

Scale invariance is useful because it enables new, hitherto-impossible aircraft configurations. However, scale invariance cannot be exploited with a drop-in solution like the Alpha (in which the piston engine is replaced with an electric motor, without more substantial design changes). Instead, multiple motors and propellers are used. This design strategy is known as Distributed Electric Propulsion, or DEP.

The X-57 Maxwell, an X-plane under development by NASA and several partner companies, is a good example of some of the potential benefits of DEP. It is depicted in Figure 1-2.



Figure 1-2: The X-57 Maxwell [8].

The Maxwell is a modified Tecnam P2006T [9]. It incorporates an all-new wing, with two new design features not typically seen in conventional aircraft: high-lift propellers; and wingtip propellers. As depicted in Figure 1-2, the Maxwell has 12 high-lift propellers distributed along the wing leading edge. These propellers are only used during takeoff/climb and landing; they fold up during cruise. When in operation,

these propellers increase the wing maximum lift coefficient to as high as 5.0 (a value of 1.6 would be typical for this class of aircraft). This allows a smaller wing to be used, while still attaining a low stall speed (61 knots) and a short runway length (2,000 ft). The smaller wing is more aerodynamically efficient, and also offers improved ride quality due to the higher cruise wing loading [1]. This would be much more difficult to do with piston engines, because small piston engines are less efficient and have a lower power-to-weight ratio than large ones (see above). 12 piston engines would also be a challenge to maintain.

The Maxwell's cruise propellers are mounted on the wingtips, which reduces induced drag during cruise [1], [9]. While this can be done with piston engines, the resulting aircraft would have to have a very large vertical tail to balance one-engine-operative (OEI) control moments. It would also be very difficult for a pilot to control the aircraft under OEI conditions for the same reasons. Instead, the Maxwell exploits synergy between the high-lift propellers and wingtip propellers. If a Maxwell wingtip motor fails, the high-lift propellers on that wing can be turned on, helping to balance the moments and ensuring a more controllable design.

1.1.5 Disadvantages

Arguably the most important hypothesized disadvantage of battery-electric propulsion for aircraft is severely limited range and endurance. Note from Table 1.1 that the Alpha Electro is essentially equivalent to the Alpha on weight, as well as on key performance metrics such as rate of climb, takeoff distance, and landing distance. However, it is severely compromised in terms of both range (81 vs. 390 nmi) and endurance (1 hr vs. 3hr 36min).

The main reason for this is the low energy density of current batteries. The Maxwell uses state-of-the-art lithium-ion batteries with an energy density of approximately 200 Wh/kg [8]; batteries with more than twice this energy density are on the horizon (for example, see Reference [10]). However, aviation fuel has an energy density of approximately 12,000 Wh/kg. Even assuming a 30% piston-engine efficiency, as compared to an 85% electrical efficiency (including the motor), current electric

propulsion systems cannot compete with conventional internal-combustion systems on the basis of energy density. For this reason, battery-powered aircraft are much more sensitive to range and/or endurance requirements (this is analyzed later in Section 5.1.1). Energy density is also known as specific energy; the two terms are used interchangeably.

1.1.6 Certification

Until very recently, it was seen as impossible to certify an electric aircraft for commercial use in the United States. This is because of FAA (Federal Aviation Administration) Part 23, the section of US aviation law under which most small aircraft are certified. Previously, the rules were written in a prescriptive manner, specifying how requirements should be met [11]. For example, many regulations for small aircraft specified reciprocating piston engines. Casting the rules in this manner was meant to forestall the use of turbine or rocket engines on small aircraft, but it also had the unintended consequence of banning the use of electric aircraft for profit.

However, in December 2016, the FAA released a rewrite of Part 23 [12]. Under the new rules, the previous “prescriptive design requirements [were replaced] with performance-based airworthiness standards” [11]. Many in the electric aircraft community cheered the move [12], which for the first time should allow an electric aircraft to be certified for commercial use in the United States.

A number of problems remain, however. For example, the Alpha can legally be operated in the United States in the Light Sport Aircraft (LSA) category, but the Alpha Electro cannot. This is because the FAA definition of a LSA still specifies that the aircraft must have “[a] single, reciprocating engine, if powered” [13]. Pilots wishing to fly the Alpha Electro in the United States can still do so under the Experimental category, but flying for profit in this category is prohibited. Therefore, despite the analysis in Section 1.1.2 illustrating the cost advantages of the Alpha Electro it cannot legally be used by flight training schools.

1.2 On-Demand Aviation

On-demand aviation is a promising new application to which electric propulsion is well suited. This section will give an overview of on-demand aviation, including a concept of operations, and a discussion of some of the technical challenges.

1.2.1 Overview

On-Demand Aviation (ODA), also known as On-Demand Mobility (ODM) or eVTOL (Electric Vertical Takeoff and Landing), is an envisaged air taxi service. The service would use small, 1-4 place aircraft for trips of approximately 200 nautical miles or less [14]. Most proposed aircraft concepts are fully electric, although some are hybrid-electric. In general, Distributed Electric Propulsion is used. The aircraft are capable of VTOL (Vertical Takeoff and Landing). On-demand aviation offers a number of advantages over existing transport solutions, including the aforementioned cost and environmental-impact advantages (Sections 1.1.2 and 1.1.3 respectively).

Other hypothesized advantages include:

- Greatly reduced commute times and/or greatly increased Mobility Reach (accessible land area with a given commute time [14]), by avoiding gridlock.
- Lower (or no) pilot operating costs, due to autonomy.

Uber published a white paper in October 2016 outlining their vision for an on-demand aviation service, which they call Uber Elevate [15]. In it, they describe what they see as the key market feasibility barriers, including battery technology, vehicle efficiency, air traffic control, cost, safety, noise, and emissions. Uber also held a summit in Dallas in April 2017 to bring together stakeholders from industry, academia, and government [16]. Demonstration programs are planned for 2020 in Dallas and Los Angeles, with commercial operations beginning in 2023 [17], [18].

1.2.2 Concept of Operations

Uber's Vision

As described by Uber, the first interaction between an on-demand air service and a user would be via a smartphone app, similar to today's Uber app. Users would be shown a range of proposed transportation options, as well as estimated wait times and commute times. They would then book their flight through the app. Screenshots of the proposed app are shown in Figure 1-3.

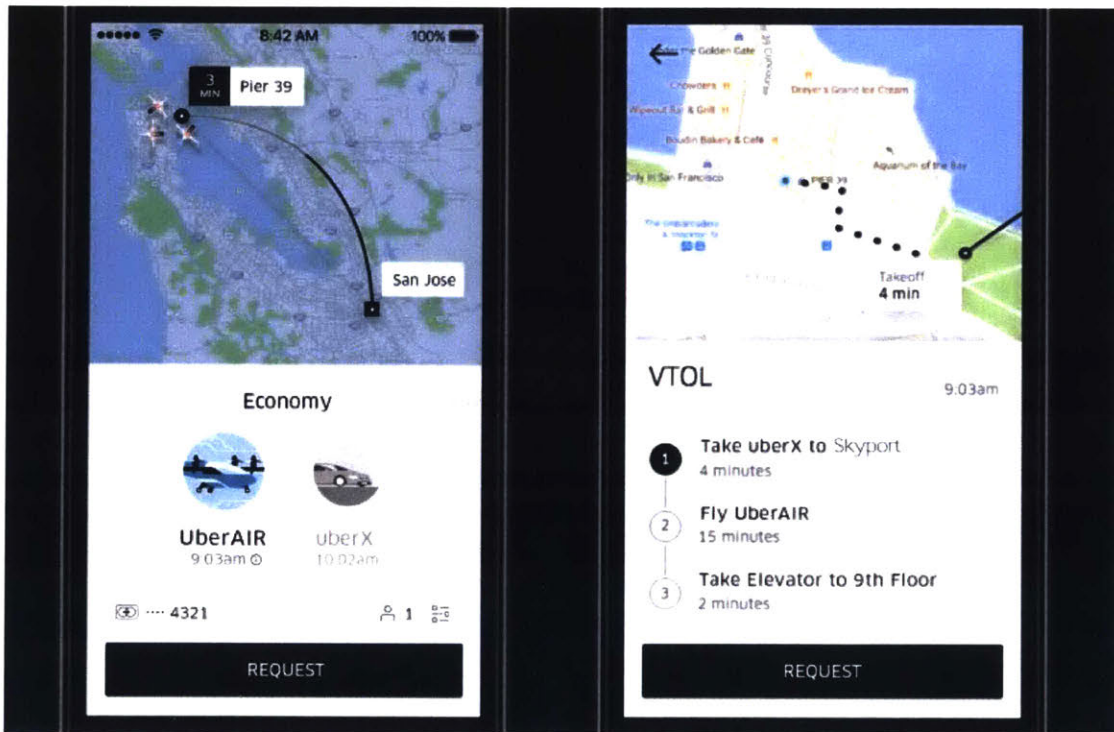


Figure 1-3: A screenshot of the proposed UberAIR app [17].

Air vehicles would typically not fly directly to a user's location. Instead, trips would be multimodal, potentially involving a combination of walking, flying, and/or ground transportation. The air vehicles would utilize a network of takeoff and landing areas:

It has been proposed that the repurposed tops of parking garages, existing helipads, and even unused land surrounding highway interchanges could form the basis of an extensive, distributed network of "vertiports" (VTOL

hubs with multiple takeoff and landing pads, as well as charging infrastructure) or single-aircraft “vertistops” (a single VTOL pad with minimal infrastructure) [15].

Customer-identification, safety, security, and baggage checks would all be conducted at the vertiport or vertistop. An artist’s conception of a vertiport, taken from the Uber white paper, is shown in Figure 1-4.



Figure 1-4: An artist’s conception of a vertiport [15].

Current Helicopter Air Taxi Operations

Voom, an on-demand helicopter air taxi service developed by Airbus, resembles Uber’s vision in many ways [19]. The service currently operates in two notoriously gridlocked cities: Sao Paulo (Brazil) and Mexico City.

Voom does not own any helicopters or helipads. Instead, their online application connects riders with existing helicopter operators and helipads. Users book their flights online, as little as one hour in advance. According to Voom, their service costs “up to 80 percent less than traditional helicopter services - about the cost of a private

car service” [19]. As of this writing, Voom services nine helipads in Sao Paulo, and four helipads in Mexico City.

Airbus is using Voom to better understand the business case for urban air mobility, and also to provide information useful for vehicle design [20]. Example issues uncovered by Voom include baggage capacity requirements (especially for riders travelling to and from airports), customer price sensitivity, and the effects of weather on vehicle availability.

1.2.3 Autonomy

Under Uber’s vision, the air vehicles would initially be piloted. However, the goal is to eventually switch to fully autonomous flight. The implications of aircraft autonomy, including technical feasibility, advantages, and barriers to adoption are discussed in this section.

Technical Feasibility

Unmanned, autonomous aircraft are increasingly common nowadays, ranging in scale from small hobby UAVs to the US military’s 32,250 lbf Global Hawk. These aircraft are capable of flying themselves using waypoints, without direct human intervention. The Global Hawk also takes off and lands autonomously [21].

However, in order to implement an autonomous air taxi system, the aircraft must be capable of much more than just autonomous flight between waypoints. For example, a Detect and Avoid capability is required in order to comply with 14 CFR Part 91 (General Operating and Flight Rules, the section of US aviation law that governs how aircraft must be operated) [22]. Other required capabilities include identifying landing sites, including obstacles; and communicating with air traffic control.

Some of these capabilities were recently demonstrated by Aurora Flight Sciences using a retrofitted helicopter [23]. The helicopter, equipped with an inertial navigation system (INS), LIDAR, and other sensors, was designed to resupply soldiers at the front lines [24]. It is capable of successfully identifying landing sites, including obstacles

ranging from power lines to people, without a previously loaded map. It can then avoid obstacles and land, or else decide to abort. A tablet-equipped operator at the scene can also issue a wave-off command if necessary. Such technology could conceivably be applied to on-demand electric air vehicles.

Advantages of Autonomy

Two main advantages of autonomy are hypothesized: cost and safety. By eliminating the pilot, costs could potentially be reduced. This is only true if the number of people actually involved in the operation of the system is reduced.

It is anticipated that if fully autonomous aircraft are to operate, a Remote Operations Center (ROC) will be required. Operators at the ROC, called “bunker pilots” by Uber [15], would each be responsible for several aircraft. Requirements for ROCs are discussed in Reference [25].

The second hypothesized advantage is safety. While airline travel is about two orders of magnitude safer than driving on the basis of fatalities per passenger mile, current air taxi operations are about twice as dangerous as driving [15]. Moreover, two of the most common causes of aircraft accidents are loss of control and controlled flight into terrain. Both types of accidents can in theory be mitigated using autonomous technologies. For example, flight envelope protection can be used to prevent loss of control accidents. Almost all current airliners have some form of envelope protection, but the technology is not currently applied to most general-aviation aircraft. Similarly, terrain collision avoidance systems (which are already saving lives on military aircraft [15]) can be used to prevent controlled flight into terrain accidents.

Barriers to Adoption

The barriers to adoption of autonomy are significant. While the FAA Part 23 rewrite (Section 1.1.6) should allow for electric aircraft to be certified, no current regulatory structure exists that would allow for the certification of an autonomous, passenger-carrying aircraft. This is not expected to change soon. Also, it is unclear as to whether customers will feel comfortable on an autonomous aircraft, despite the (hypothesized)

cost and safety benefits.

In conclusion, while autonomy does promise to improve aircraft safety as well as reduce costs, the hypothesized safety improvements will have to be demonstrated in practice before they become widely accepted by both regulators and the public. Full vehicle autonomy is not expected to be possible for many years, despite promising technological advancements in the field.

1.3 Research Goals

This research examines on-demand aviation from the perspective of a vehicle designer. The goal is to determine whether on-demand air vehicles are technically feasible; to identify any critical enabling technologies; and to gain estimates for key vehicle design parameters such as size, weight and cost. Vehicle noise is also identified as critical, and as such is analyzed in detail.

Dozens of companies are working on eVTOL aircraft designs, including Joby Aviation, Lilium Aviation, *A³* by Airbus, and Aurora Flight Sciences. A variety of fundamentally different design approaches are employed. For example, Joby Aviation's S4 is a tilt-rotor design; Lilium Aviation uses a tilt-duct design; Airbus' Vahana is a tilt-wing; and Aurora Flight Sciences uses a lift + cruise design (a design with separate rotors for cruise and for hover, with no folding or tilting components). Other postulated configurations include the multirotor, the autogyro, the conventional helicopter, the tilt duct, the coaxial-rotor helicopter, and the compound helicopter [26]. This research aims to provide guidance to vehicle designers on the strengths and weaknesses of each configuration.

The rest of this thesis is structured as follows. A vehicle design and optimization tool is developed in Chapter 2, incorporating weight, cost and noise estimates. The tool is used in Chapter 3 to conduct a trade study between various on-demand air vehicle configurations. Six case studies are conducted in Chapter 4. A series of sensitivity studies are conducted in Chapter 5, to evaluate the influence of key design parameters and vehicle requirements on the results. Finally, avenues for future work

are discussed in Chapter 6, before the conclusion in Chapter 7.

Chapter 2

Methodology

A vehicle design and optimization tool was developed for this research. The tool is formulated as a geometric program (GP), a type of constrained optimization problem. An introduction to geometric programming is given in Section 2.1.

The tool uses vehicle and mission models similar to those used by McDonald & German [26]. Some key vehicle parameters, such as empty weight fraction and battery energy density, are held constant between vehicle configurations. Other parameters, such as cruising speed, cruise lift-to-drag ratio, and hover disk loading, are varied between configurations, using representative values for a given configuration.

However, in this study, optimization is used instead of sizing. Instead of assuming a fixed vehicle weight and empty weight fraction, then computing the range, this work assumes a fixed empty weight fraction and mission range, then computes the required vehicle weight during the optimization process. This means that all configurations have the same range, enabling comparisons between them.

The tool is fully open source; it is available for download under an MIT license [27]. The API is given in Appendix E. The geometric programs are solved using the open-source Python package GPkit [28], with MOSEK as the backend solver.

2.1 Geometric Programming

An introduction to geometric programming is given in this section. The reader is referred to References [29] and [30] for a more detailed discussion.

2.1.1 Definition

A geometric program is a type of convex optimization problem, in which the objective and constraint functions are written in terms of monomials and posynomials. A monomial function $m(\mathbf{x})$ can be written as follows:

$$m(\mathbf{x}) = c \prod_{j=1}^n x_j^{a_j} \quad (2.1)$$

c and x_j must be positive, while a_j can be any real number. Meanwhile, a posynomial $p(\mathbf{x})$ is defined as a sum of monomials:

$$p(\mathbf{x}) = \sum_{i=1}^K c_i \prod_{j=1}^n x_j^{a_{ij}} \quad (2.2)$$

A geometric program can therefore be written as follows:

$$\begin{aligned} & \text{Minimize} && p_0(\mathbf{x}) \\ & \text{Subject to} && p_i(\mathbf{x}) \leq 1, \quad i = 1 \dots n_p \\ & && m_i(\mathbf{x}) = 1, \quad i = 1 \dots n_m \end{aligned} \quad (2.3)$$

$p_0(\mathbf{x})$ is the objective function (a posynomial), subject to posynomial inequality constraint functions $p_i(\mathbf{x})$ and monomial equality constraint functions $m_i(\mathbf{x})$. The vector \mathbf{x} represents the design variables.

2.1.2 Discussion

Geometric programs offer three main advantages as compared to more general optimization algorithms: they offer extremely fast solve times, they require no initial guesses, and a globally optimal solution is guaranteed. For these reasons, geometric programming is increasingly being used for aircraft design optimization. For example, a GP model for high-altitude communications UAVs is developed in Reference [31].

The power of GP comes from a logarithmic change of variables, which results in a convex problem. In Reference [30], a simple geometric program is solved using MATLAB's `fmincon` function, both with and without the logarithmic change of variables. The results show that if the log transform is included, the problem converges in fractions of a second to the globally optimal solution, regardless of the initial guess. If the logarithmic change of variables is not included, the problem typically takes much longer to converge (if it converges at all); the solution is also highly sensitive to the initial guess. This is true regardless of whether `fmincon` is provided with analytical gradients.

The main limitation of geometric program stems from the fact that the problem must be posed in the form given by Equation 2.3. Although all of the models used in this research were GP-compatible, this is occasionally a problem in other studies. Fits to data, generated offline, are often used in such cases. For example, an eight-term posynomial fit to airfoil drag data, generated offline using Xfoil, is used in Reference [29].

One particularly troublesome limitation of Equation 2.3 is that posynomial equality constraints are not allowed. For example, a simple weight buildup equality constraint is not GP-compatible:

$$W_{takeoff} = W_{empty} + W_{battery} + W_{passengers} + W_{crew} \quad (2.4)$$

Equation 2.4 is a posynomial equality constraint, which is not GP-compatible. A technique called posynomial equality relaxation is used to convert it to a posynomial

inequality:

$$W_{total} \geq W_{empty} + W_{battery} + W_{passengers} + W_{crew} \quad (2.5)$$

Although Equation 2.5 is an inequality, it will be exactly satisfied at the optimum. This is because the objective function of any typical aircraft design problem (including this one) is monotone increasing in W_{total} ; i.e Equation 2.6 must hold:

$$\frac{\partial(\text{objective})}{\partial W_{total}} \geq 0 \quad (2.6)$$

Posynomial equality relaxation is discussed further in Reference [29]; it is used throughout this research.

Posynomial equality relaxation is not applicable in all circumstances. For example, the standard atmospheric model (see Andersen [32]) is not GP-compatible, and cannot be relaxed. This can be solved in several ways: by holding altitude constant and precomputing atmospheric design variables (as was done in this study); by performing local monomial fits to atmospheric data; or by instead using signomial programming (SP). Signomial programming is significantly more general than geometric programming, as both negative leading coefficients c_i (see Equation 2.2) and posynomial equality constraints are allowed. However, the guarantee of global optimality is lost. Signomial programming is also increasingly being used for aircraft design applications. For example, a signomial programming model for airliner design is developed in Reference [33].

2.2 Vehicle Model

2.2.1 Components

The vehicle model is divided into five components: structure, battery, electrical system, avionics, and rotors. The structural model assumes an empty weight fraction, relative to the maximum takeoff weight; the battery model assumes a battery specific energy and specific power, and sizes the battery accordingly. 20% of the battery

energy is unusable (even for reserves), to prevent current spikes at low charge levels and also to extend battery life. This is in accordance with the practice of Reference [26].

The electrical system applies a constant efficiency to the power coming from the batteries in both hover and cruise; the avionics model is only used for cost modeling if vehicle autonomy is enabled (discussed in Section 2.4); and the rotor model is only used in hover. The structure and battery have their own weight models; the weight of the other three components are bookkept under empty weight.

2.2.2 Cruise Performance

The range and endurance of an electric aircraft in cruise can be computed using Equations 2.7 and 2.8 respectively:

$$Range = \eta \frac{L}{D} \frac{C}{W} \quad (2.7)$$

$$Endurance = \eta \frac{L}{D} \frac{C}{VW} \quad (2.8)$$

$\frac{L}{D}$ is the vehicle lift-to-drag ratio in cruise, C is the battery energy used, W is the vehicle weight, and V is the cruising speed. η is the system efficiency, equal to the product of electric and propulsive efficiency. Electrical efficiency accounts for losses due to the wires, controller, and motors; a value of 90% is used in both cruise and hover. For a propeller-driven aircraft, propulsive efficiency is equal to propeller efficiency; a value of 85% is used.

2.2.3 Hover Performance

In hover, the rotors must produce thrust equal to vehicle weight; the power required to generate this thrust must be computed. The rotor model developed for this purpose uses an extension of actuator-disk theory, using equations from Chapter 3 of Reference [34]. The effects of non-uniform downwash and blade profile drag are included.

The rotor thrust coefficient is defined in Equation 2.9:

$$C_T = \frac{T}{\frac{1}{2}\rho V_T^2 A} \quad (2.9)$$

C_T is the rotor thrust coefficient, T is the thrust generated by the rotor, ρ is the air density, V_T is the rotor tip speed, and A is the rotor disk area (πR^2 , where R is the rotor radius).

The power coefficient is defined in Equation 2.10:

$$C_P = \frac{P}{\frac{1}{2}\rho V_T^3 A} \quad (2.10)$$

C_P is the power coefficient, while P is the power required to turn the rotor. C_P is related to the ideal and profile power coefficients through Equations 2.11, 2.12, and 2.13:

$$C_P = k_i C_{P_i} + C_{P_p} \quad (2.11)$$

$$C_{P_i} = \frac{1}{2} C_T^{3/2} \quad (2.12)$$

$$C_{P_p} = \frac{1}{4} s C_{d_0} \quad (2.13)$$

C_{P_i} is the ideal power coefficient. If profile drag is neglected and the blade lift distribution is elliptical, then C_{P_i} is equal to C_P . The induced power factor k_i accounts for non-uniform lift distribution, while the profile drag coefficient C_{P_p} accounts for profile drag. s is the rotor solidity, computed using Equation 2.14:

$$s = \frac{A_b}{A} = \frac{BcR}{\pi R^2} \quad (2.14)$$

A_b is the rotor blade area, equal to the product of the number of blades B , average blade chord c , and blade radius R .

Figure of merit FOM is defined as the ratio of ideal to actual power required in

hover. It can be computed using Equation 2.15:

$$FOM = \frac{C_{P_i}}{C_P} \quad (2.15)$$

While not required by the optimization model, torque is required for the purpose of computing noise during post-processing. Equation 2.16 relates torque Q and torque coefficient C_Q :

$$C_Q = \frac{Q}{\frac{1}{2}\rho V_T^2 AR} \quad (2.16)$$

Torque and power coefficients are equal.

Finally, "[the rotor] mean lift [coefficient] is that which, applied uniformly across the blade span, would give the same thrust as the total blade" [34]. Rotor mean lift coefficient, denoted as \bar{C}_l , can be calculated using Equation 2.17:

$$\bar{C}_l = \frac{3C_T}{s} \quad (2.17)$$

Rotor tip speed is a design variable. The upper limit on tip speed is a limit on the tip Mach number, while a lower limit is set by limiting the blade mean lift coefficient.

Calculations are performed on a per-rotor basis. Standard sea-level values for ρ (air density) and a (speed of sound) are used.

The rotor aerodynamic model was validated using experimental data from Bagai & Leishman [35], as given by Leishman [36]. The data was obtained using a series of experiments conducted on a four-bladed model helicopter rotor, with a radius of 32.5 inches and a solidity of 0.098. Results are shown in Figure 2-1.

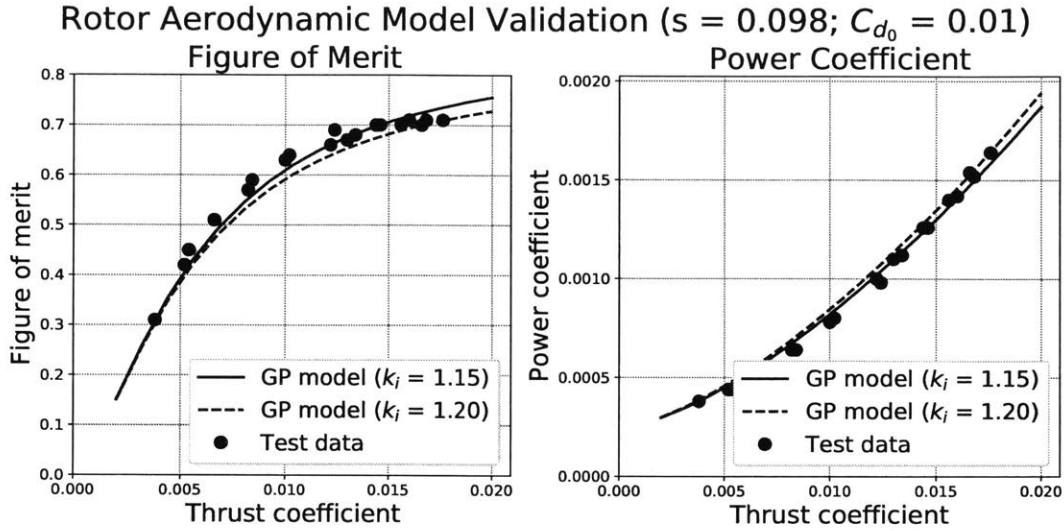


Figure 2-1: Validation of the rotor aerodynamic model.

Values of k_i and C_{d_0} of 1.15 and 0.01 respectively are recommended by Leishman. Figure 2-1 shows that using this set of parameters results in a reasonable approximation of the experimental data. However, most of the optimized designs in this study have thrust coefficients in the range of 0.025-0.035, higher than the data in Figure 2-1. On-demand air vehicles are capable of higher thrust coefficients relative to helicopters. This is due to the higher limits on blade mean lift coefficient (discussed in Section 3.1), directly leading to higher thrust coefficients through Equation 2.17. A value of $k_i = 1.2$ was used to better match the available data at higher thrust coefficients.

Parameters used by the rotor model are given in Table 2.1.

Table 2.1: Rotor model parameters.

Parameter	Symbol	Value
Induced power factor	k_i	1.2
Blade zero-lift drag coefficient	C_{d_0}	0.01
Rotor solidity	s	0.1
Tip Mach number (upper limit)	M_{tip}	0.9

2.3 Mission Model

The mission model is also similar to that in Reference [26], with three different mission profiles:

- A sizing mission, which the aircraft must be capable of flying.
- A revenue mission, in which the aircraft is carrying paying passengers.
- A deadhead mission, in which the aircraft is merely being repositioned for its next revenue-generating flight and no passengers are carried.

The sizing mission includes a longer hover time relative to the revenue and deadhead missions; it also includes a reserve. Three reserve options are available. The first is a 20-minute loiter time, required by the FAA for helicopter VFR (Visual Flight Rules) operations [37]. This requirement applies both during the day and at night, and would be applicable if on-demand vehicles are certified as helicopters. The second reserve option is a 30-minute loiter time, required for the FAA for aircraft VFR (Visual Flight Rules) operations during the day [38]. This requirement would be applicable if on-demand vehicles are certified as aircraft. The final option is a 2-nmi diversion distance, included in case a special regulatory class is created for eVTOL aircraft:

The General Aviation Manufacturers Association (GAMA) is currently developing a recommendation for performance measurement for electric VTOL aircraft by requiring a reserve segment consisting of a balked landing followed by a 2 nautical mile flight to an alternate landing site. This short distance to an alternate is reflective of the capability of VTOL aircraft to land in any suitable open area in emergency situations and of the severe challenge of extensive reserve requirements on electric aircraft feasibility [39].

A similar option was used by Reference [26]; this option is hereafter referred to as the Uber reserve requirement.

Two crew options are available: piloted and autonomous. If the mission is piloted, the pilot is assumed to add 190 lbs to the vehicle weight. If the mission is autonomous, no weight penalty is applied. 200 lbs per passenger is assumed.

Mission profiles are shown in Figure 2-2.

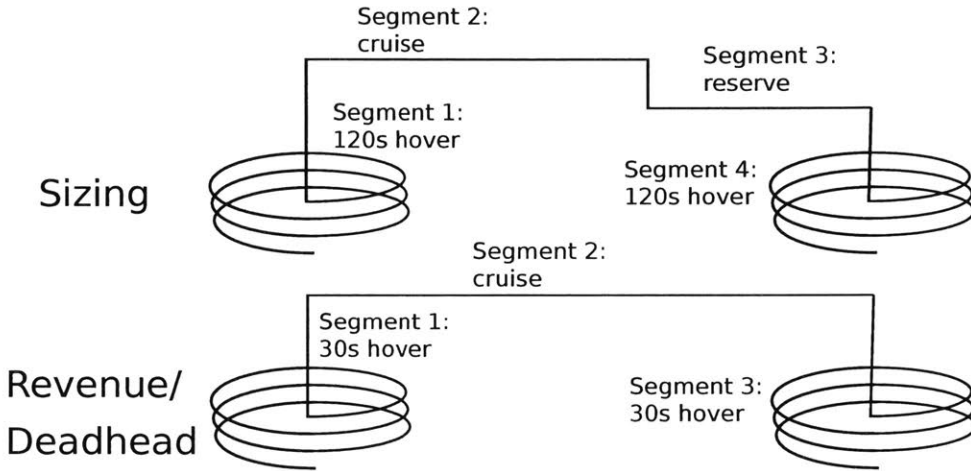


Figure 2-2: Mission profiles. Segment 4 of the revenue and deadhead missions (time on ground) is not shown.

Segment 4 of the revenue-generating and deadhead missions (time on ground; not shown in Figure 2-2) includes a segment time constrained by one of two factors. Firstly, the time has to be greater than 5 minutes, to allow for passenger loading/unloading, safety checks, etc. Secondly, the vehicle is assumed to be charging at the same time; all of the energy used during the mission is replenished. A 200 kW charger is assumed for the purposes of computing charging time.

Cruising speed and cruise lift-to-drag ratio were provided as input parameters for each configuration. These numbers are used in cruise, and also for the reserve segment if the Uber reserve requirement is used. However, the FAA reserve requirement is a loiter requirement, as opposed to a cruise requirement. For this reason, the optimal lift-to-drag ratio and flight speed differ from the cruise values.

If a parabolic drag polar is assumed, Equations 2.7 and 2.8 can be written as

Equations 2.18 and 2.19 respectively:

$$Range = \eta \frac{C_L}{C_{D_0} + k C_L^2} \frac{C}{W} \quad (2.18)$$

$$Endurance = \eta \left[\frac{\rho S C_L}{2W} \right]^{1/2} \frac{C_L}{C_{D_0} + k C_L^2} \frac{C}{W} \quad (2.19)$$

C_L is the wing three-dimensional lift coefficient, C_{D_0} is the aircraft three-dimensional zero-lift drag coefficient, and k is the aircraft induced power factor. All values are referenced to the wing area S . k is equal to $\frac{1}{\pi e AR}$, where e is the Oswald efficiency and AR is the wing aspect ratio.

The conditions for maximum range and endurance can be obtained by differentiating Equations 2.18 and 2.19 respectively, with respect to lift coefficient. This yields the values for lift coefficient, airspeed, and lift-to-drag ratio in Table 2.2.

Table 2.2: Flight conditions for maximum range and endurance.

	Lift coefficient	Airspeed	Lift-to-drag ratio
Maximum range	$C_L = \left[\frac{C_{D_0}}{k} \right]^{1/2}$	$V = \left[\frac{2W}{\rho S} \right]^{1/2} \left[\frac{k}{C_{D_0}} \right]^{1/4}$	$\frac{L}{D} = \frac{1}{2} \left[\frac{1}{k C_{D_0}} \right]^{1/2}$
Maximum endurance	$C_L = \left[\frac{3C_{D_0}}{k} \right]^{1/2}$	$V = \left[\frac{2W}{\rho S} \right]^{1/2} \left[\frac{k}{3C_{D_0}} \right]^{1/4}$	$\frac{L}{D} = \frac{1}{4} \left[\frac{3}{k C_{D_0}} \right]^{1/2}$

Therefore, if the cruising speed and lift-to-drag ratio for a given configuration are known, the loiter speed and lift-to-drag ratio can be estimated using Equations 2.20 and 2.21 respectively:

$$V_{loiter} = \left[\frac{1}{3} \right]^{1/4} V_{cruise} \quad (2.20)$$

$$\left(\frac{L}{D} \right)_{loiter} = \frac{\sqrt{3}}{2} \left(\frac{L}{D} \right)_{cruise} \quad (2.21)$$

The net effect of Equations 2.20 and 2.21 is to reduce power consumption (and by extension, energy use) during the loiter segment. This in turn provides a benefit to battery sizing. These adjustments were implemented in the optimization tool.

2.4 Cost Model

The cost model uses both the revenue mission and the deadhead mission. Costs are divided into two categories: capital expenses, and operating expenses. Key input parameters for the cost model are given in Table 2.3.

Table 2.3: Parameters used by the cost model.

Parameter	Value
Vehicle cost per unit empty weight	\$350 per lb
Avionics cost per aircraft (assuming vehicle autonomy is enabled)	\$60,000
Battery cost per unit energy capacity	\$400 per kWh
Pilot wrap rate	\$70 per hour
Pilots per aircraft (assuming a piloted mission)	1.5
Aircraft per bunker pilot (assuming an autonomous mission)	8
Mechanic wrap rate	\$60 per hour
Price of electricity	\$0.12 per kWh
Maintenance man-hours per flight hour	0.6
Deadhead ratio	0.2

2.4.1 Capital Expenses

Capital expenses are subdivided into three categories: vehicle purchase price, battery purchase price, and avionics purchase price. Vehicle purchase price is computed using a fixed price per unit empty vehicle weight, while battery purchase price is computed using a fixed price per unit energy capacity. If vehicle autonomy is enabled, the avionics add a fixed amount per aircraft. Avionics cost is neglected if vehicle autonomy is not enabled. These last two assumptions are identical to those in Reference [15].

Estimates for vehicle cost per unit empty weight were obtained for several different vehicle categories, ranging from business jets to electric cars. A summary of the results is in Table 2.4. Battery weight and cost were deducted from the Tesla Model S estimates by assuming a vehicle curb weight, purchase price, battery weight, battery

energy density, and battery cost of 4,749 lbf, \$70,000, 1,200 lbf, 200 Wh/kg, and \$200 per kWh respectively.

Table 2.4: Empty weight (W_e) and cost estimates for several representative vehicles.

Vehicle	Vehicle type	W_e (lbf)	Price (\$US)	\$US/ W_e
Cessna Citation Mustang	Very light jet	5,600	\$3,350,000	\$598.2
Robinson R44	Light helicopter	1,450	\$425,000	\$293.1
Cessna 172R	GA aircraft	1,691	\$274,900	\$162.6
Ferrari 488	Sports car	3,362	\$272,700	\$81.1
Tesla Model S (75D)	Electric car	3,549	\$48,182	\$13.6
Honda Accord	Sedan	3,170	\$22,455	\$7.1

Table 2.4 shows that cost per unit empty weight varies widely depending on the vehicle type. Therefore, a relatively conservative estimate of \$350 per lbf is used. However, if production rates increase to levels approaching those typical in the automotive industry, Table 2.4 shows that significant cost savings are expected. Meanwhile, battery prices per unit energy capacity are based upon Department of Energy projections, as referenced in [15].

Capital expenses are then amortized over the mission, in order to estimate their effects on the cost of providing air taxi service. In financial terms, this is analogous to straight-line depreciation with zero salvage value. Vehicle and avionics costs are amortized using a 20,000-hour vehicle life, while the battery is amortized using a 2,000-cycle battery life.

2.4.2 Operating Expenses

Operating expenses are divided into direct operating cost (DOC) and indirect operating cost (IOC). Direct operating cost is further divided into three categories: pilot cost, maintenance cost, and energy (electricity) cost.

Pilot and maintenance costs are estimated using wrap rates, which include salary payments as well as benefits, overhead, training, administrative costs, etc [38]. Wrap

rates of \$50-150 per hour for pilots and \$53-67 per hour for mechanics are typical [40].

Pilot and maintenance cost per mission are then computed using Equations 2.22 and 2.23 respectively:

$$\text{Pilot cost} = (\text{Pilot wrap rate}) \times (\text{Pilots per aircraft}) \times (t_{mission}) \quad (2.22)$$

$$\text{Maintenance cost} = (\text{Mechanic wrap rate}) \times (MMH/FH) \times (t_{mission}) \quad (2.23)$$

$t_{mission}$ is the mission time (including time spent on the ground), while MMH/FH is the number of maintenance man-hours required per flight hour. Values of 0.25-1 are typical for light aircraft [38].

Equation 2.22 assumes a piloted mission. If the mission is flown autonomously, the pilot cost model uses ROCs and bunker pilots instead (see Section 1.2.3). Pilot cost is then computed using Equation 2.24:

$$\text{Pilot cost} = \frac{(\text{Pilot wrap rate}) \times (t_{mission})}{\text{Aircraft per bunker pilot}} \quad (2.24)$$

Energy cost is computed by multiplying the amount of electricity used during the mission by the price of electricity: \$0.12 per kWh, the average price of electricity in the United States [15]. A 90% charging efficiency is assumed. Finally, indirect operating cost is estimated as a fixed fraction of direct operating cost. Values of 33%-100% are typical for airlines, depending on the business model [38]. However, the proposed on-demand air service does not require large airports, sophisticated baggage-handling systems, etc. IOC should therefore be significantly lower; a value of 12% of DOC is used.

2.4.3 Effect of Deadhead

Some missions flown by the air taxi service will inevitably be deadhead missions: missions in which the aircraft is merely being repositioned for its next revenue-generating flight and no passengers are carried. In order to account for the effect of deadhead

missions on cost, the aircraft is “flown” over both missions, and costs are computed for both.

The total cost of flying N_r revenue-generating missions at a cost c_r per mission and of flying N_d deadhead missions at a cost c_d per mission can be calculated using Equation 2.25:

$$\text{Total cost} = N_r c_r + N_d c_d \quad (2.25)$$

The cost per trip (including the effect of deadhead) is therefore calculated using Equation 2.27, obtained after some algebraic manipulation:

$$\text{Cost per trip} = \frac{\text{Total cost}}{N_r} = c_r + \frac{N_d}{N_r} c_d \quad (2.26)$$

$$\text{Cost per trip} = c_r + \frac{dr}{1 - dr} c_d \quad (2.27)$$

dr is the deadhead ratio: number of deadhead flights as a percentage of total number of flights.

2.4.4 Limitations

A number of important effects are not included in the cost model. For example, the same vehicle cost per unit empty weight is used for all configurations. This may not be an accurate assumption. For example, the lift + cruise vehicle configuration is aeromechanically quite simple as compared to configurations with more moving parts like the tilt wing and tilt rotor (these configurations are depicted in Figure 3-1). It should therefore benefit from lower development, certification, and manufacturing costs, resulting in a reduced cost ratio. Taxes, insurance, landing fees, air traffic control (ATC) fees, and profit margin are all neglected by the cost model as well.

2.5 Noise Model

A model for vehicle noise is developed in this section. The model is not compatible with geometric programming, so it was not integrated into the optimization model. Instead, vehicle noise is computed during post-processing.

2.5.1 Importance of Noise

Low noise is essential in order to achieve community acceptance for on-demand aviation. Community opposition to increased noise is already an important consideration for commercial airliners [41], supersonic jet concepts [42], and helicopters [6]. Both the Federal Aeronautics Administration (FAA) and European Aviation Safety Administration (EASA) already have noise limits in place for various types of aircraft, but Uber anticipates that a much stricter standard will be required for on-demand aviation.

A significant portion of the Uber Elevate paper is devoted to defining a set of quantitative noise goals. They eventually select a target noise level of 62 dBA (A-weighted decibels) with the vehicle hovering 500 ft overhead. This is half the noise generated by a medium-size truck at 50 ft, and comparable to a Prius at 25 ft [15]. A-weighting is discussed further in Section 2.5.7.

This research focuses on vehicle noise in hover, as opposed to in cruise. This is done for two reasons. First of all, according to the noise model in Equation 2.32, noise is strongly correlated with thrust. Thrust required in cruise is related to thrust required in hover (equal to vehicle weight) through Equation 2.28:

$$T_{cruise} = T_{hover} \left(\frac{L}{D} \right)_{cruise}^{-1} \quad (2.28)$$

The configurations with wings examined in this research have cruise lift-to-drag ratios on the order of 10-14 (see Table 3.3). Therefore, according to Equation 2.28, cruise thrust is an order of magnitude less than hover thrust, with a corresponding significant reduction in noise. Using wings instead of rotors is one way of reducing noise, relative to helicopters.

Secondly, cruise noise can be reduced through operational procedures, as well as through vehicle design. Examples of operational procedures include flying higher, avoiding noise-sensitive areas, and/or flying near existing noise sources (such as highways) to mitigate the noise impact of the vehicle. By comparison, hover noise at the landing site cannot be reduced nearly as easily, and is therefore the focus of this research.

2.5.2 Noise Metrics

Metrics for aircraft noise measurement can be divided into five categories and/or steps, with each category building upon the previous one. The first and simplest category is unweighted sound pressure level, or SPL. SPL is defined in Appendix A; it is measured in decibels (dB).

Humans are capable of hearing sounds at frequencies between about 20 Hz and 20 kHz; also, human ears have different responses at different frequencies [43]. For example, humans will perceive a 2.5-kHz tone as being much louder than a 40-Hz tone if the two tones have identical sound pressure levels. The second step is therefore to introduce noise exposure levels, noise metrics that takes human response into account [44]. Examples include A-weighted decibels (dBA) and perceived noise level (PNL). dBA is designed such that the average human will perceive two sounds with the same noise exposure level as being equally loud, regardless of frequency. Meanwhile, PNL is based upon annoyance criteria rather than equal loudness.

The third step is to introduce effective noise levels. Metrics in this category adjust the noise exposure level to account for the length of time of the noise event. [44]. Examples include Single Event Level (SEL), which when applied to A-weighted decibel measurements is typically referred to as L_{AE} . “[L_{AE}] is the [equivalent] A-weighted sound pressure level lasting one second that contains the same energy as an entire aircraft event such as takeoff or overflight” [15]. Meanwhile, Effective Perceived Noise Level (EPNL) is based upon PNL, and is the standard metric for aircraft noise regulations [44].

The fourth step is to introduce noise indices, which adjust the effective noise level

to account for the number of noise sources present. Variation of noise levels with time is also accounted for. Examples include the A-weighted Equivalent Continuous Sound Level ($L_{A_{eq}}$) and the Day Night Average Sound Level (L_{dn} or DNL).

The final step is to introduce noise criteria. A simple example is the percentage of the population in a given area that experiences noise above a certain level [44].

This work is concerned with metrics in the first and second category; all noise data uses either unweighted or A-weighted decibels. However, two additional noise metrics (in addition to A-weighted sound pressure level) are defined in the Uber white paper: long-term annoyance (measured in terms of the DNL) and short-term annoyance (measured in terms of the SEL). Future work should focus on incorporating these metrics, as well as metrics in the other categories listed above.

2.5.3 Sources of Noise

Lowson and Ollerhead conducted a comprehensive review of the helicopter noise prediction problem. [7]. A list of helicopter noise sources, in decreasing order of importance, is included in that reference:

- Blade slap (when it occurs)
- Piston-engine exhaust noise
- Tail-rotor rotational noise
- Main-rotor vortex noise
- Main-rotor rotational noise
- Gearbox noise
- Turbine engine noise

The noise problem for an on-demand aircraft is more straightforward than that of a helicopter, because gearbox noise and turbine engine noise are absent. Piston-engine exhaust noise is also absent, unless the vehicle is a hybrid. Therefore, the noise model in this report accounts for blade slap, rotational noise, and vortex noise.

2.5.4 Blade Slap

Blade slap is the most significant source of noise for a helicopter. Three causes of blade slap are identified in Reference [45]. The first is shockwave formation, which typically occurs at high rotor blade tip Mach numbers. It is shown in Section 3.2 that optimized tip Mach numbers for on-demand electric aircraft are typically in the range of 0.35-0.55, significantly lower than values typical for helicopters [34]. Therefore, this form of blade slap is neglected. Blade stall is also cited as a cause of blade slap, but this problem can be mitigated by the selection of appropriate constraints on blade mean lift coefficient. In addition, blade stall tends to be a problem in cruise, rather than in hover. Therefore, concepts that use wings instead of rotors in cruise should not suffer from blade stall.

The final form of blade slap is known as blade-vortex interaction (BVI); it occurs when one rotor blade passes through the bound vortex emanating from another blade. This form of blade slap is common during descent to landing. Helicopters can avoid this form of noise using correct approach and departure procedures, examples of which are given in Reference [46]. It is hypothesized in this work that on-demand electric aircraft can take advantage of similar procedures. Therefore, BVI noise is neglected as well.

2.5.5 Rotational Noise

Rotor noise in the absence of blade slap can be divided into two main components: rotational noise, which occurs at integer multiples of the blade passage frequency (blade rotational frequency \times number of rotor blades); and vortex noise, which is broadband in nature. Rotational noise is also referred to as harmonic noise.

Rotational noise can be divided into two categories: loading noise, which is a direct consequence of thrust generation; and thickness noise, caused by finite rotor blade thickness. These two forms of noise can be modeled by the Gutin and Deming formulae respectively. They are derived in equivalent-radius form in Appendix C.

The resulting noise model is repeated here as Equations 2.29, 2.30, and 2.31:

$$p_{m_L} = \frac{mB\Omega}{2\sqrt{2}\pi a(\Delta S)} \left[T \cos \theta - Q \frac{a}{\Omega R_e^2} \right] J_{mB} \left(\frac{mB\Omega}{a} R_e \sin \theta \right) \quad (2.29)$$

$$p_{m_T} = \frac{-\rho(mB\Omega)^2 B}{3\sqrt{2}\pi(\Delta S)} ct R_e J_{mB} \left(\frac{mB\Omega}{a} R_e \sin \theta \right) \quad (2.30)$$

$$SPL = 10 \log_{10} \left[N \left(\frac{p_{m_L}^2 + p_{m_T}^2}{p_{ref}^2} \right) \right] \quad (2.31)$$

p_{m_L} and p_{m_T} are the root mean square (RMS) sound pressures for loading and thickness noise respectively. m is the harmonic number (a positive integer), N is the number of rotors, B is the number of rotor blades, Ω is the rotor angular velocity, a is the speed of sound, and ΔS is the distance between the rotor and the observer. T is the rotor thrust, Q is the rotor torque, and θ is the observer azimuthal location. ρ is the air density, c is the blade chord, and t is the blade maximum thickness. J_{mB} is a Bessel function of the first kind of order mB . A diagram showing ΔS and θ is given in Figure 2-3.

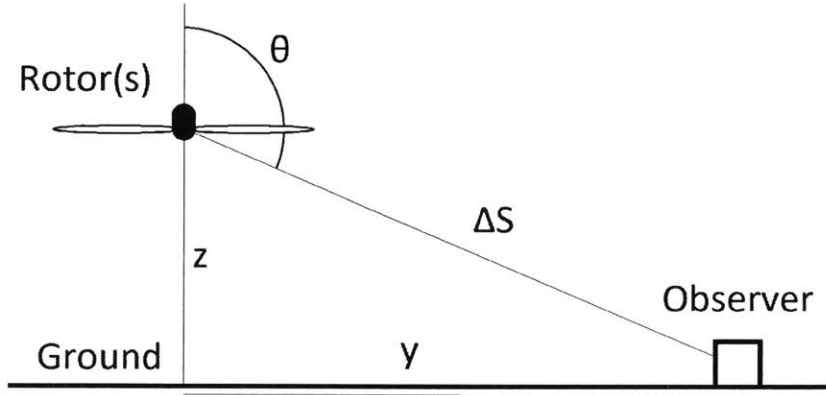


Figure 2-3: Azimuthal angle diagram.

An effective rotor radius of $R_e = 0.8R$ is recommended by Reference [47], and is used throughout this work. Blade chord is estimated using the definition of solidity (Equation 2.14). Since the NACA 0012 airfoil is a traditional choice for helicopter

rotor blades [34], the blade thickness is calculated using an assumed thickness-to-chord ratio of 12%. Finally, p_{ref} is the reference pressure, equal to 2×10^{-5} Pa.

Unless otherwise stated, all rotational noise calculations assume a five-bladed rotor. Combined with the solidity value from Table 2.1, this results in a blade aspect ratio of 15.9, a reasonable compromise between blade efficiency and structural integrity for helicopters [34].

Note that $\theta = 180^\circ$ directly underneath a rotor, so $J_{mB} \left(\frac{mB\Omega}{a} R_e \sin \theta \right) = 0$. Therefore, rotational noise is negligible for an observer underneath the aircraft, something that is not true for vortex noise. Because the Uber noise requirement is for an observer 500 ft underneath the aircraft, all studies (unless otherwise noted) neglect rotational noise. This assumption is investigated further in Section 3.3.

2.5.6 Vortex Noise

A model for vortex noise is derived in Appendix D.1, and is repeated here as Equation 2.32:

$$SPL = 20 \log_{10} \left[K_2 \frac{V_T}{\rho(\Delta S)} \sqrt{\frac{NT}{s} \left(\frac{T}{A} \right)} \right] \quad (2.32)$$

T/A is the rotor disk loading; K_2 is a constant, equal to $1.206 \times 10^{-2} s^3/ft^3$.

All of the non-constant parameters in Equation 2.32 both provide a benefit to vehicle sizing and reduce noise. For example, K_2 , ρ , and ΔS are constants. Meanwhile, lowering tip speed, increasing rotor solidity, and decreasing rotor disk loading all result in sizing benefits. Finally the product of number of rotors and rotor thrust is equal to vehicle weight; a lighter vehicle both costs less (see Section 2.4) and is quieter.

Equation 2.32 was validated using data in Reference [48] for two different helicopter main rotors: the CH-3C and the CH-53A. Results are given in Appendix D.1. It is shown that the model is accurate to within 3 dB of test data.

Although vortex noise is broadband in nature, it has a peak frequency (frequency

at which the amplitude is highest). It can be estimated using Equation 2.33 [45]:

$$f_{peak} = \frac{(V_{0.7})St}{h} \quad (2.33)$$

f_{peak} is the vortex-noise peak frequency (in Hz), St is the Strouhal number, $V_{0.7}$ is the blade velocity at a radial location $r/R = 0.7$ (i.e. 0.7 times the tip speed), and h is the projected blade thickness (see Appendix D.2). An estimate of $St = 0.28$ is used; this is a reasonable value for a helicopter [45].

Once peak frequency is known, the vortex-noise frequency spectrum can be obtained using the method in Appendix D.2. This is required if noise weighting schemes are to be applied.

2.5.7 A-Weighting Scheme

As discussed in Section 2.5.2, human ears have different responses at different frequencies. Various decibel weighting schemes have been proposed to account for this, the most widely used of which is the A-weighting scheme. This scheme applies a response function to a given sound pressure level, in order to compensate for the frequency response of the human ear. The A-weighting response function $A(f)$ as a function of frequency is plotted in Figure 2-4.

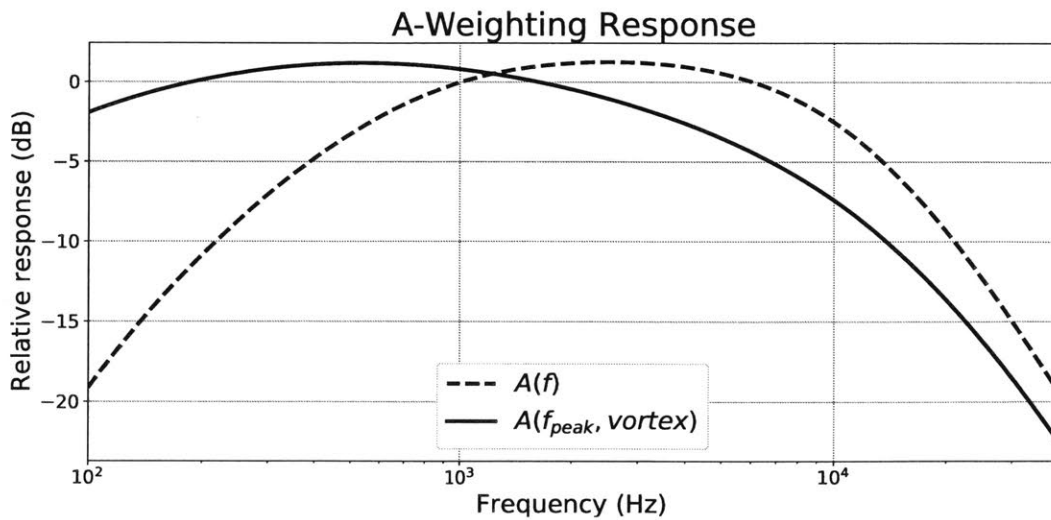


Figure 2-4: The A-weighting response function.

Figure 2-4 reveals that $A(f)$ is maximized at a frequency of approximately 3 kHz, indicating that humans are particularly sensitive to sounds at this frequency. In order to reduce subjective annoyance, the designer should strive to avoid sound frequencies near 3 kHz as much as possible.

The Gutin and Deming model for rotational noise produces a discrete array of frequencies and sound pressure levels. Therefore, the A-weighted sound pressure level can be obtained by applying $A(f)$ to the sound pressure level for each harmonic, then adding the results using the method in Appendix B. This method cannot be applied to vortex noise because the resulting frequency spectrum is continuous. Instead, an approximate procedure for applying A-weighting to vortex noise is derived in Appendix D.3.

It is shown in Appendix D.2 that the vortex-noise frequency spectrum ranges from $0.5f_{peak}$ to $16f_{peak}$. Therefore, most of the sound produced is at frequencies higher than the peak frequency; the peak frequency at which human ears are most sensitive is therefore somewhat lower than 3 kHz. Figure 2-4 also shows $A(f)$ as a function of f_{peak} , revealing a maximum around $f_{peak} = 600$ Hz. The designer should therefore strive to obtain a peak frequency as far away from 600 Hz as possible.

A-weighted sound pressure level is known to be far from perfect in predicting human perception of loudness, in part because of its bias against low frequencies [43]. It is used in this study for three primary reasons. First of all, it is by far the most common metric for noise prediction, allowing comparisons with data from other noise sources such as cars and helicopters (see Section 2.5.1). Secondly, it is often used for regulatory purposes. Thirdly, a recent psychoacoustic study demonstrated a correlation between noise and annoyance [49]. The study used an acoustically treated room with human subjects to gather data, and auralizations of sounds from small UAVs and cars as noise inputs. An example correlation is depicted in Figure 2-5.

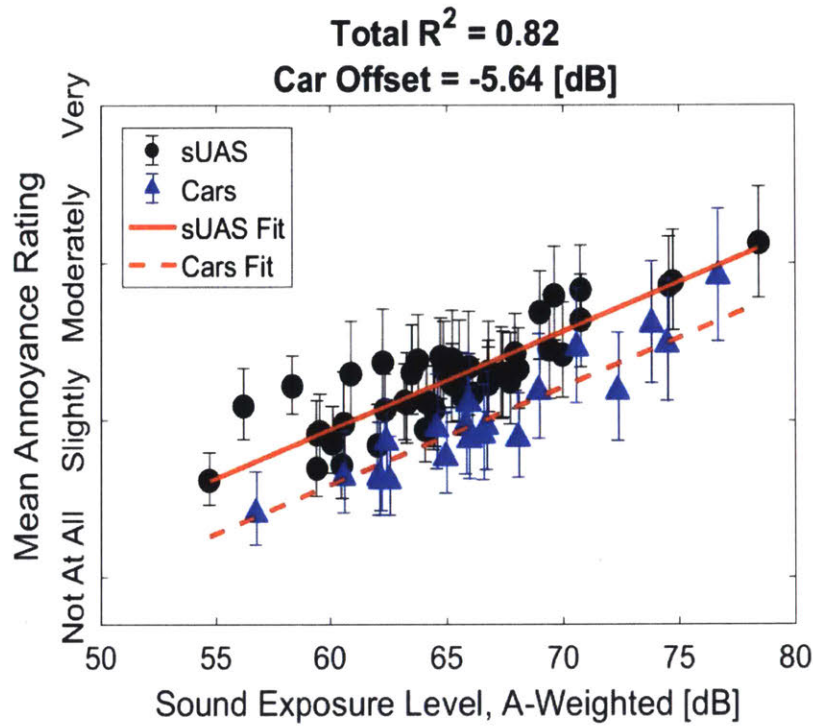


Figure 2-5: Correlation between noise and annoyance, from Reference [49].

Figure 2-5 shows that A-weighted sound exposure level is correlated with annoyance. The correlation is much weaker for both C-weighted SEL (another form of noise weighting that lacks a bias against low frequencies) and EPNL. However, the correlation is different for cars and UAVs. As Figure 2-5 also shows, UAVs were perceived as being approximately 6 dB more annoying than cars at the same sound exposure level.

These results are preliminary in nature, and technically only apply to small UAVs. Their suitability to on-demand air vehicles has not been established [49]. However, they provide evidence that A-weighting is a reasonable first step at predicting human annoyance. Therefore, A-weighted SPL forms a reasonable starting point, and is used throughout this study.

2.5.8 Limitations

The noise model is not immediately applicable to all vehicle configurations. For example, a coaxial helicopter will produce additional noise due to the interaction of the flow field between the rotors. This effect was not taken into account.

Conventional and compound helicopters have tail rotors, to counteract the torque of the main rotor. According to Lawson and Ollerhead, helicopter tail rotors are subjectively louder than main rotors [7]. Many modern helicopters use shrouded tail rotors, which substantially reduce noise [38]. Therefore, it is assumed that the conventional and compound helicopters use shrouds, and tail-rotor noise is neglected. This approximation should be treated with extreme caution.

Chapter 3

Configurational Trade Study

In this section, the vehicle design and optimization tool developed in Chapter 2 is used to conduct a trade study between various vehicle configurations. Estimates are obtained for vehicle weight, cost, noise, and other key design parameters.

3.1 Inputs

Input parameters are divided into two categories: generic inputs, for which the same value is used for all configurations; and configuration-specific inputs, where different values are used for each configuration. Generic input parameters are given in Table 3.1.

Table 3.1: Generic vehicle input parameters.

Parameter	Value
Battery specific energy	400 Wh/kg
Battery specific power	3 kW/kg
Vehicle autonomy enabled?	Yes

Mission parameters are given in Table 3.2. Inputs specific to the cost model were previously given in Table 2.3.

Table 3.2: Mission input parameters.

Mission	Sizing	Revenue	Deadhead
Mission type	Piloted	Piloted	Autonomous
Mission range	50 nmi	30 nmi	30 nmi
Number of passengers	3	2	0
Reserve type	FAA helicopter VFR	None	None

Table 3.2 specifies that the deadhead mission is flown autonomously, although the other missions are piloted. In practice, the deadhead mission cannot always be autonomous, as pilots will need to be relocated along with their aircraft in order to fly piloted revenue missions. Autonomous deadhead missions are used here to demonstrate the utility of the methodology; a sensitivity analysis is conducted as part of the case study on technology assumptions (Section 4.2).

Most manufacturers plan to certify their vehicles to FAA Part 23, which governs aircraft [50]. However, the helicopter reserve requirement (from FAA Part 27) is listed in Table 3.2. Based on conversations between the author and some in the industry, the consensus appears to be that an entirely new reserve requirement will be created for electric VTOL aircraft. Progress towards such a requirement was discussed previously in Section 2.3. Other eVTOL optimization studies (ex. Reference [51]) tend to use a 20-minute loiter reserve requirement. It was adopted here for this reason; a sensitivity analysis and further discussion is given in Section 5.1.3.

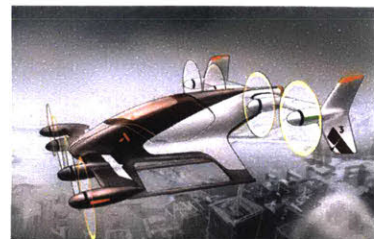
Representative images of each configuration are shown in Figure 3-1.



(a) An example lift + cruise aircraft: the Aurora Flight Sciences prototype [52].



(b) An example compound helicopter: the Carter SR/C [53].



(c) An example tilt wing aircraft: the A³ Vahana [54].



(d) An example tilt rotor: the Joby S2 [55].



(e) An example conventional helicopter: the Robinson R44 [56].



(f) An example coaxial helicopter: the Kamov Ka-32 [57].



(g) An example multirotor: the Ehang 184 [58].



(h) An example autogyro: the Magni M16 [59].



(i) An example tilt duct: the Lilium Jet [60].

Figure 3-1: Configuration representative images. Note that the example conventional helicopter, coaxial helicopter, and autogyro are gasoline-powered; they do not represent eVTOL concepts.

Configuration-specific input data is given in Table 3.3. Cruising speed values were taken from Reference [26]. Reference [26] also gives a range of values for cruise lift-to-drag ratio and hover disk loading; the median values are used in this study. Values for number of rotors were taken from the vehicles in Figure 3-1.

Table 3.3: Input data for each configuration [26].

Configuration	V_{cruise} (mph)	$(\frac{L}{D})_{cruise}$	$\frac{T}{A}$ (lb/ft 2)	W_e/W_0	\bar{C}_l	N
Lift + cruise	150	10	15	0.53	1.0	8
Compound helicopter	150	9	4.5	0.5	0.8	1
Tilt wing	150	12	15	0.55	1.0	8
Tilt rotor	150	14	15	0.55	1.0	12
Conventional helicopter	100	4.25	4.5	0.43	0.6	1
Coaxial heli	150	5.5	7	0.43	0.6	2
Multirotor	50	1.5	3.75	0.43	0.6	8
Autogyro	100	3.5	3.75	0.5	0.8	1
Tilt duct	150	10	40	0.55	1.0	36

As discussed in Section 2.2, a constant empty weight fraction W_e/W_0 is assumed for each configuration. A recent study by Boeing [51] used configuration-specific structural, propulsion-system, and fixed-equipment weight models. Three eVTOL configurations were evaluated: a helicopter, a stopped rotor (lift + cruise), and a tilt rotor. Empty weight fraction estimates of 0.43, 0.53, and 0.55 were respectively obtained, and used here to estimate the values in Table 3.3.

As discussed in Section 2.2.3, rotor tip speed is a design variable. The optimizer tended to reduce the tip speed as much as possible, to reduce blade profile drag. Because the lower limit on tip speed is set by blade mean lift coefficient, understanding of this constraint is critical.

Helicopters typically operate with \bar{C}_l between 0.3 and 0.6 [34]. This is because helicopters with higher values of \bar{C}_l would be prone to retreating blade stall in forward flight. For this reason, \bar{C}_l is constrained to below 0.6 for the conventional and coaxial helicopter.

Retreating blade stall is only an issue for configurations that use their rotors to provide lift in cruise. Therefore, configurations like the tilt rotor and lift + cruise, which do not use their rotors to provide lift in cruise, use a \bar{C}_l constraint of 1.0. In theory, values as high as 1.5-1.6 could be used before the rotor stalls; the value of

1.0 provides a margin for control in hover. The compound helicopter uses its rotor to provide some (but not all) lift in cruise; a \bar{C}_l constraint of 0.8 is used. The same value is used for the autogyro.

Although Table 3.3 includes parameter estimates for the autogyro and the tilt duct, they were not included in the trade study. This is because the vehicle performance model does not accurately describe these two configurations. For example, all three mission profiles include hover segments, but an autogyro is incapable of hover. Instead, the main rotor is unpowered, and autorotates in flight. Meanwhile, the tilt duct uses multiple ducted fans to provide lift in hover. These ducts provide an efficiency and noise benefit, relative to an unducted rotor [38]. In the absence of a model for taking these two benefits into account, the tilt duct was neglected.

The conventional and compound helicopters both have tail rotors, which consume additional power. The tail rotor of a typical helicopter consumes approximately 10-15% of the power consumed by the main rotor [34]. This adjustment can be applied to the conventional helicopter in both cruise and hover. However, the wing of a compound helicopter unloads the main rotor in cruise, causing it (and by extension, the tail rotor) to consume less power. As the wing and rotor power for the compound helicopter in cruise cannot be separated by the mission model, the additional power percentage applied to the compound helicopter was reduced.

Power increase assumptions for both configurations are given in Table 3.4.

Table 3.4: Power increase percentages for configurations with a tail rotor.

Configuration	Power increase (hover)	Power increase (cruise)
Conventional helicopter	15%	15%
Compound helicopter	15%	10%

Sound pressure level is computed during post-processing with the vehicle hovering 500 ft overhead (i.e. $z = \Delta S = 500 \text{ ft}$). This is in accordance with the Uber noise requirement (see Section 2.5.1).

3.2 Results

A bar chart with some key results from the configurational trade study is shown in Figure 3-2.

Aircraft parameters: battery energy density = 400 Wh/kg; 5 rotor blades; autonomy enabled
 Sizing mission (piloted): range = 50 nmi; 3 passengers; 120s hover time; reserve type = FAA helicopter VFR (20-minute loiter time)
 Revenue mission (piloted): range = 30 nmi; 2.0 passengers; 30s hover time; no reserve; charger power = 200 kW
 Deadhead mission (autonomous): range = 30 nmi; 0.0 passengers; 30s hover time; no reserve; deadhead ratio = 0.2

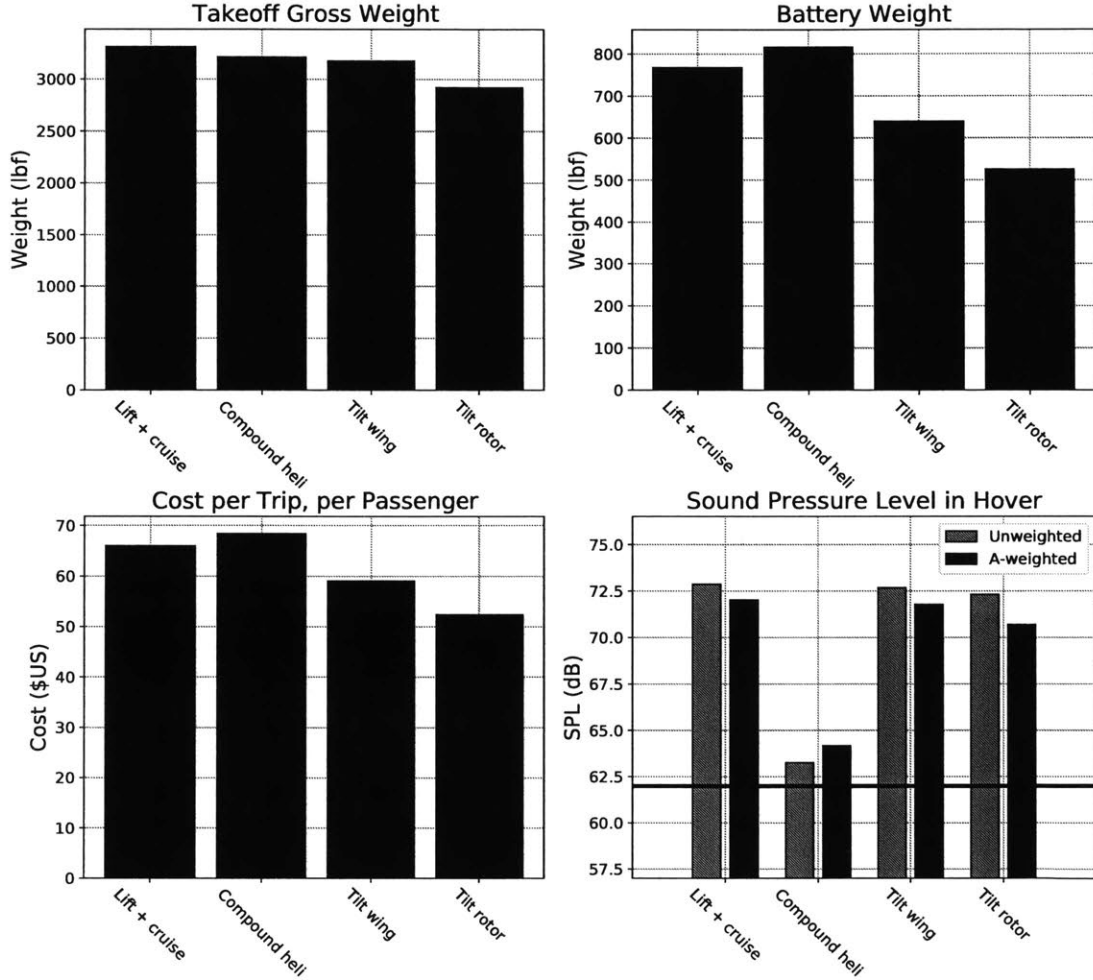


Figure 3-2: Results of the configurational trade study. SPL values are from the sizing mission; the horizontal line represents the 62-dBA Uber noise requirement [15].

Several things are apparent from Figure 3-2. First of all, the multirotor, conventional helicopter, and coaxial helicopter are all missing. In the case of the multirotor, the optimizer returns Primal Infeasible; i.e. a solution for this configuration that

satisfies all of the requirements and constraints does not exist. The conventional and coaxial helicopters do close, but at significantly higher weights: above 10,000 lbf and above 6,000 lbf respectively. Costs are also significantly higher. They were therefore dropped from consideration.

The four remaining configurations are the lift + cruise aircraft, the compound helicopter, the tilt wing, and the tilt rotor. These four configurations all have a relatively high lift-to-drag ratio, but also (with the exception of the compound helicopter) a relatively high disk loading. Since a high lift-to-drag ratio translates to increased efficiency in cruise, while a low disk loading translates to increased efficiency in hover, this means that cruise efficiency takes precedence over hover efficiency for the mission under consideration.

The sound pressure level varies widely between configurations, with unweighted values ranging from a low of about 63 dB for the compound helicopter to above 73 dB for the lift + cruise aircraft. A-weighting affects the results by at most 1-2 dB.

The compound helicopter is the most expensive configuration, but it is also the quietest. However, recall from Section 2.5.3 that tail rotor noise, potentially the dominant source of noise for this configuration, is neglected. Furthermore, no configuration is capable of meeting the 62-dBA Uber noise requirement. This indicates that vehicle noise is a critical issue for on-demand aviation.

Additional results from the configurational trade study are given in Figure 3-3.

Aircraft parameters: battery energy density = 400 Wh/kg; 5 rotor blades; autonomy enabled
Sizing mission (piloted): range = 50 nmi; 3 passengers; 120s hover time; reserve type = FAA helicopter VFR (20-minute loiter time)
Revenue mission (piloted): range = 30 nmi; 2.0 passengers; 30s hover time; no reserve; charger power = 200 kW
Deadhead mission (autonomous): range = 30 nmi; 0.0 passengers; 30s hover time; no reserve; deadhead ratio = 0.2

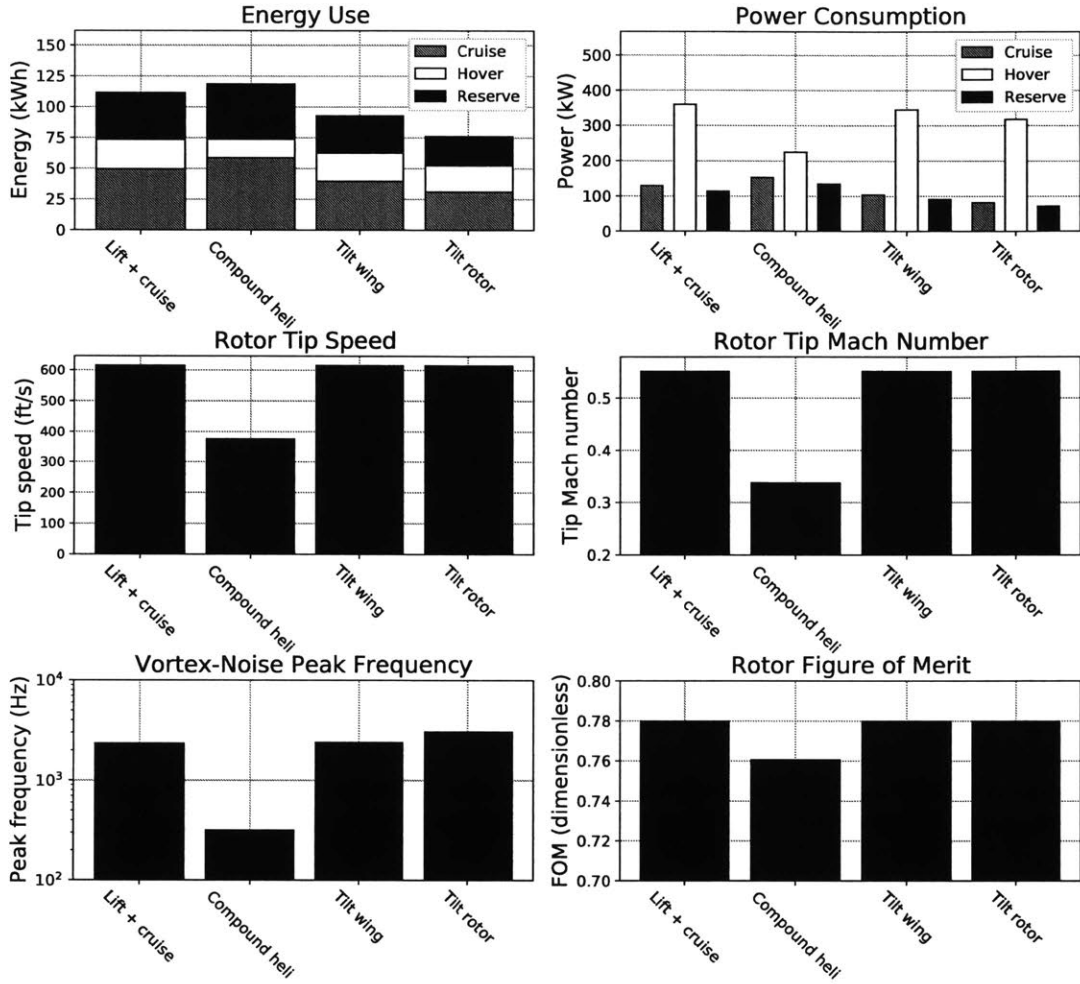


Figure 3-3: More results from the configurational trade study. All data presented is from the sizing mission. Energy use in hover is the sum from all four hover segments.

Figure 3-3 shows that significant amounts of energy are consumed during all three categories of mission segment (cruise, hover, and reserve). Reserve power is lower than cruise power, due to the loiter adjustments discussed in Section 2.3. Also, all four aircraft consume significantly more power in hover than in cruise.

Helicopters may experience tip Mach numbers in forward flight approaching 0.9 [34]. Compressibility and thickness effects (which adversely impact both vehicle effi-

ciency and noise) pose significant problems in this regime. However, from Figure 3-3, rotor tip Mach numbers range from below 0.35 to slightly above 0.55. As discussed in Section 2.5.4, tip Mach effects are therefore not a problem for on-demand aircraft.

Note from Figure 3-2 that the compound helicopter actually becomes slightly louder if A-weighting is considered. This is because the compound helicopter has a vortex-noise peak frequency of about 300 Hz. It can be seen from Figure 2-4 that applying A-weighting to a sound at this frequency increases the sound pressure level. The other configurations have peak frequencies above 2,000 Hz; applying A-weighting therefore lowers the sound pressure level.

For all configurations included in the trade study, the revenue flight takes 14.8 minutes (including hover and cruise). However, it is also important to consider time required to fully charge the battery. In a presentation at the Uber Elevate summit, McDonald & German demonstrated that reducing vehicle charging time is critical to maintaining a high cadence of vehicle operations [16]. This is particularly important during rush hour operations.

Recharge times from the revenue mission, broken down by configuration, are listed in Table 3.5.

Table 3.5: Charging times for the revenue mission.

Configuration	Charging time (minutes)
Lift + cruise	11.1
Compound helicopter	12.2
Tilt wing	9.2
Tilt rotor	7.4

Table 3.5 shows that in some cases, charging the battery takes almost as long as flying the mission. Recall from Section 2.3 that the mission model assumes a 200 kW charger. For comparison, a Supercharger (the most powerful charger available for Tesla electric cars) can produce a maximum of 145 kW. Therefore, in order to increase the number of missions that can be conducted during rush hour, more powerful chargers will be required.

A cost breakdown is shown in Figure 3-4.

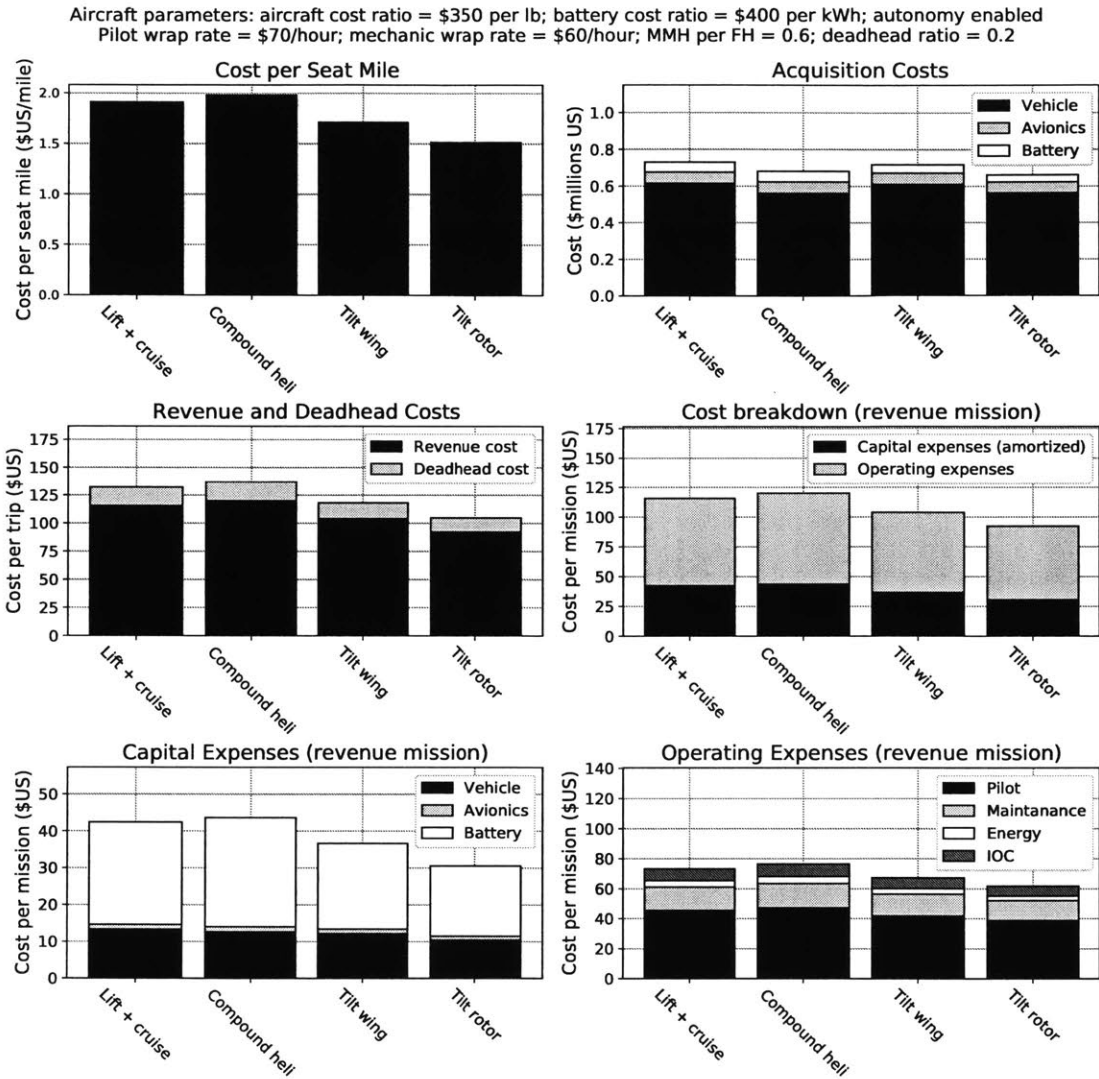


Figure 3-4: Cost breakdown. Cost per seat mile is given in terms of statute miles, instead of nautical miles.

Figure 3-4 shows that cost per seat mile does not vary widely between configurations. Values range from as low as \$1.50 per seat mile for the tilt rotor, to about \$2.00 per seat mile for the compound helicopter. Operating expenses account for a somewhat larger share of revenue mission cost than capital expenses.

Interestingly, the deadhead mission cost is not very large as compared to the revenue-generating mission cost. This is partly because of the low deadhead ratio

(Table 2.3); it is also because the deadhead mission is flown autonomously, with correspondingly lower pilot costs.

Despite the relatively small share of acquisition costs attributable to the battery, the battery accounts for a much larger share (about two-thirds) of amortized capital expenses. This is because the battery is amortized differently as compared to the vehicle and avionics. The latter two items are amortized using a 20,000 hour service life, while the battery is amortized using a 2,000-cycle life (i.e. 2,000 missions). Within operating expenses, pilot cost is dominant as compared to maintenance cost, energy cost, and indirect operating cost. Therefore, the keys to reducing the cost per trip are to 1) reduce battery manufacturing cost and increase cycle life (which lowers battery amortized cost) and 2) implement vehicle automation (which lowers pilot cost). This is discussed further in Section 4.2.

3.3 Noise Analysis

In this section, the assumption that vortex noise is negligible (discussed in Section 2.5.5) is reexamined, by comparing the vortex- and rotational-noise levels. Example noise spectra, for an altitude $z = 500$ ft and observer ground location $y = 982$ ft, are presented in Figure 3-5. The resulting azimuthal angle is $\theta = 117^\circ$. See Figure 2-3 for definitions of y , z , and θ . Only the first harmonic of rotational noise is shown; the other harmonics are negligibly small by comparison.

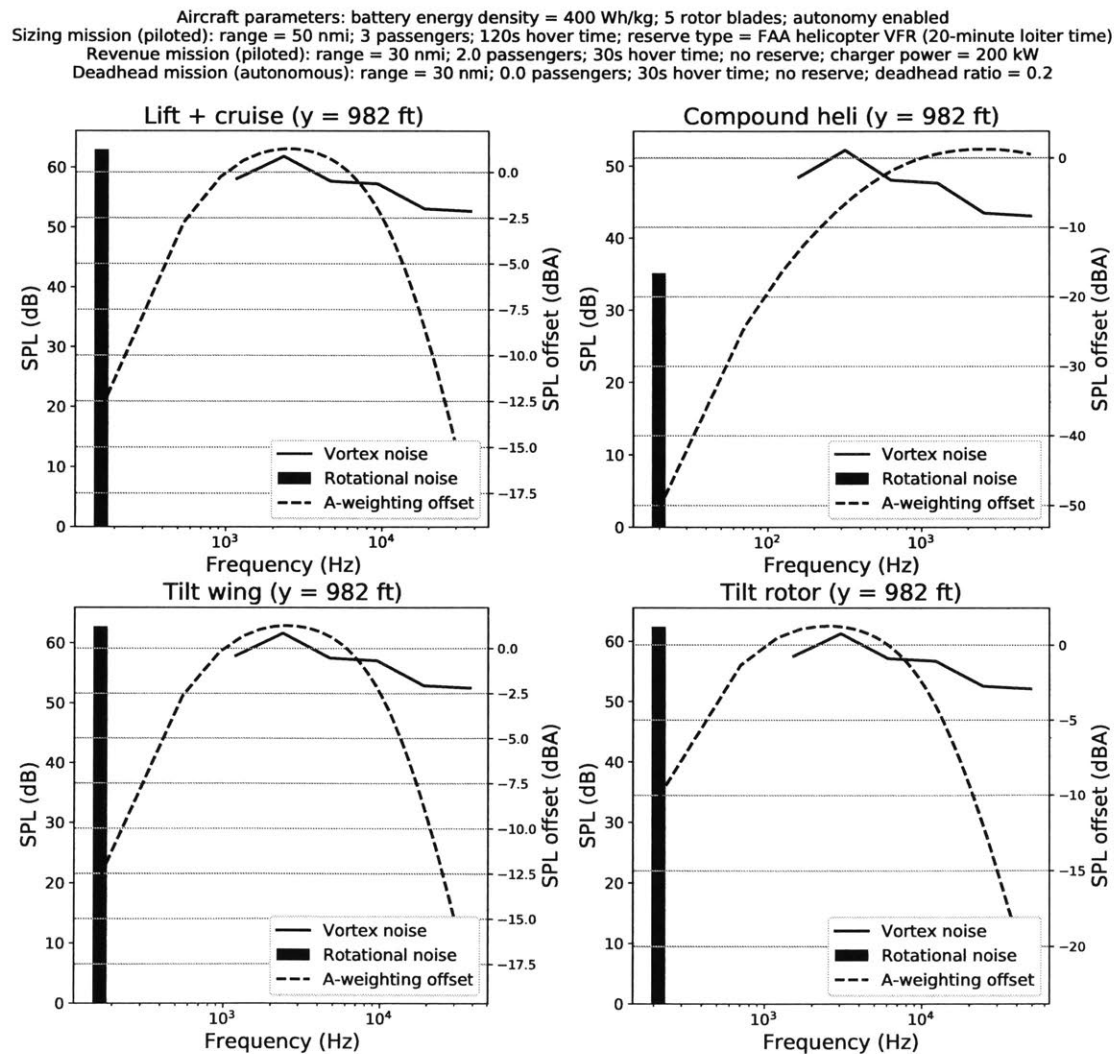


Figure 3-5: Example noise spectra. Both rotational and vortex noise values are unweighted.

Figure 3-5 reveals that (with the exception of the compound helicopter) rotational and vortex noise are comparable in magnitude. However, rotational noise occurs at a much lower frequency. The A-weighting frequency response function $A(f)$ is also plotted. Much of the vortex noise occurs in a regime between 1 and 7 kHz, where $A(f)$ is maximized. Meanwhile, rotational noise occurs at a much lower frequency, with a corresponding large negative weight. This suggests that A-weighted rotational noise is negligible for on-demand aircraft as compared to vortex noise.

A plot showing noise as a function of observer ground location y ($z = 500$ ft) is presented in Figure 3-6. Rotational noise values included the first 10 harmonics.

Aircraft parameters: battery energy density = 400 Wh/kg; 5 rotor blades; autonomy enabled
Sizing mission (piloted): range = 50 nmi; 3 passengers; 120s hover time; reserve type = FAA helicopter VFR (20-minute loiter time)
Revenue mission (piloted): range = 30 nmi; 2.0 passengers; 30s hover time; no reserve; charger power = 200 kW
Deadhead mission (autonomous): range = 30 nmi; 0.0 passengers; 30s hover time; no reserve; deadhead ratio = 0.2

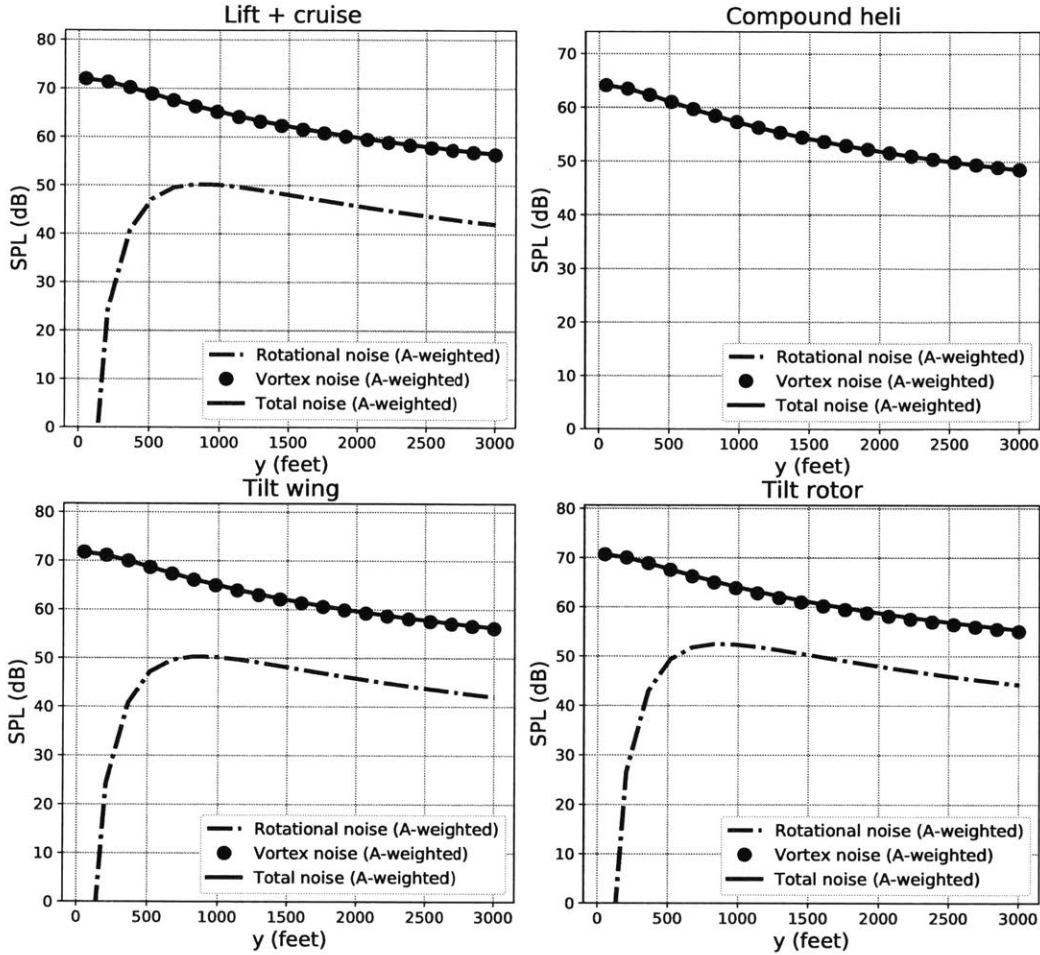


Figure 3-6: Noise as a function of observer location, for constant $z = 500$ ft.

Figure 3-6 shows that A-weighted vortex noise dominates the spectrum for all values of y . Total noise (including both rotational and vortex noise) is plotted to show this more clearly. Therefore, if the relevant sound metric is A-weighted sound pressure level, rotational noise is negligible. This is true not just directly underneath the vehicle (where rotational noise is 0), but for all relevant observer positions while the vehicle is in hover. Also, because vortex noise is independent of azimuthal angle, noise directly underneath the vehicle at $z = \Delta S = 500$ ft is useful as a benchmark by which different vehicles can be compared.

Chapter 4

Case Studies

Six case studies are presented in this chapter. The case studies examine different aspects of vehicle design, including technological forecasts, analysis of existing vehicles, and example initial markets.

The rest of this chapter is structured as follows. Section 4.1 looks at New York City as an example market for on-demand aviation. Meanwhile, Section 4.2 looks at how technology improvements over time affect vehicle cost and noise. The configurational trade study (Section 3.2) identified vehicle noise as a critical issue; Section 4.3 examines methods for reducing noise. The S4 (a four-seat eVTOL under development by Joby Aviation [61]) is analyzed in Section 4.4. In Section 4.5, a type of plot for rapidly examining the vehicle design space is developed. Finally, the impact of some of the model fidelity limitations are addressed in Section 4.6, via comparison with work by other authors.

4.1 New York City Airport Transfers

New York City was selected as an example city in which to implement an on-demand aviation service. Air taxi services already exist in the city, provided by companies such as Blade [62] and New York Helicopter [63]. New York Helicopter provides airport transfer services between downtown helipads and local airports. Three downtown helipads are listed on their website: East 34th Street, West 30th Street, and Pier 6.

Transfers are provided to three airports: John F. Kennedy (JFK), LaGuardia (LGA), and Newark (EWR).

The trip distance between each helipad and each airport was computed using Google Maps. Two sets of assumptions were used: a direct route, and an overwater-only route. As-the-crow-flies routes are generally not permitted in New York City. Instead, the city has defined routes that helicopters must follow. The direct route was selected as the shortest of the existing helicopter routes, as obtained from the maps in Reference [64].

Overwater-only routes were included in case on-demand aircraft are not permitted to fly over populated areas for noise reasons. Given the current controversy in New York City centered on noise generated by helicopter tour operators [6], overwater-only flights may become a necessity.

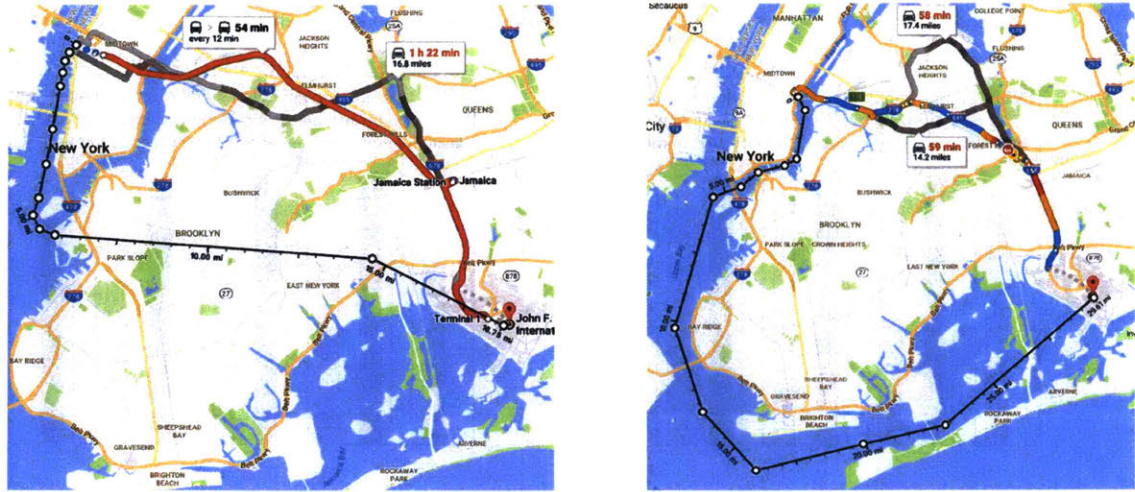
Computed trip distances are presented in Table 4.1. Note that in some cases, no direct route exists that is shorter than the overwater route. In these cases, direct and overwater route distances are identical.

Table 4.1: Trip distance for the airport transfer routes, computed using Google Maps.

Heliport	Airport	Distance (direct, nmi)	Distance (overwater, nmi)
West 30th Street	JFK	16.3	24.4
	LGA	14.2	14.2
	EWR	13.3	13.3
East 34th Street	JFK	9.9	25.7
	LGA	6.4	6.4
	EWR	14.3	14.3
Pier 6	JFK	10.3	21.7
	LGA	10.0	10.0
	EWR	10.6	10.6

The longest direct and overwater routes in Table 4.1 are West 30th Street to JFK (16.3 nmi) and East 34th Street to JFK (25.7 nmi) respectively. They are shown in

Figure 4-1.



(a) The longest direct route: West 30th Street to JFK.

(b) The longest overwater route: East 34th Street to JFK.

Figure 4-1: New York City helicopter routes (black lines). Note that the direct route passes over Brooklyn. While this is in accordance with the established helicopter route [64], an overwater-only route is also included in case this route is shut down for noise reasons.

Based on Table 4.1, trip distances of 19 nmi for the direct flight and 30 nmi for the overwater flight were selected. A comparative study was conducted, using three sets of assumptions:

1. A 19 nmi sizing mission and a 19 nmi revenue mission. This corresponds to a vehicle that is solely capable of flying the direct route.
2. A 30 nmi sizing mission and a 19 nmi revenue mission. This corresponds to a vehicle that typically flies the direct route, but has the range to fly the overwater route if necessary.
3. A 30 nmi sizing mission and a 30 nmi revenue mission. This corresponds to a vehicle that always flies the overwater route.

The deadhead mission range is the same as the revenue mission range. Results are in Figure 4-2.

Aircraft parameters: battery energy density = 400 Wh/kg; 5 rotor blades; autonomy enabled
Sizing mission (piloted): 3 passengers; 120s hover time; reserve type = FAA helicopter VFR (20-minute loiter time)
Revenue mission (piloted): 2.0 passengers; 30s hover time; no reserve; charger power = 200 kW
Deadhead mission (autonomous): 0.0 passengers; 30s hover time; no reserve; deadhead ratio = 0.2

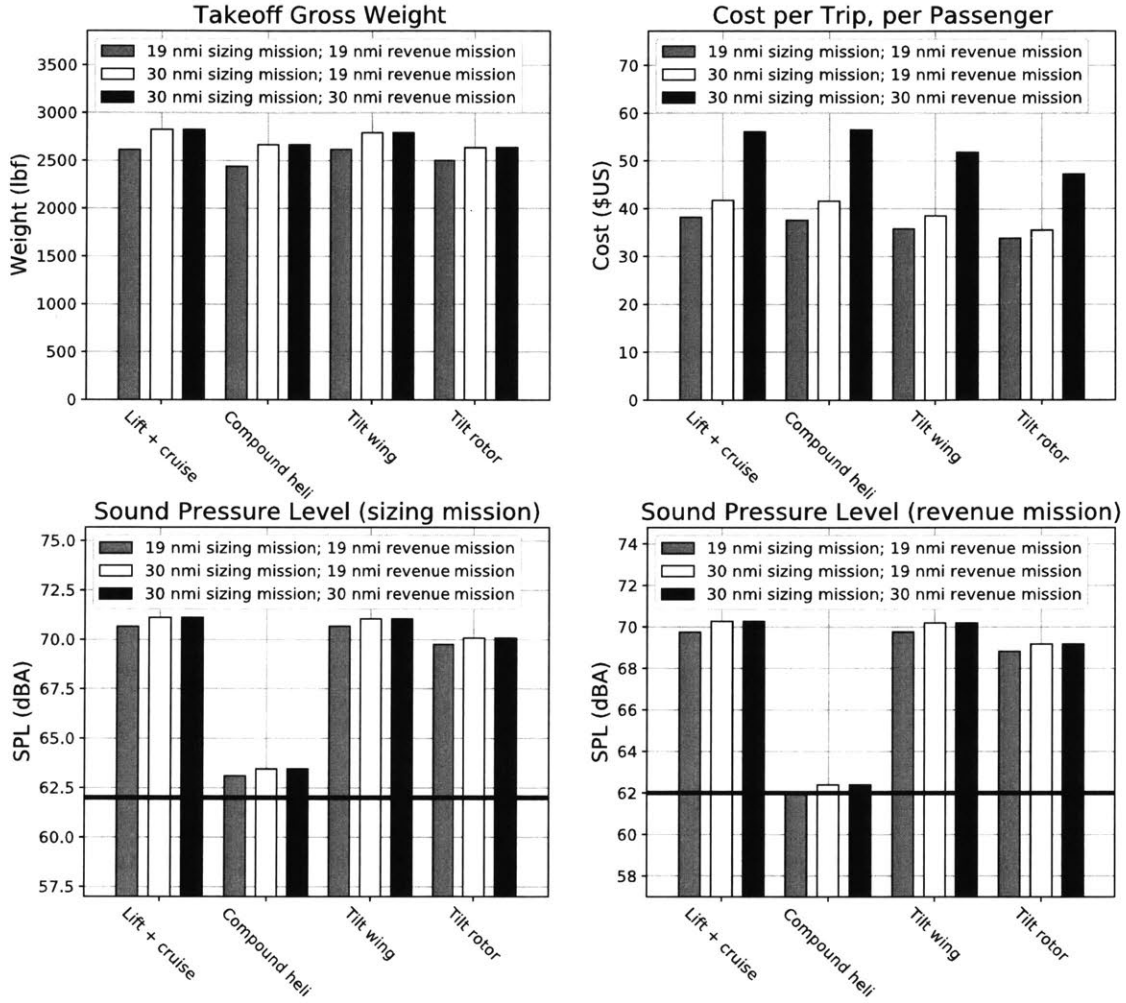


Figure 4-2: Results from the New York City study.

Figure 4-2 shows that an on-demand electric air service will cost significantly less to operate than an equivalent helicopter service. The compound helicopter, the most expensive of the configurations in Figure 4-2, costs approximately \$55 per passenger for an overwater flight. For comparison, New York Helicopter quotes a price of \$1,900 per airport transfer, or \$875 per passenger for a 2-passenger trip [63]. These two prices cannot be directly compared, as the New York Helicopter quote includes costs neglected by the model (see Section 2.4.4). However, an order-of-magnitude cost reduction illustrates that on-demand aviation has the potential to supplant existing

services.

Vehicle weight and noise are not strongly affected by the mission assumptions. In particular, there is no difference between Options 2 and 3. However, the effect on cost per trip is much more significant. Flying a direct route results in substantial cost savings, even if the vehicle is sized to fly the overwater mission; this is mainly due to the reduced pilot and maintenance costs. Note that the noise level is somewhat lower during the revenue mission, as compared to the sizing mission. This is because fewer passengers are carried, resulting in a lighter aircraft.

New York City would be a difficult place to roll out an on-demand air service, because the primary restrictions on market size are particularly acute there. Vascik and Hansman [65] identified three primary constraints on on-demand aviation market size: availability of ground infrastructure, interaction with air traffic control, and community acceptance of aircraft noise. New York City has some of the highest real-estate prices in the world, so obtaining space for additional helipads, charging stations, and maintenance facilities would be very expensive; with three large international airports and numerous smaller ones in the area, the airspace ranks among the world's busiest (second only to London); and community opposition to noise is already a major issue for the city's helicopter tour operators [6]. On-demand aviation operators must take these factors into account.

4.2 Technological Assumptions by Time Frame

Uber includes economic forecasts in their white paper, for three different time frames: initial, near term, and long term. They show that costs are strongly affected by the technological assumptions associated with each time frame. In this section, further investigations into this phenomenon are carried out.

Input parameters for each time frame are given in Table 4.2. Vehicle cost per unit empty weight ranges from business-jet levels at the high end, to current general-aviation levels at the low end (see Table 2.4). Battery cost per unit energy capacity is assumed to drop in accordance with US Department of Energy projections [15]. Deadhead ratios are reduced and use of autonomy is increased as on-demand aviation becomes more acceptable to consumers and regulators respectively, while battery specific energy is assumed to improve somewhat as well.

Table 4.2: Input parameters for the different time frames.

Time frame	Initial	Near term	Long term
Vehicle autonomy enabled?	No	Yes	Yes
Battery specific energy	400 Wh/kg	450 Wh/kg	500 Wh/kg
Sizing mission type	Piloted	Piloted	Piloted
Revenue mission type	Piloted	Piloted	Autonomous
Deadhead mission type	Piloted	Autonomous	Autonomous
Deadhead ratio	0.5	0.35	0.2
Vehicle cost ratio	\$600 per lb	\$400 per lb	\$200 per lb
Battery cost ratio	\$400 per kWh	\$200 per kWh	\$100 per kWh

Figure 4-3 contains an overview of the results.

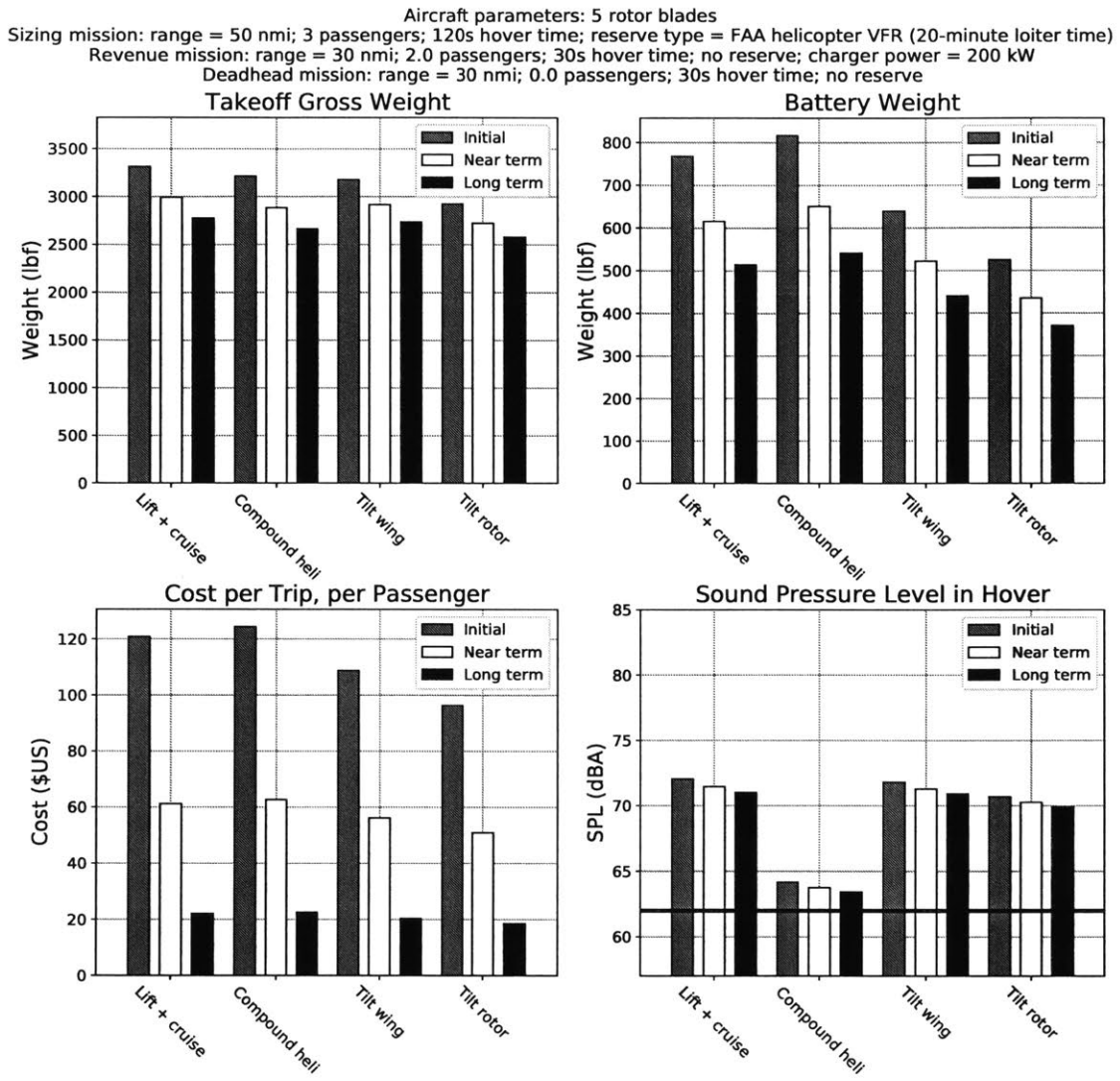


Figure 4-3: Time frame study results.

Figure 4-3 shows that vehicle weight and battery weight decrease in accordance with technological assumptions associated with each time frame. Cost per trip decreases even more dramatically: by a factor of 5-6 between Initial and Long Term, depending on configuration. Recall from Section 3.2 that the two main cost drivers are pilot salary and battery amortization. These costs are greatly reduced via vehicle automation and reduced battery manufacturing costs respectively.

However, the effect on noise is not nearly as large. Furthermore, even in the long term, no configuration is capable of meeting the Uber 62-dBA noise requirement.

Therefore, a substantial amount of engineering effort should be expended on reducing vehicle noise, since simply relying on technology improvements will not suffice.

A cost breakdown is shown in Figure 4-4.

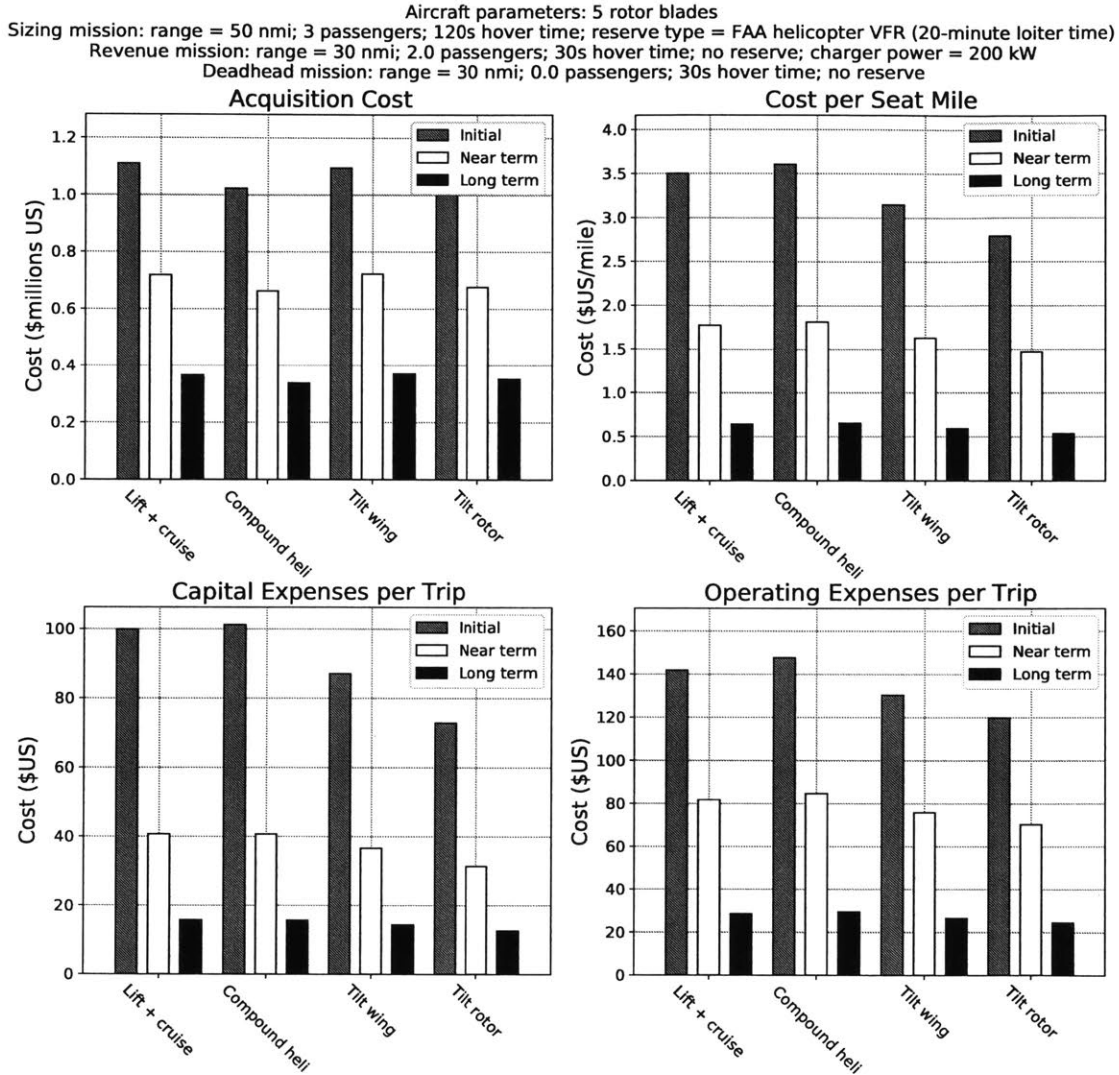


Figure 4-4: Cost breakdown from the time frame study. Capital and operating expenses are per trip; i.e. the effect of deadhead is included. Cost per seat mile is given in terms of statute miles.

Figure 4-4 shows that all costs decrease substantially depending on the time frame assumption. In the case of the compound helicopter (the most expensive configuration), cost per seat mile decreases from almost \$3.50 per mile initially, to as little as

\$0.60 per mile in the long term. For comparison, the average prices of UberX (car ridesharing, where the ride is paid for by one passenger) and UberPool (in which the ride is shared between multiple paying passengers) rides in the United States in 2016 were \$2.34 per mile and \$1.38 per mile respectively [15]. Recall again from Section 2.4.4 that a number of costs are neglected, so a direct comparison is not possible. However, it appears as if the proposed on-demand air service has the long-term potential to compete on price not just for expensive New York City airport transfers, but for everyday commutes as well.

4.3 Low-Noise Design

It is shown in Section 4.2 that while the costs of an on-demand air service decrease dramatically as technology improves, the same is not true for noise. The goal of this section is to identify and evaluate methods of reducing noise.

Five parameters were identified as having a significant impact on noise, without substantially affecting vehicle sizing: number of rotors, number of rotor blades, rotor solidity, blade thickness-to-chord ratio, and maximum mean lift coefficient. It was discovered during sensitivity analysis (Section 5.2.5) that number of rotors does not affect vehicle weight or cost, as long as disk loading is held constant. The goal of this case study is to investigate the design space formed by these five parameters, and try to determine combinations that reduce noise.

Three design categories were created. The first is the baseline, in which the same parameters from the configuration trade study (Section 3.2) are used. The second category is called Rotor Replacement. Here, the vehicle rotors are replaced with a different set, designed specifically for low noise. Only number of rotor blades and blade thickness-to-chord ratio are modified; rotor solidity is left unchanged. In the third category, called Aircraft Redesign, the entire vehicle is aggressively redesigned to reduce noise. All five identified parameters are modified.

The goal of the Rotor Replacement category is to design rotors that reduce noise, without affecting vehicle sizing. This requires a distinction to be drawn between the

compound helicopter and the other configurations. Recall from Section 3.2 that the compound helicopter has a vortex-noise peak frequency of around 300 Hz, below the value (600 Hz) at which the A-weighting response function is maximized. In this regime, reducing the peak frequency will decrease A-weighted sound pressure level. Towards this end, the number of blades was reduced from 5 to 3 (while holding solidity constant), and the rotor blade thickness-to-chord ratio was increased from 12% to 15%. Both changes have the effect of increasing the blade projected thickness, which in turn decreases the peak frequency (see Appendix D.2).

The three other configurations have peak frequencies well above 600 Hz. In this regime, Figure 2-4 shows that the opposite rule applies: increasing the peak frequency will decrease A-weighted sound pressure level. Therefore, the number of blades was increased from 5 to 7, and the rotor blade thickness-to-chord ratio was decreased to 10%. Both changes have the effect of decreasing the blade projected thickness, which in turn increases the peak frequency. Note that this selection of blade count results in a blade aspect ratio of 22.3, which is quite high for a helicopter [34]. The resulting rotors may suffer from structural issues.

In the Aircraft Redesign category, a more aggressive approach is employed. The number of rotors is increased for all configurations except the compound helicopter. Although this does not affect vehicle weight, cost, or unweighted sound pressure level, it results in smaller rotors with correspondingly lower projected thicknesses. This in turn increases peak frequency.

Rotor mean lift coefficient is increased for all configurations. This results in a small benefit to vehicle weight and cost, but a large benefit to unweighted sound pressure level due to reduced tip speed (see the discussion in Section 3.1). However, it requires accepting smaller control margins in hover.

Finally, rotor solidity is increased to 0.14 for all configurations except the compound helicopter. This has a small, beneficial effect on vehicle sizing and a significant, beneficial effect on unweighted sound pressure level. (see Equation 2.32). Blade aspect ratio is maintained at a more-reasonable value of 15.9. Rotor solidity for the compound helicopter is unchanged, resulting in a reduced blade aspect ratio (9.6).

Parameter selections are summarized in Table 4.3.

Table 4.3: Input parameters for the low-noise design study. While the Aircraft Redesign category uses all five parameter values, the Rotor Replacement category only uses the values for number of rotor blades and blade thickness-to-chord ratio. Number of rotors, rotor solidity, and maximum mean lift coefficient for Rotor Replacement are the same as those from the configurational trade study.

Configuration	N	B	s	$(t/c)_{blade}$	\bar{C}_l
Lift + cruise	12	7	0.14	0.1	1.2
Compound heli	1	3	0.1	0.15	1.0
Tilt wing	12	7	0.14	0.1	1.2
Tilt rotor	16	7	0.14	0.1	1.2

Figure 4-5 contains an overview of the results.

Aircraft parameters: battery energy density = 400 Wh/kg; autonomy enabled
Sizing mission (piloted): range = 50 nmi; 3 passengers; 120s hover time; reserve type = FAA helicopter VFR (20-minute loiter time)
Revenue mission (piloted): range = 30 nmi; 2.0 passengers; 30s hover time; no reserve; charger power = 200 kW
Deadhead mission (autonomous): range = 30 nmi; 0.0 passengers; 30s hover time; no reserve; deadhead ratio = 0.2

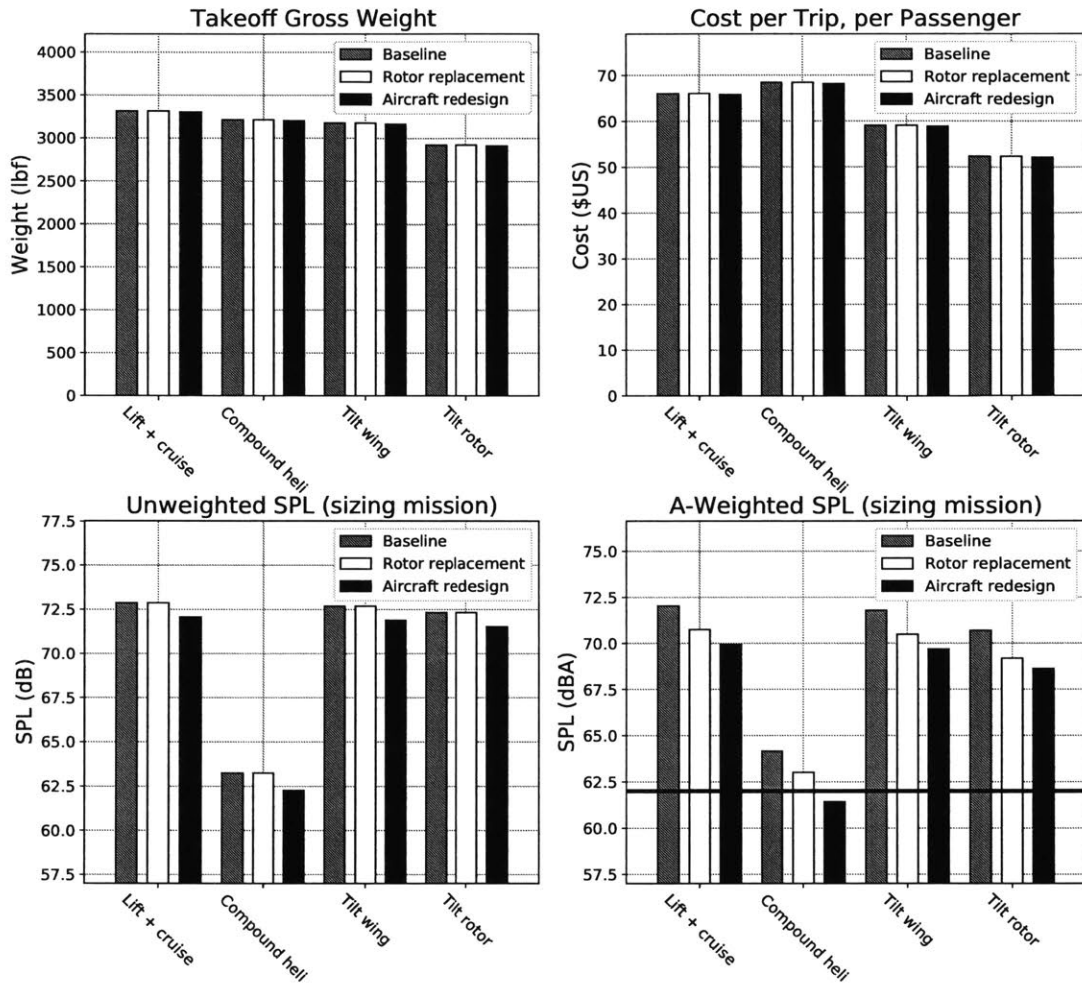


Figure 4-5: First set of results from the low-noise design study.

Figure 4-5 shows that the Rotor Replacement strategy does not affect vehicle weight, cost, or unweighted sound pressure level. However, A-weighted sound pressure level is reduced by about 1 dBA on average. Meanwhile, the Aircraft Redesign strategy has a tiny, beneficial effect on weight and cost, but a significant effect on both unweighted and A-weighted sound pressure level. Therefore, while some noise benefits can be obtained by replacing the rotors, redesigning the aircraft with noise as a primary concern results in significantly larger reductions in noise.

Additional data is shown in Figure 4-6.

Aircraft parameters: battery energy density = 400 Wh/kg; autonomy enabled
Sizing mission (piloted): range = 50 nmi; 3 passengers; 120s hover time; reserve type = FAA helicopter VFR (20-minute loiter time)
Revenue mission (piloted): range = 30 nmi; 2.0 passengers; 30s hover time; no reserve; charger power = 200 kW
Deadhead mission (autonomous): range = 30 nmi; 0.0 passengers; 30s hover time; no reserve; deadhead ratio = 0.2

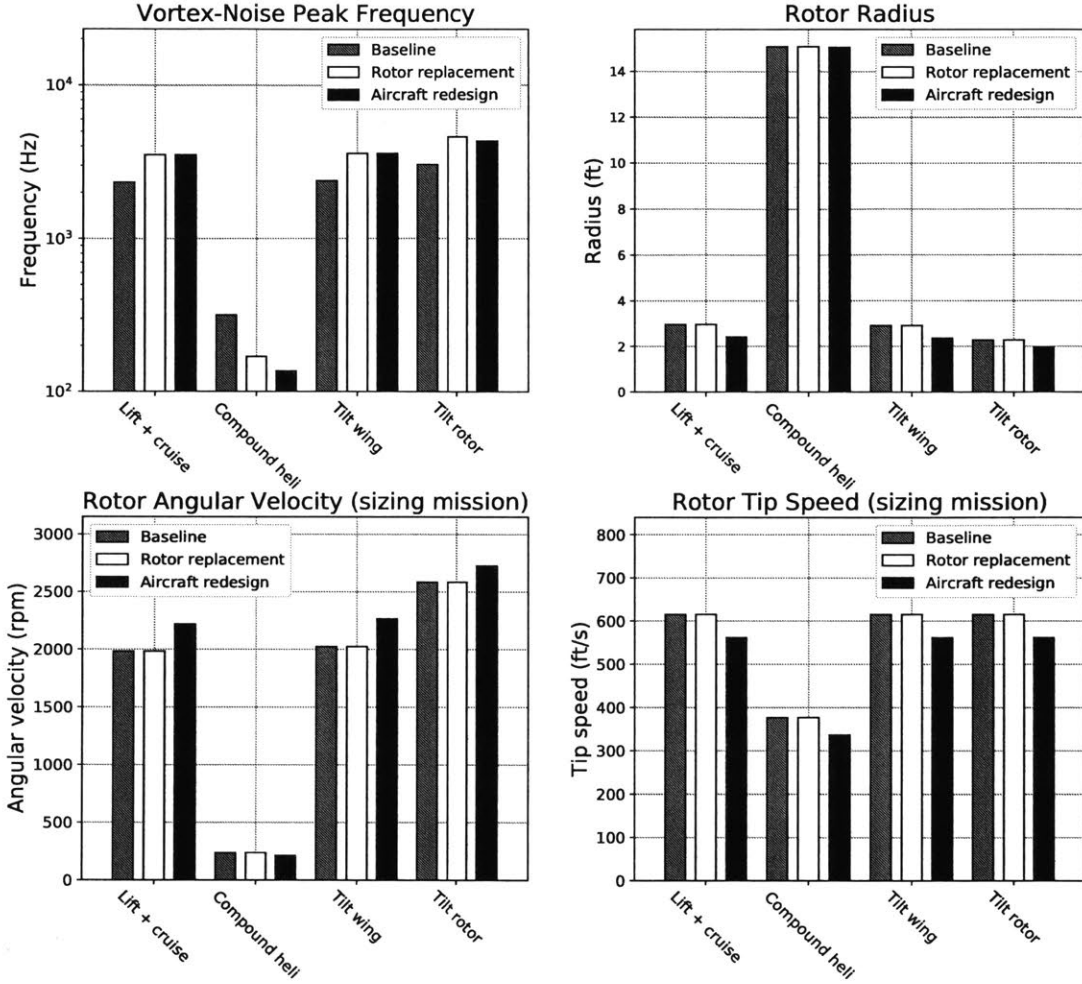


Figure 4-6: Second set of results from the low-noise design study.

Figure 4-6 shows that the Rotor Replacement strategy produced the intended effect: vortex-noise peak frequency decreased for the compound helicopter, but increased for all other configurations. This was achieved without affecting rotor radius or tip speed, indicating that rotor replacement works as a drop-in solution for noise reduction. The Aircraft Redesign strategy results in more substantial design changes.

Some design choices made as part of this design study may not be feasible. For example, a blade aspect ratio of 22.3 (used for the Rotor Replacement category) is very high for a helicopter. The feasibility of such a rotor must be verified using

structural analysis.

Increasing mean lift coefficient and increasing rotor solidity both result in significant noise reductions, but the upper limit on these parameters is at present unclear. Mean lift coefficient is expected to be constrained by control margins in hover; additional analysis is required to determine the mean lift coefficient above which reasonable control margins cannot be maintained. Similarly, solidity is limited by blade interference; an upper limit is required.

The only configuration that meets the 62-dBA noise requirement is the compound helicopter. This is only achievable with the Aircraft Redesign approach, and only if tail-rotor noise is neglected. Substantial engineering effort to reduce noise will therefore be required.

A number of ideas for reducing noise were not investigated in this work, including: ducted rotors; swept, pointed, and/or split rotor blade tips; serrated rotor blade edges; and asynchronous blade design (used on the MacBook Pro cooling fan [66]). In addition, a number of new methods of reducing rotor noise are enabled by Distributed Electric Propulsion. Reference [1] cites two examples: motor digital control synchronization, and asynchronous RPM. These techniques should be investigated as part of a more detailed study; they are discussed further in Chapter 6.

4.4 The Joby S4 Configuration Change

A case study on the S4 tilt rotor, currently under development by Joby Aviation, was conducted. This study was selected to illustrate the utility of the optimization tool, in that different vehicle configurations can be rapidly compared with only limited inputs. However, it also illustrates a key limitation: the sensitivity of the results to the required inputs.

In 2014, Joby Aviation published a conference paper presenting the conceptual design of the S2, a two-seat tilt-rotor with 12 lifting rotors [67]. An image of the S2 configuration presented in that paper is shown in Figure 3-1. However, in November 2016, a Joby engineer was quoted in *Vertiflite* discussing the S4, a four-seat tilt-rotor

with six, larger rotors [61]. A CFD image of the new configuration was released at the same time. The goal of this study is to determine the rationale behind the switch from 12 rotors to 6.

Sketches of the two different configurations are in Figure 4-7. They were generated using OpenVSP (Open Vehicle Sketch Pad) [68].

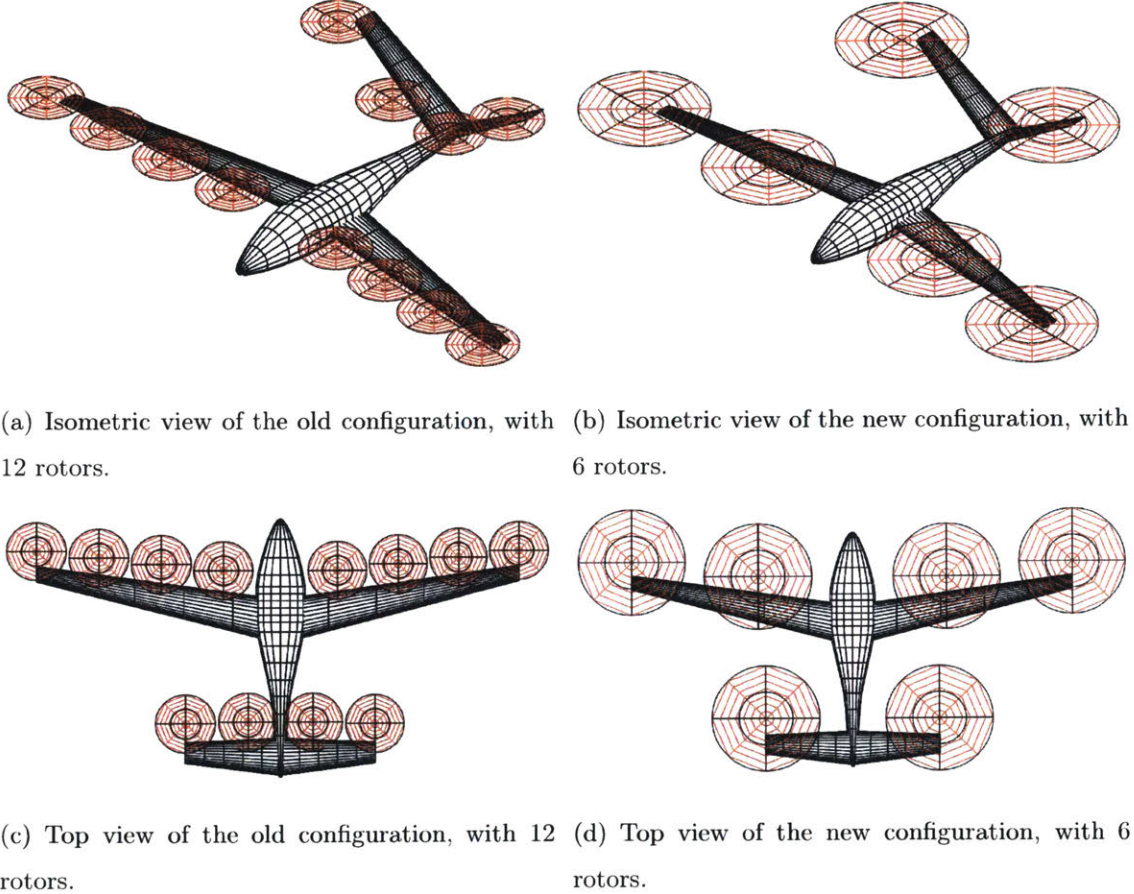


Figure 4-7: VSP sketches of the Joby S4.

One simple way to improve the Joby S2 design is to increase the rotor radius, decreasing the disk loading. As discussed in Section 3.2, lower disk loading means less power (and energy) required in hover. This shrinks the battery, leading to a sizing benefit across the board. However, as can be seen from Figure 4-7, increasing the rotor radius of the old S4 configuration would cause the rotor disks to overlap. This would at best lead to reduced efficiency and increased noise, and would be catastrophic if

the blades were to collide.

A better way of reducing the disk loading is to halve the number of rotors, and double the rotor radius. Since rotor disk area is proportional both to the number of rotors and the square of the rotor radius, this configuration change effectively decreases the disk loading by half. This is apparently what the Joby engineers did; this change is depicted in Figure 4-7.

A study was performed to determine the effect of this improvement on vehicle sizing. Most of the input parameters used were identical to those used in the other studies in this paper (Tables 3.2 and 3.3). However, a longer range was selected. In addition, some other parameters were changed to better reflect those given for the S2 in Reference [67]. Changed parameters are given in Table 4.4. The disk loading for the old configuration is the same as that given in Reference [67], but that of the new configuration is halved.

Table 4.4: Input parameters for the Joby S4 configuration study.

Configuration	Old	New
Number of rotors	12	6
Disk loading	16.3 lbf/ft ²	8.15 lbf/ft ²
Sizing mission range	100 nmi	100 nmi
Typical mission range	50 nmi	50 nmi
Deadhead mission range	50 nmi	50 nmi
Cruising speed	200 mph	200 mph

Results are in Figures 4-8 and 4-9.

Aircraft parameters: battery energy density = 400 Wh/kg; 5 rotor blades; autonomy enabled
Sizing mission (piloted): range = 100 nmi; 3 passengers; 120s hover time; reserve type = FAA helicopter VFR (20-minute loiter time)
Revenue mission (piloted): range = 50 nmi; 2.0 passengers; 30s hover time; no reserve; charger power = 200 kW
Deadhead mission (autonomous): range = 50 nmi; 0.0 passengers; 30s hover time; no reserve; deadhead ratio = 0.2

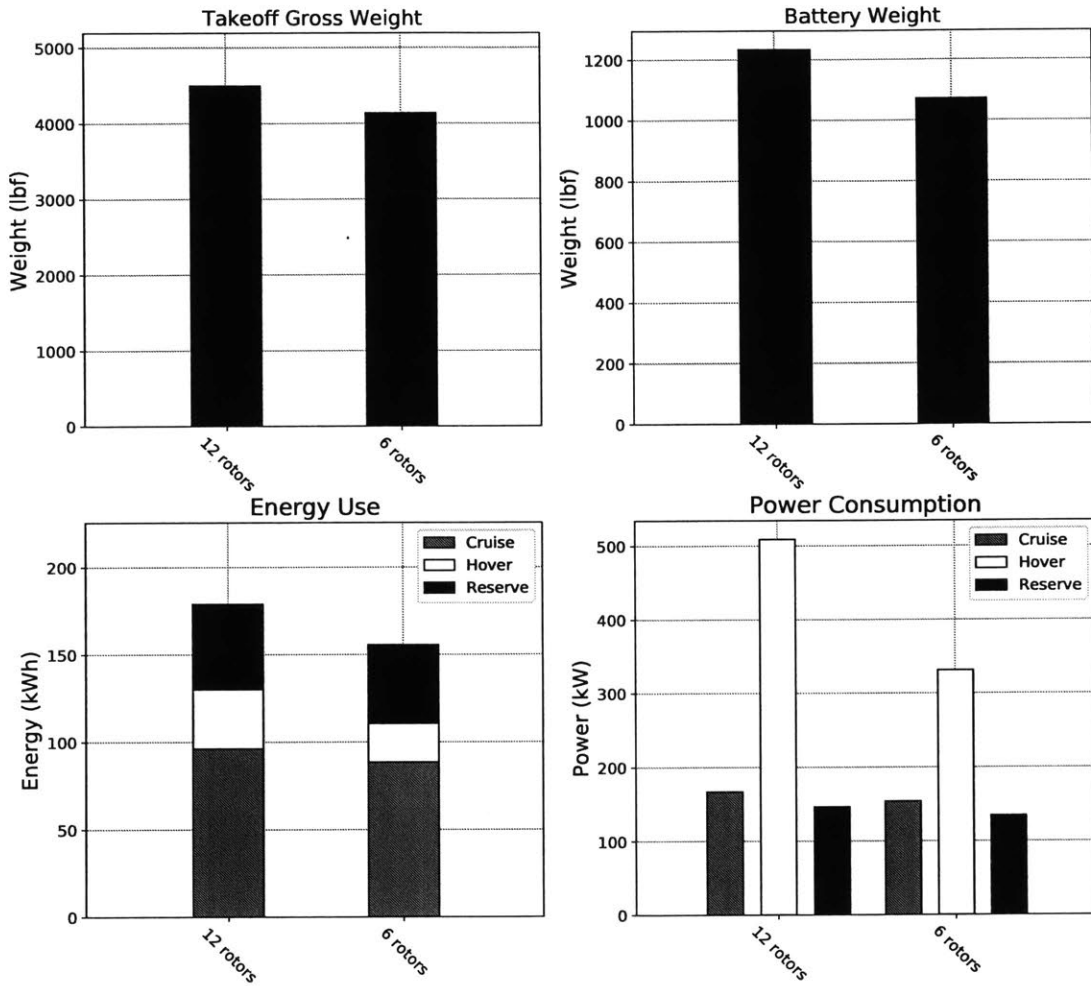


Figure 4-8: First set of results from the Joby S4 configuration study.

Figure 4-8 shows that the configuration change is beneficial in terms of weight and cost. However, the most significant benefit is in terms of noise, as shown in Figure 4-9: the new configuration benefits from an A-weighted sound pressure level that is approximately 5 dB lower than the old one.

Aircraft parameters: battery energy density = 400 Wh/kg; 5 rotor blades; autonomy enabled
Sizing mission (piloted): range = 100 nmi; 3 passengers; 120s hover time; reserve type = FAA helicopter VFR (20-minute loiter time)
Revenue mission (piloted): range = 50 nmi; 2.0 passengers; 30s hover time; no reserve; charger power = 200 kW
Deadhead mission (autonomous): range = 50 nmi; 0.0 passengers; 30s hover time; no reserve; deadhead ratio = 0.2

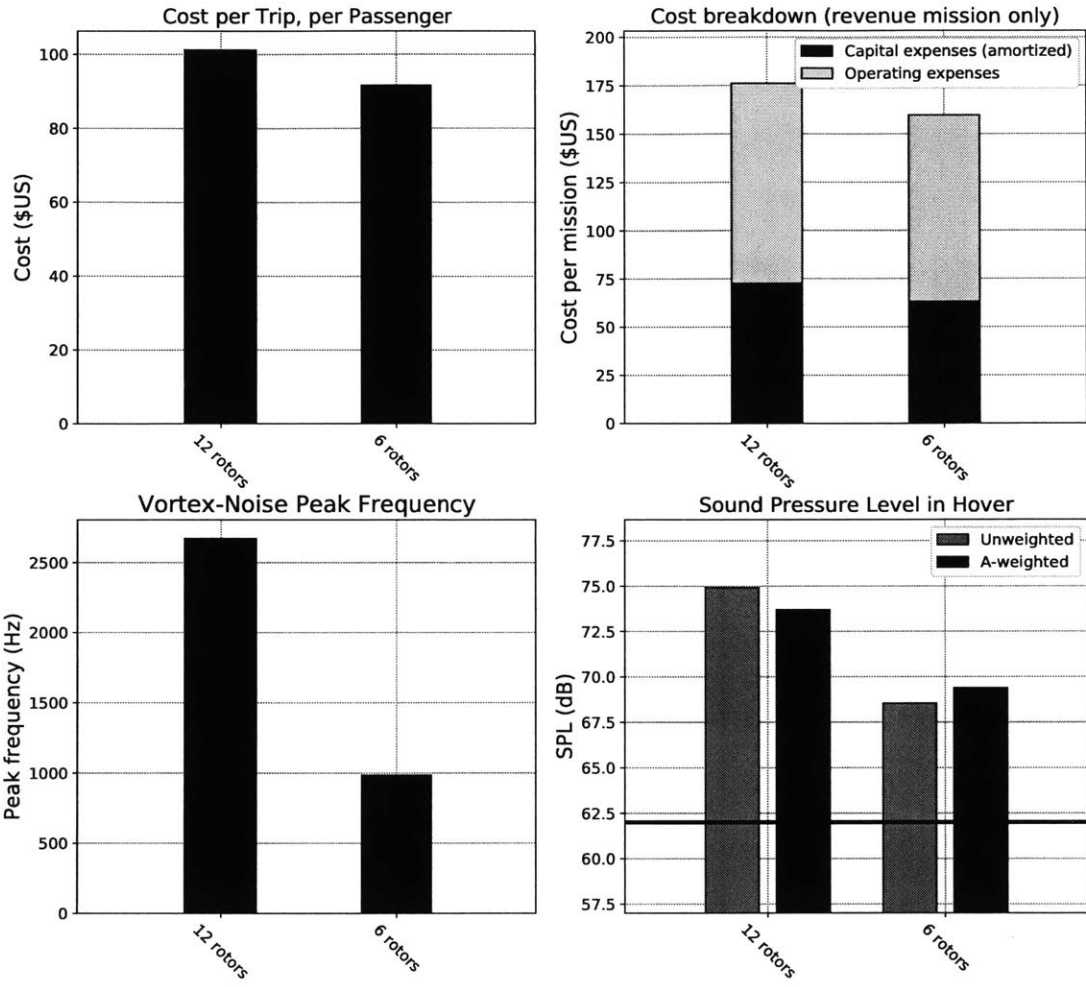


Figure 4-9: Second set of results from the Joby S4 configuration study.

The new configuration is not without drawbacks. The rotors, and by extension, the motors, are larger; this may result in cooling issues in hover. Also, control in hover with one rotor inoperative may also be more of an issue.

This case study exemplifies both the strengths and the weaknesses of the optimization tool. Comparisons between configurations with known input parameters (cruising speed, cruise lift-to-drag ratio, hover disk loading, rotor mean lift coefficient, etc.) can easily be made. However, accurate values for these parameters are essential to achieve meaningful results.

4.5 Sizing Plot

Recall from Section 3.2 that the compound helicopter is the most expensive configuration, but it is also the quietest. Table 3.3 shows that this configuration has the lowest cruise lift-to-drag ratio, but also the lowest disk loading. Therefore, a tradeoff between cruise and hover efficiency is hypothesized, depending on whether low cost or low noise is the priority. One way of illustrating this is with a carpet plot (hereafter called a sizing plot), in which optimized cost per trip and sound pressure level are plotted as a function of cruise lift-to-drag ratio and hover disk loading. In particular, the importance of hover disk loading was illustrated in Section 4.4.

An example sizing plot is shown in Figure 4-10. Three configurations from Table 3.3, as well as two configurations from the aforementioned Boeing eVTOL study [51], are also shown. The Boeing lift + cruise configuration assumes a cruise lift-to-drag ratio of 9.1 and a disk loading of 7.3 lbf/ft²; the Boeing tilt rotor assumes a cruise lift-to-drag ratio of 11.0 and a disk loading of 12.8 lbf/ft². These values were obtained from Reference [51]. Aside from these two parameters, all other assumptions are consistent with those previously described for the lift + cruise configuration.

Aircraft parameters: empty weight fraction = 0.53; battery energy density = 400 Wh/kg; cruising speed = 150 mph
8 rotors; 5 rotor blades; mean lift coefficient = 1.0; autonomy enabled. Lift + cruise configuration.
Sizing mission (piloted): range = 50 nmi; 3 passengers; 120s hover time; reserve type = FAA helicopter VFR (20-minute loiter)
Revenue mission (piloted): range = 30 nmi; 2.0 passengers; 30s hover time; no reserve; charger power = 200 kW
Deadhead mission (autonomous): range = 30 nmi; 0.0 passengers; 30s hover time; no reserve; deadhead ratio = 0.2

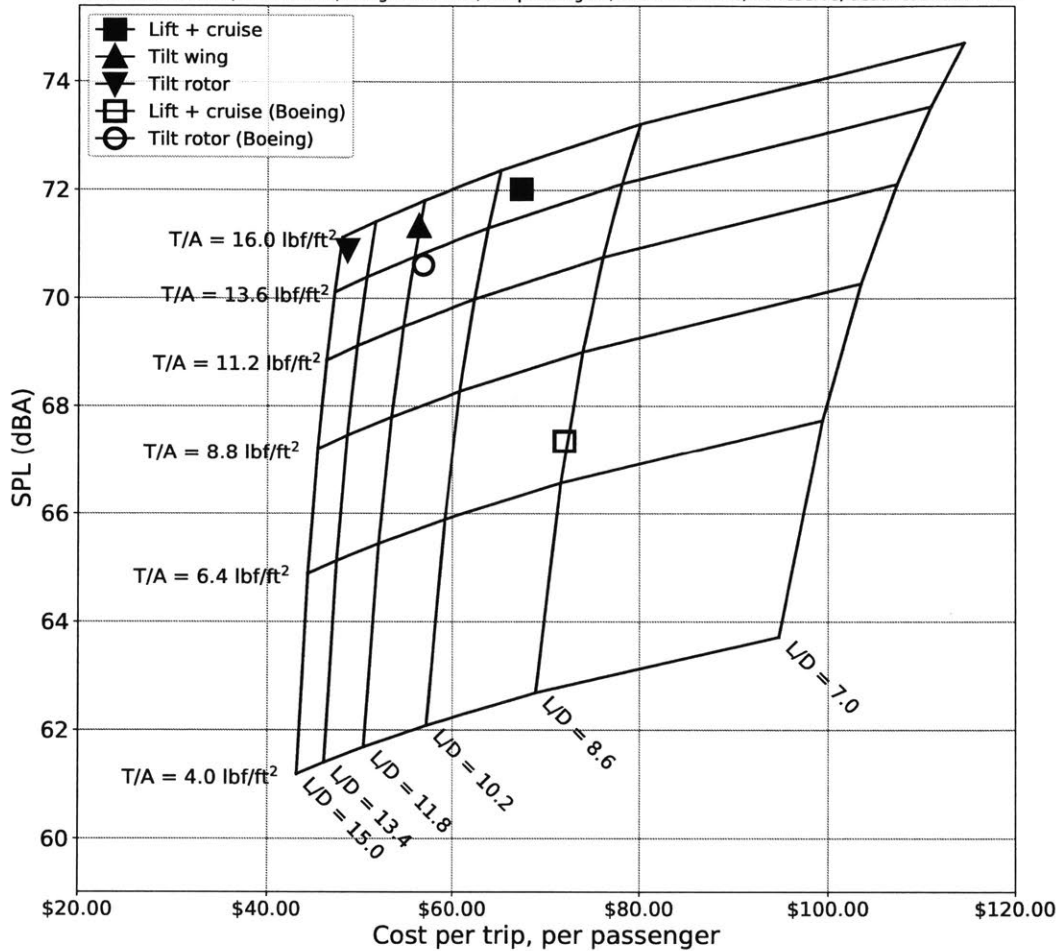


Figure 4-10: Sizing plot for the lift + cruise configuration. An intersection between any two lines on the plot represents an optimized vehicle design, for that combination of cruise lift-to-drag ratio and hover disk loading.

Figure 4-10 shows that cost primarily depends on cruise lift-to-drag ratio; it is relatively insensitive to hover disk loading. However, the opposite is true for noise, implying that vehicle configuration selection may be driven by whether cost or noise is a primary requirement. As an example, take the tilt rotor and the Boeing lift + cruise configuration. The tilt rotor has a higher lift-to-drag ratio (14 vs. 9.1), which translates to lower power and energy requirements in cruise. This makes the tilt rotor

significantly less expensive. However, the tilt rotor has a much higher disk loading (15 vs. 7.3 lbf/ft²), resulting in greater noise.

The sizing plot is limited in the sense that it technically only applies to one configuration. While lift-to-drag ratio and disk loading can be varied, other inputs must be held constant. For example, the compound helicopter is not shown, because it has a lower empty weight fraction (Table 3.3) and greater power requirements due to its tail rotor (Table 3.4). The sizing plot is therefore better suited to making trades between similar configurations than to compare helicopters with winged vehicles. However, it does provide a simple yet powerful view of the eVTOL design space.

4.6 Boeing Study Comparison

In this section, the results from the GP optimization tool are compared in more detail with those of the Boeing eVTOL study [51]. Instead of assuming values for empty weight fraction, cruise lift-to-drag ratio, and hover disk loading, the Boeing study computed these parameters as part of the optimization process. For example, empty weight was based on configuration-specific composite structural models, subject to bending stress and minimum-gauge constraints. Also, configuration-specific aerodynamic modeling, including blade-element momentum theory and equivalent skin-friction drag estimation for hover and cruise performance respectively, was employed.

Three different eVTOL configurations were analyzed: a (conventional) helicopter, a stopped rotor (lift + cruise), and a tilt rotor. Key parameters from the Boeing study were used as inputs to the GP tool developed in this research. Parameters whose values differ from those given earlier in this study (Chapters 2 and 3) are listed in Tables 4.5 and 4.6.

The Boeing study assumed that the vehicle could dip into the 20% battery reserve during the reserve mission segment in the sizing mission, but nowhere else. To account for this, the GP battery usable energy fraction was increased to 1. It was verified manually that the 20% battery reserve was not used anywhere but during the reserve

segment. Also, the sizing-mission range was increased to 87 nmi (100 miles) with 3 passengers and 1 pilot, all weighing 200 lbf each (800 lbf total). The 20-minute reserve requirement was retained.

Table 4.5: Generic Boeing study input parameters.

Parameter	Value
Battery usable energy fraction	1
Pilot weight	200 lbf
Sizing mission range	87 nmi

Cruise lift-to-drag ratios are given in [51] for the lift + cruise and tilt rotor configurations, but not for the helicopter. However, lift-to-drag ratio can be estimated by differentiating Equation 2.7 with respect to time, then rearranging:

$$\frac{L}{D} = \frac{VW}{\eta P_{cruise}} \quad (4.1)$$

Modifying Equation 4.1 to account for power consumed by the tail rotor results in Equation 4.2:

$$\frac{L}{D} = \frac{1 + \chi_{cruise}}{\eta} \frac{VW}{P_{cruise}} \quad (4.2)$$

χ_{cruise} is the tail-rotor power fraction: tail-rotor power divided by main-rotor power (in cruise).

Using Equation 4.2; power, velocity, and weight estimates from the Boeing study; an estimate of $\chi_{cruise} = 0.08$ from the included mission-profile power plots; and an efficiency of $\eta = 0.85 \times 0.9$ (product of cruise and propulsive efficiency), the helicopter cruise lift-to-drag ratio was estimated as 7.84. This is significantly higher than the value in Table 3.3. $\chi_{hover} = 0.10$ for the helicopter was estimated in a similar manner to χ_{cruise} .

An additional modification concerns rotor solidity. Values for rotor tip speed and disk loading are given in the Boeing study. Assuming sea-level atmospheric conditions, thrust coefficients of 0.0229 and 0.0466 were obtained for the lift + cruise

and tilt rotor respectively. Since the Boeing study states that the mean lift coefficients of these two configurations are equal, Equation 2.17 can be rearranged to produce Equation 4.3:

$$\frac{s_{\text{tilt rotor}}}{s_{\text{lift + cruise}}} = \frac{C_{T_{\text{tilt rotor}}}}{C_{T_{\text{lift + cruise}}}} \quad (4.3)$$

Equation 4.3 implies that the solidity of the tilt rotor must be more than twice that of the lift + cruise configuration. This adjustment was implemented, resulting in the solidity values in Table 4.6: 0.1 and 0.203 for the lift + cruise and tilt rotor respectively. Typical helicopter rotor solidities range from 0.06 to 0.12, although values as high as 0.23 are encountered in Reference [36]. Also, it should be noted that the tilt rotor uses identical rotors for hover and cruise, to reduce maintenance costs.

Table 4.6: Configuration-specific Boeing study inputs.

Configuration	Lift + cruise	Tilt rotor	Helicopter
V_{cruise} (mph)	150	150	150
$(\frac{L}{D})_{\text{cruise}}$	9.1	11.0	7.84
$\frac{T}{A} \left(\frac{\text{lbf}}{\text{ft}^2} \right)$	7.3	12.8	4.1
Empty weight fraction	0.53	0.55	0.43
χ_{cruise}	0	0	0.08
χ_{hover}	0	0	0.10
Number of hover rotors	8	8	1
Rotor solidity	0.1	0.203	0.1

One of the most significant disadvantages of using a constant empty weight fraction is that the effect of motor weight on vehicle sizing is not modeled. As discussed in Section 3.1, the GP optimizer tends to select the lowest rotor tip speed possible, subject to a constraint on blade mean lift coefficient.

A different behavior is expected if a motor weight model is included. Since motor weight is approximately proportional to torque [69] and rotor power is the product of torque and angular velocity ($P = Q\omega$), the optimizer may choose to use higher rotor

angular velocities (and by extension, rotor tip speeds). This would reduce torque (and by extension, motor weight), but would also increase vehicle noise.

In order to estimate the effect of this omission, two cases were prepared. One uses an unmodified form of the GP optimization tool; while the other constrains the rotor angular velocity to a value equal to that from the Boeing study. To first order, this constraint should remove the effect of motor weight on vehicle sizing, allowing for a fairer comparison with data from the Boeing study. In the case of the tilt-rotor, this results in a reduction of rotor tip speed, and so the rotor mean lift coefficient constraint was increased to compensate.

Results are shown in Figure 4-11; data from the Boeing study is included for comparison.

Aircraft parameters: battery energy density = 400 Wh/kg; 5 rotor blades; autonomy enabled
Sizing mission (piloted): range = 87 nmi; 3 passengers; 120s hover time; reserve type = FAA helicopter VFR (20-minute loiter time)
Revenue mission (piloted): range = 30 nmi; 2.0 passengers; 30s hover time; no reserve; charger power = 200 kW
Deadhead mission (autonomous): range = 30 nmi; 0.0 passengers; 30s hover time; no reserve; deadhead ratio = 0.2

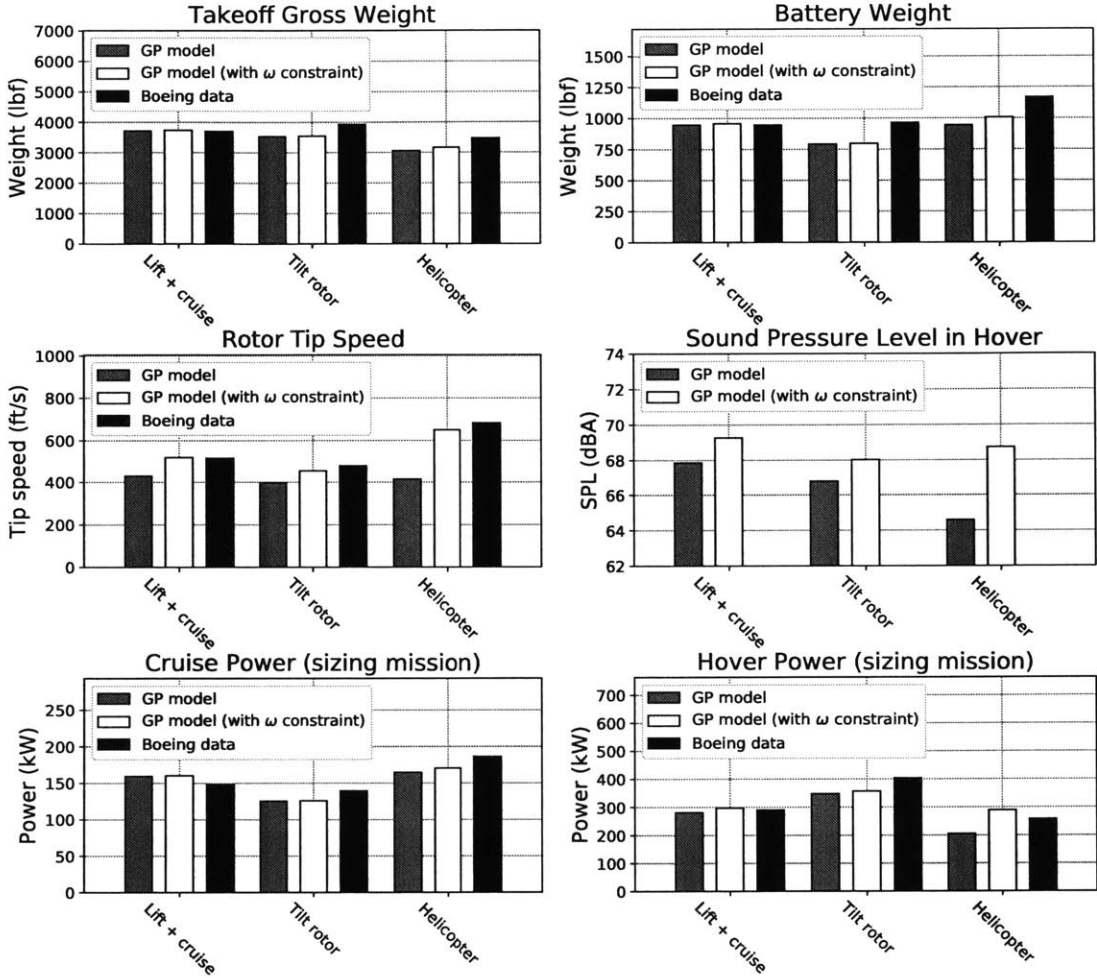


Figure 4-11: Comparison with the Boeing study.

Figure 4-11 shows that in general, the takeoff gross weights from the GP are reasonably close to those from the Boeing study. If the ω constraint is used, all weights are within 10%. This is also shown in Table 4.7.

Table 4.7: Takeoff gross weight percentages differences, relative to those from the Boeing study.

Configuration	No ω constraint	ω constraint
Lift + cruise	0.2%	0.8%
Tilt rotor	-10.0%	-9.6%
Helicopter	-11.7%	-8.6%

The effect on noise is more significant, especially for the helicopter. Figure 4-11 shows that adding the ω constraint results in noise increases of 1.4 dBA, 1.2 dBA, and 4.1 dBA for the lift + cruise, tilt rotor and helicopter respectively. Therefore, the effect of motor weight is non-negligible for the purpose of noise analysis.

One potential way of mitigating the effect of motor weight would be to add a gearbox to the hover motors. Adding a gearbox would reduce the rotor angular velocity, leading to lower rotor tip speeds (and by extension, lower noise). It would also reduce the torque requirements on the motors, allowing them to be lighter. For this reason, the Boeing helicopter uses a gear reduction system on its main rotor [51]. However, gearbox weight is expected to scale with gear ratio, potentially mitigating the motor weight savings; a gearbox would also increase maintenance cost and reduce reliability. This should be considered as part of a more detailed trade study.

It can be concluded from this section that weight estimates from the GP optimization tool compare reasonable with those generated using higher-fidelity methods. However, the effect of motor weight on noise is significant, and should be modeled as part of a more detailed design study.

Chapter 5

Sensitivity Studies

In this section, the sensitivity of the optimized designs to various design requirements and vehicle parameters is explored. Each point on each plot represents an optimized design.

5.1 Design Requirements

5.1.1 Mission Range

A sweep was conducted to determine the importance of mission range. The same range requirement is used for the sizing, revenue, and deadhead missions. Results are shown in Figure 5-1.

Aircraft parameters: battery energy density = 400 Wh/kg; 5 rotor blades; autonomy enabled
Sizing mission (piloted): 3 passengers; 120s hover time; reserve type = FAA helicopter VFR (20-minute loiter time)
Revenue mission (piloted): same range as sizing mission; 2.0 passengers; 30s hover time; no reserve; charger power = 200 kW
Deadhead mission (autonomous): same range as sizing mission; 0.0 passengers; 30s hover time; no reserve; deadhead ratio = 0.2

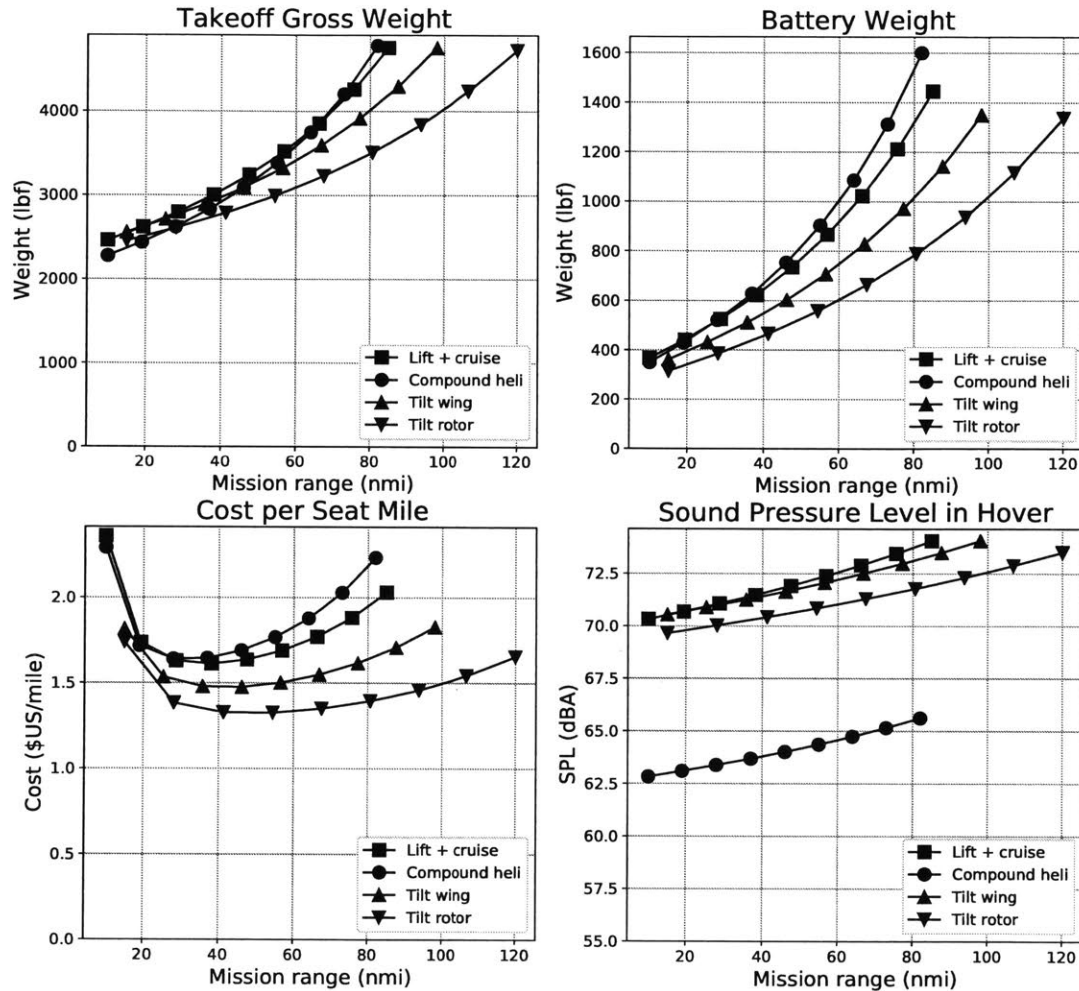


Figure 5-1: Sensitivity to mission range. Cost per seat mile is plotted instead of cost per passenger.

Figure 5-1 shows that some configurations are more sensitive to mission range than others. The defining parameter input appears to be the cruise lift-to-drag ratio. The compound helicopter ($\frac{L}{D} = 9$, the lowest value) weighs and costs the most at longer ranges, while the tilt rotor ($\frac{L}{D} = 14$, the highest value) weighs and costs the least. Cost per seat mile is minimized at a mission range of about 30 nmi. On-demand aviation is at its most cost-competitive at this range; it may therefore be wise to use 30 nmi as a design requirement.

Beyond 30 nmi, the cost per seat mile of all configurations increases steadily. At these ranges, the size and weight of the battery makes up an increasingly large share of the costs. Therefore, hybrid-electric propulsion may be more useful at ranges beyond about 80-100 nmi. A hybrid-electric aircraft would be able to fly shorter missions on electric power alone, taking advantage of the cost and environmental benefits of electric propulsion. However, the ability to fly missions beyond 100 nmi would be retained, albeit with greater operational costs. A similar concept is developed in Reference [69]: a series of fixed-wing hybrid-electric aircraft, designed for thin-haul air travel (100-400 nmi) rather than urban air mobility.

5.1.2 Number of Passengers

On-demand vehicle concepts produced by different companies vary in terms of number of passengers. For example, the A³ Vahana carries one passenger and no pilot [54]. Meanwhile, the Uber white paper assumes a vehicle with four seats. If the vehicle is piloted, then three seats are available for passengers; all four seats can be occupied by passengers if the vehicle is autonomous [15].

A sweep was conducted to determine the importance of number of passengers carried on the sizing mission. The load factor was set to 2/3; i.e. the number of passengers carried on the typical mission was set equal to 2/3 times the number of passengers carried on the sizing mission. Results are shown in Figure 5-2.

Aircraft parameters: battery energy density = 400 Wh/kg; 5 rotor blades; autonomy enabled
Sizing mission (piloted): range = 50 nmi; 120s hover time; reserve type = FAA helicopter VFR (20-minute loiter time)
Revenue mission (piloted): range = 30 nmi; load factor = 0.67; 30s hover time; no reserve; charger power = 200 kW
Deadhead mission (autonomous): range = 30 nmi; 0.0 passengers; 30s hover time; no reserve; deadhead ratio = 0.2

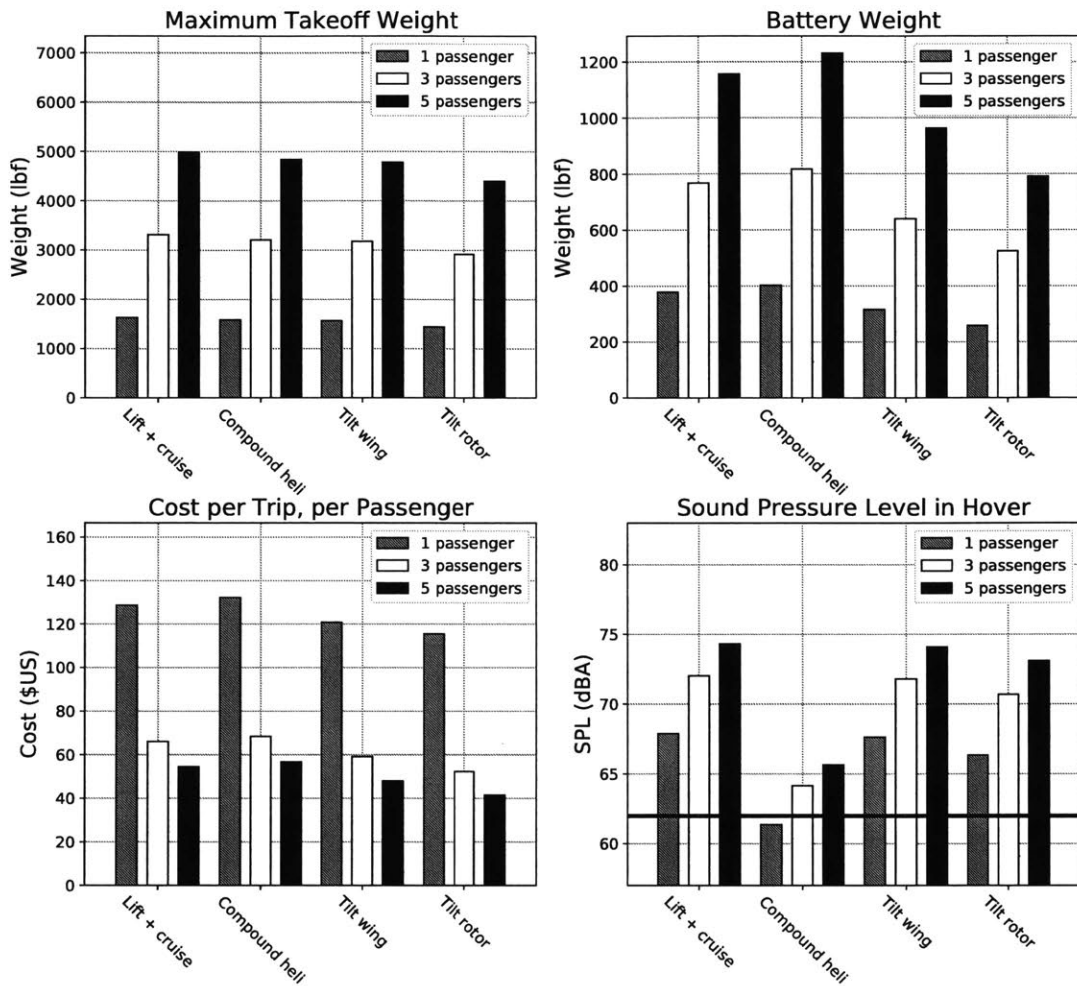


Figure 5-2: Sensitivity to number of passengers carried on the sizing mission.

Figure 5-2 shows that weight and noise increase significantly with number of passengers. Cost per trip decreases, although diminishing returns are encountered beyond 3 passengers. Therefore, although 3 passengers seems reasonable, a decision on number of passengers must consider both cost and noise.

5.1.3 Reserve Requirement

On-demand aircraft companies are faced with a choice: should they certify their aircraft as airplanes or as helicopters? The FAA definitions are as follows [37]: “[airplane] means [a] fixed-wing aircraft...that is supported in flight by the dynamic reaction of the air against its wings”, while “[helicopter] means [an] aircraft that depends principally for its support in flight on the lift generated by one or more rotors.” For configurations with wings as well as rotors, either definition applies, and so a choice must be made.

From a certification perspective, the most important difference is in the reserve requirement: 30 minutes for airplanes vs. 20 minutes for helicopters. A study was conducted to determine the importance of this requirement. A 2-nmi diversion requirement was also included, in case a special regulatory class is created for eVTOL aircraft (this was discussed in Section 2.3). Results are in Figure 5-3.

Aircraft parameters: battery energy density = 400 Wh/kg; 5 rotor blades; autonomy enabled
Sizing mission (piloted): range = 50 nmi; 3 passengers; 120s hover time
Revenue mission (piloted): range = 30 nmi; 2.0 passengers; 30s hover time; no reserve; charger power = 200 kW
Deadhead mission (autonomous): range = 30 nmi; 0.0 passengers; 30s hover time; no reserve; deadhead ratio = 0.2

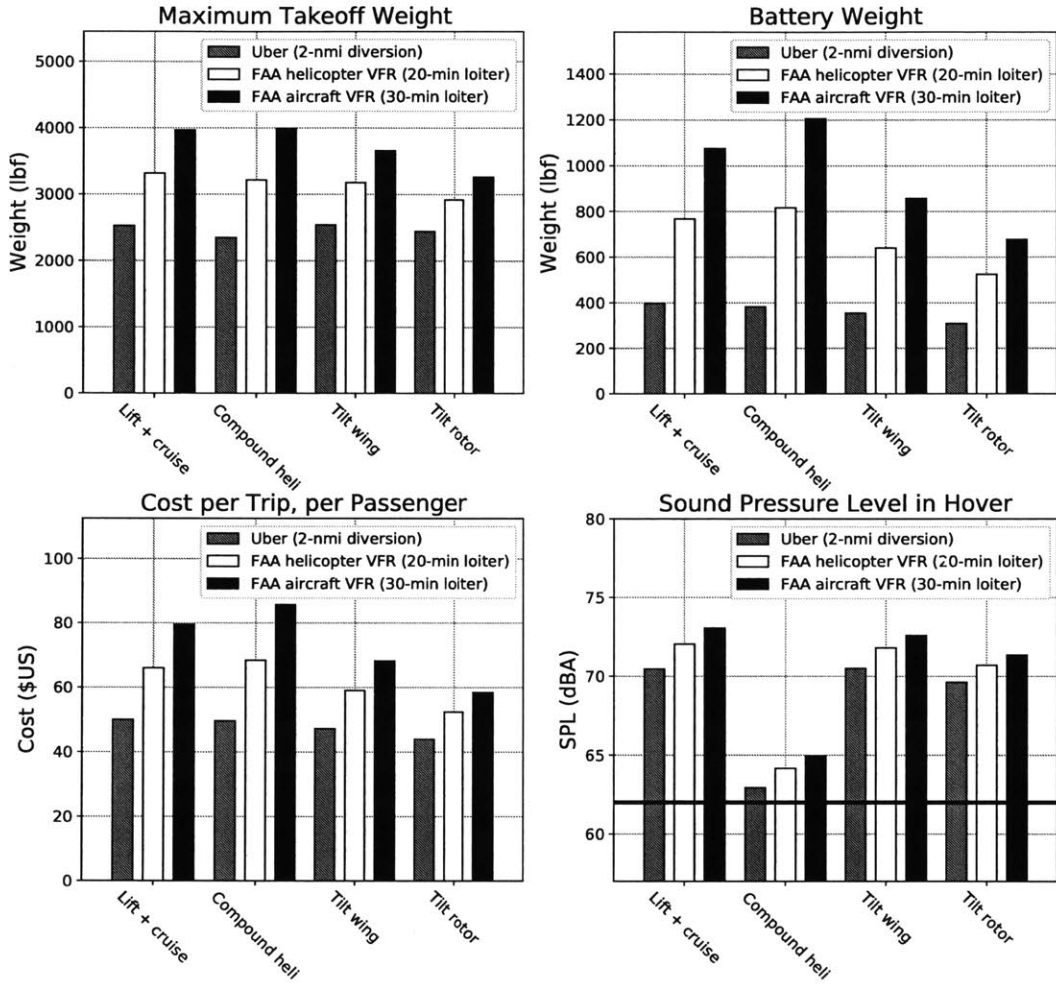


Figure 5-3: Sensitivity to reserve requirement.

Figure 5-3 shows that the reserve requirement is critical. Vehicle weight, cost, and noise are all strongly affected. It seems at first glance that the logical choice is the helicopter requirement. This choice takes advantage of the existing certification framework, while providing a sizing benefit relative to the aircraft requirement. However, helicopter pilots are in short supply relative to aircraft pilots. In 2016, approximately 96,000 pilots held commercial ratings in the US; an additional 158,000 pilots held airline ratings [70]. By contrast, only 16,000 pilots held rotorcraft ratings. Barring full vehicle autonomy (impossible under current regulations), a pilot shortage

would seriously impair the widespread adoption of on-demand aviation. Therefore, unless the regulations are changed, the choice of certification pathway should be carefully considered.

5.1.4 Time in Hover

A sweep was conducted to determine the importance of the hover requirement for the sizing mission. The hover requirements for the revenue and deadhead missions were left unchanged. Results are shown in Figure 5-4.

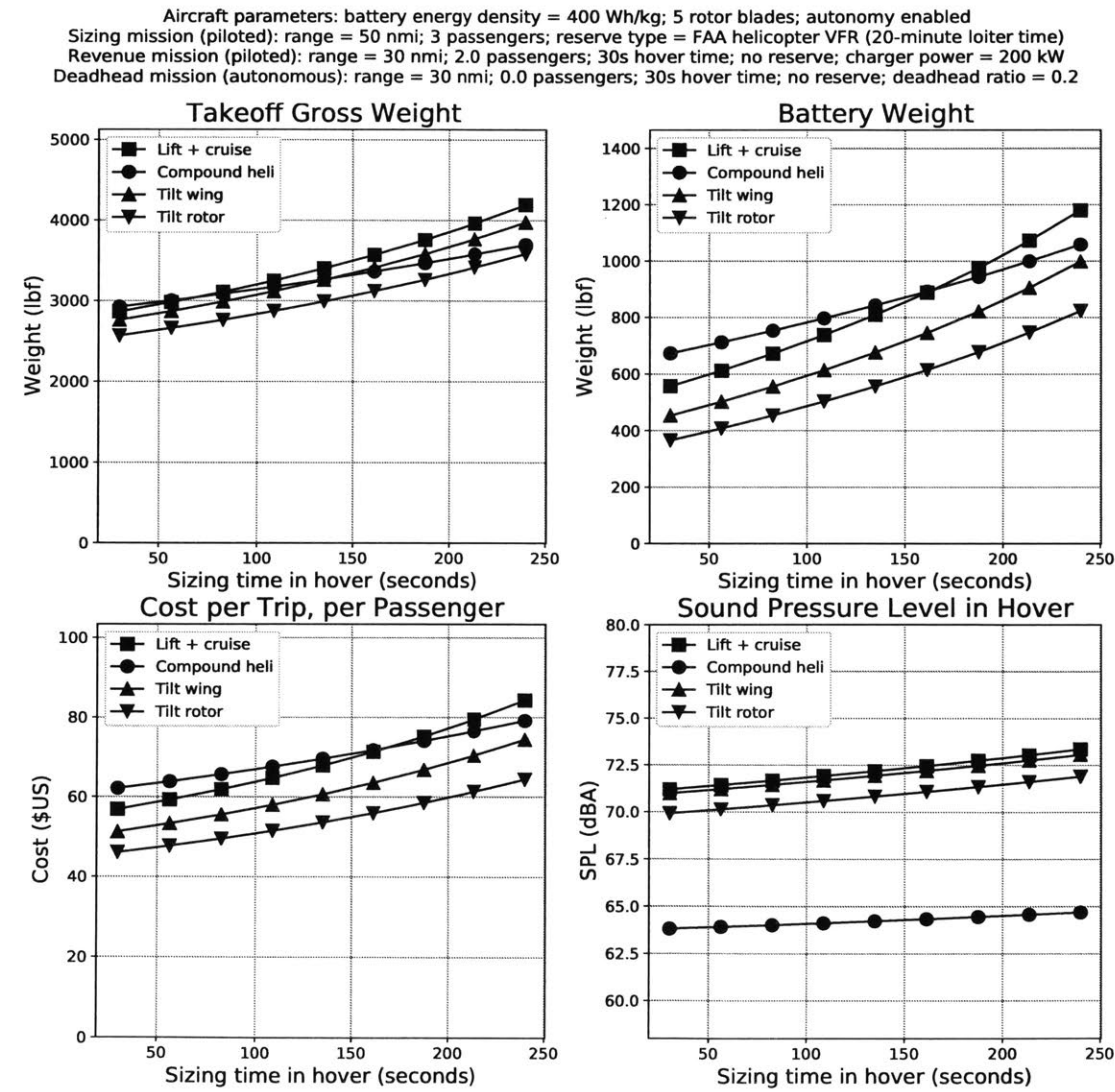


Figure 5-4: Sensitivity to time in hover (sizing mission).

Figure 5-4 reveals that all configurations are sensitive to the hover time requirement. The lift + cruise configuration is most sensitive. Also, crossover is encountered. The tilt wing is superior to the compound helicopter on weight and cost for low hover time values, but becomes inferior at high values. This indicates that time in hover is a critically important requirement.

5.2 Vehicle Parameters

5.2.1 Battery Energy Density

As discussed in Section 1.1.5, one of the principal hypothesized disadvantages of electric propulsion (as compared to hydrocarbon-based propulsion) is energy density. The selected battery energy density used throughout this study (400 Wh/kg) is about twice as high as the best batteries currently available. Therefore, understanding of the sensitivity to this parameter is critical.

There are two different definitions of battery energy density of interest to vehicle designers. The first is cell-level energy density. This is the amount of electrical energy that a given cell can store per unit weight, and is the usual metric given by battery manufacturers.

However, batteries installed in aircraft must include additional weight, to protect from battery fires. In the event of a short-circuit in one cell, the resulting thermal runaway must not propagate to other cells; otherwise, the battery pack would catch fire and be destroyed. This issue was identified and solved as part of the X-57 Maxwell design process [71]. Pack-level energy density accounts for the weight of the thermal protection system as well as the weight of controllers; it is therefore lower than cell-level specific energy. Pack-level energy density is the relevant metric for vehicle optimization tools. As such, any reference to battery energy density in this thesis refers to pack-level energy density, unless otherwise stated.

A sweep was conducted to determine the importance of battery energy density. Results are shown in Figure 5-5.

Aircraft parameters: 5 rotor blades; autonomy enabled
Sizing mission (piloted): range = 50 nmi; 3 passengers; 120s hover time; reserve type = FAA helicopter VFR (20-minute loiter time)
Revenue mission (piloted): range = 30 nmi; 2.0 passengers; 30s hover time; no reserve; charger power = 200 kW
Deadhead mission (autonomous): range = 30 nmi; 0.0 passengers; 30s hover time; no reserve; deadhead ratio = 0.2

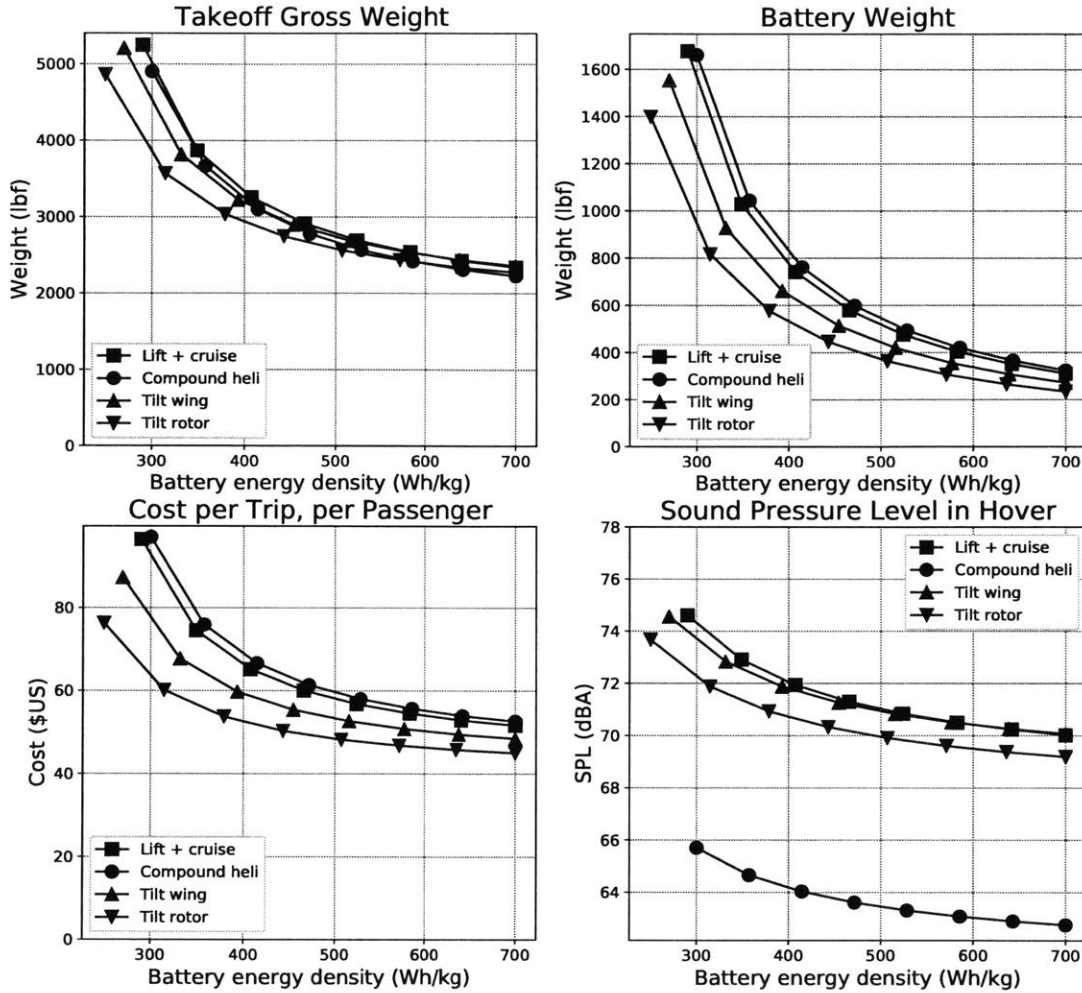


Figure 5-5: Sensitivity to battery energy density.

Figure 5-5 shows that all four configurations are quite sensitive to battery energy density below around 400 Wh/kg, but less so above this point. Similar results have been obtained for other types of electric aircraft; ex. see Reference [1]. A battery energy density of 400 Wh/kg can therefore be seen as a critical enabling value for on-demand aviation. In addition, the United States Department of Energy (DOE) is funding research with a goal of 500 Wh/kg by 2021 [72]. This explains why 400 Wh/kg was used for this study, even though it is significantly better than what current batteries can achieve.

The battery model used in this research only includes specific energy and power; a number of effects are neglected. Firstly, the higher the specific energy of a battery, the lower its specific power. This is known as the Ragone relation [73]. Secondly, only battery power and energy are modeled; current and voltage are not included. In practice, the effective energy capacity of a battery depends on the rate of current draw; this phenomenon is known as the Peukert effect [74]. These effects should be investigated as part of a more detailed study.

5.2.2 Empty Weight Fraction

A sweep was conducted to determine the importance of empty weight fraction. Results are shown in Figure 5-6.

Aircraft parameters: battery energy density = 400 Wh/kg; 5 rotor blades; autonomy enabled
 Sizing mission (piloted): range = 50 nmi; 3 passengers; 120s hover time; reserve type = FAA helicopter VFR (20-minute loiter time)
 Revenue mission (piloted): range = 30 nmi; 2.0 passengers; 30s hover time; no reserve; charger power = 200 kW
 Deadhead mission (autonomous): range = 30 nmi; 0.0 passengers; 30s hover time; no reserve; deadhead ratio = 0.2

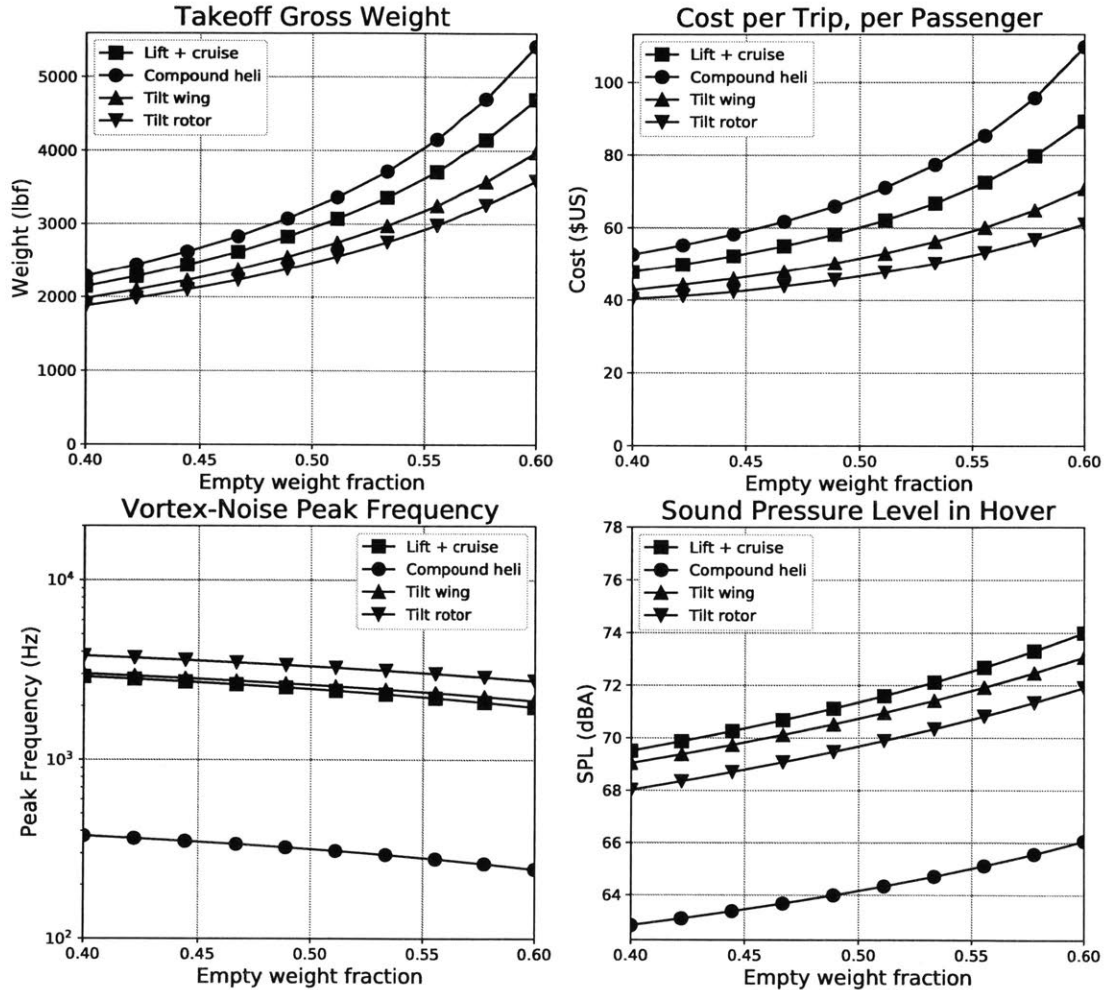


Figure 5-6: Sensitivity to empty weight fraction.

Figure 5-6 shows that the weight, cost, and noise level of all configurations are sensitive to empty weight fraction. As with battery specific energy, there is no crossover between configurations.

5.2.3 Rotor Solidity

A sweep was conducted to determine the importance of rotor solidity (quotient of rotor blade area and rotor disk area, as given in Equation 2.14). Results are shown in Figure 5-7.

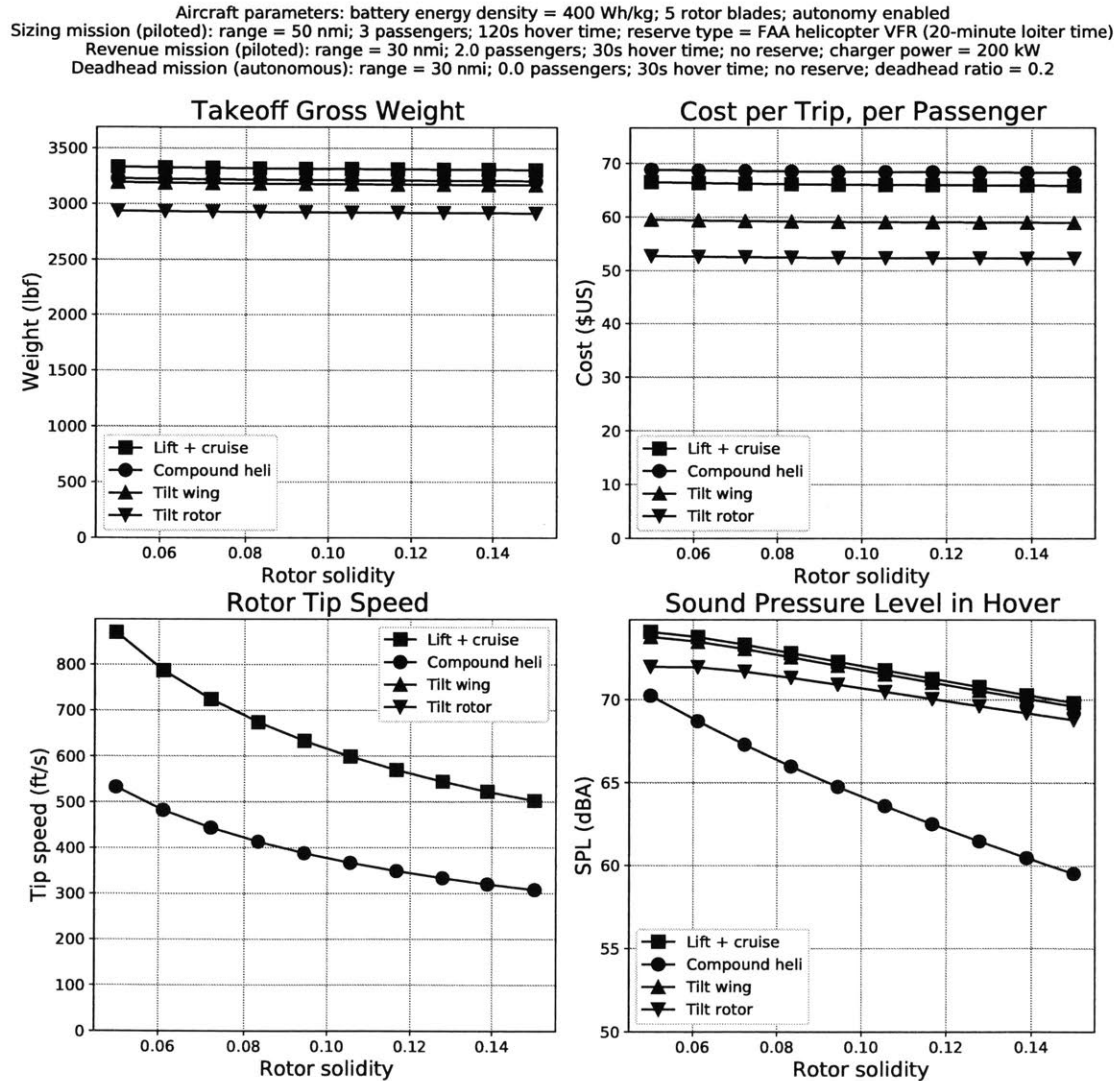


Figure 5-7: Sensitivity to rotor solidity.

Figure 5-7 shows that there is a tiny, beneficial effect of increased solidity on vehicle weight and cost. However, the benefit to noise is substantial. This is as expected, given the direct dependence of unweighted sound pressure level on solidity

(see Equation 2.32). Also, increased rotor solidity results in reduced rotor tip speed, further reducing noise. Increasing rotor solidity is therefore an effective way to reduce noise, without substantially affecting the design of the rest of the vehicle.

A-weighted noise levels for the compound helicopter are strongly affected by solidity. This is because of the effect of vortex-noise peak frequency (not plotted here). Reducing solidity tends to reduce vortex-noise peak frequency. Recall from Section 2.5.7 that a peak frequency of 600 Hz should be avoided at all costs. The compound helicopter has a peak frequency below this value; reducing it further will therefore increase the benefit from A-weighting. Meanwhile the other configurations have peak frequencies above 600 Hz. As solidity is reduced, peak frequency also reduces, decreasing the benefit from A-weighting.

5.2.4 Rotor Mean Lift Coefficient

A sweep was conducted to determine the importance of rotor mean lift coefficient. Guidelines used to select the values of \bar{C}_l were presented in Section 3.1, while results are shown in Figure 5-8.

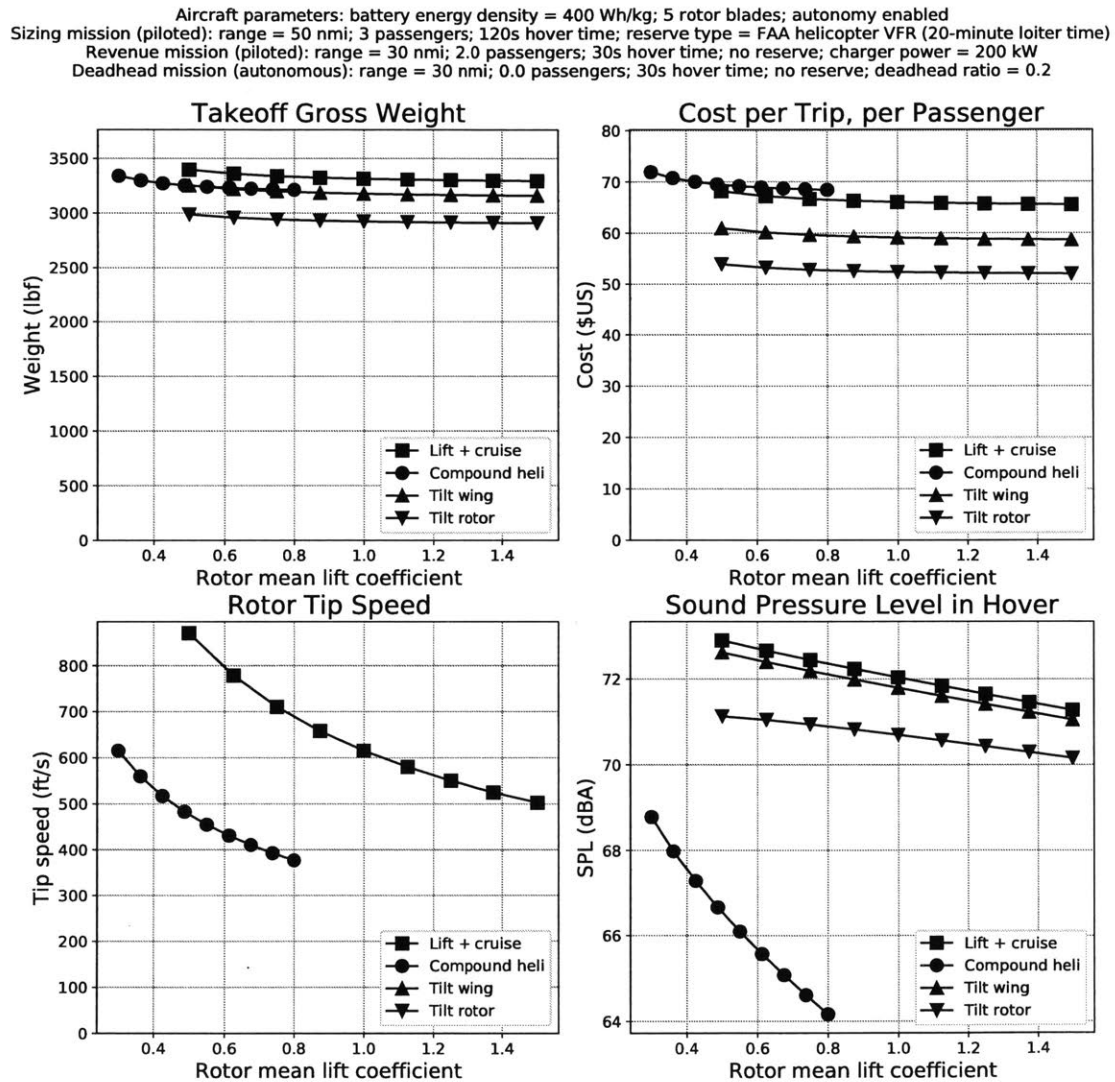


Figure 5-8: Sensitivity to rotor mean lift coefficient.

Figure 5-8 shows that increasing the allowed mean lift coefficient benefits both weight and cost. The sizing benefit is greatly diminished for \bar{C}_l values above 0.6. However, the noise benefit is significant for all values considered, because increasing

mean lift coefficient reduces rotor tip speed (this can also be seen from Figure 5-8). Therefore, like rotor solidity, rotor mean lift coefficient represents an opportunity for the acoustician to substantially reduce noise without substantially affecting vehicle sizing. However, suitable margins for control in hover must be maintained.

A-weighted noise levels for the compound helicopter are more strongly affected by mean lift coefficient than those of the other three configurations. This is true in part due to the effect of peak frequency (see Section 5.2.3), and also due to the increased effect of mean lift coefficient on takeoff weight below $\overline{C}_l = 0.6$.

5.2.5 Number of Rotors

A sweep was conducted to determine the importance of number of rotors. Results are shown in Figure 5-9. Note that the compound helicopter can only have either one or two rotors.

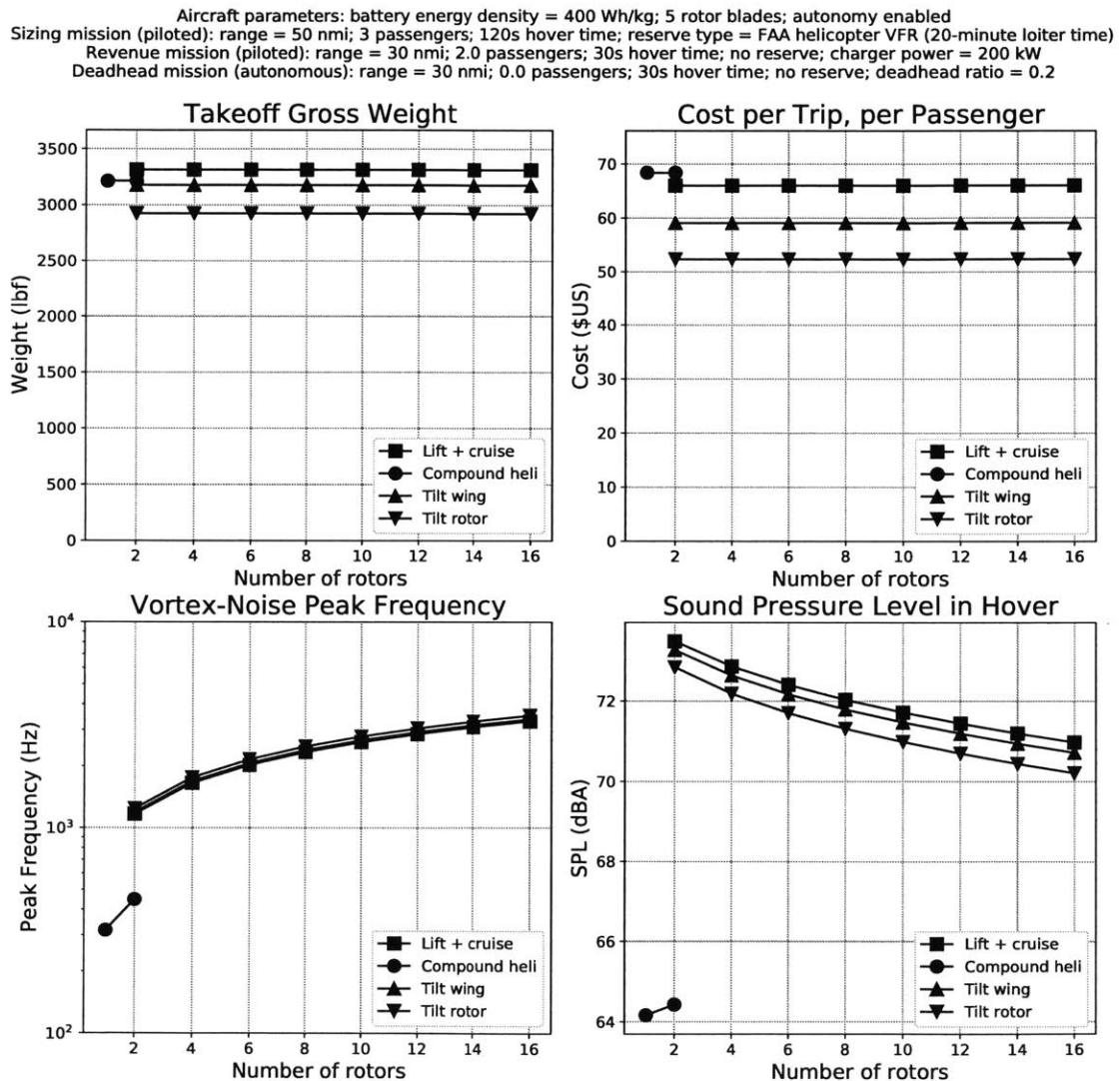


Figure 5-9: Sensitivity to number of rotors.

Figure 5-9 shows that changing the number of rotors does not affect vehicle weight or cost. While not shown, unweighted sound pressure level is also unaffected. This is because disk loading is held constant.

However, the vortex-noise peak frequency is affected. This is because increasing the number of rotors while maintaining constant disk loading results in smaller, thinner rotor blades. The blade projected thicknesses are therefore lower, resulting in higher peak frequencies (see Appendix D.2). The peak frequencies for the lift + cruise aircraft, the tilt wing, and the tilt rotor are all above 600 Hz. In this regime, increasing the peak frequency increases the benefit from A-weighting (see Figure 2-4), resulting in lower A-weighted sound pressure levels. Number of rotors can therefore be used as a design parameter to reduce noise.

5.2.6 Deadhead Ratio

A study was conducted to determine the sensitivity of various cost metrics to the deadhead ratio. Results are shown in Figure 5-10.

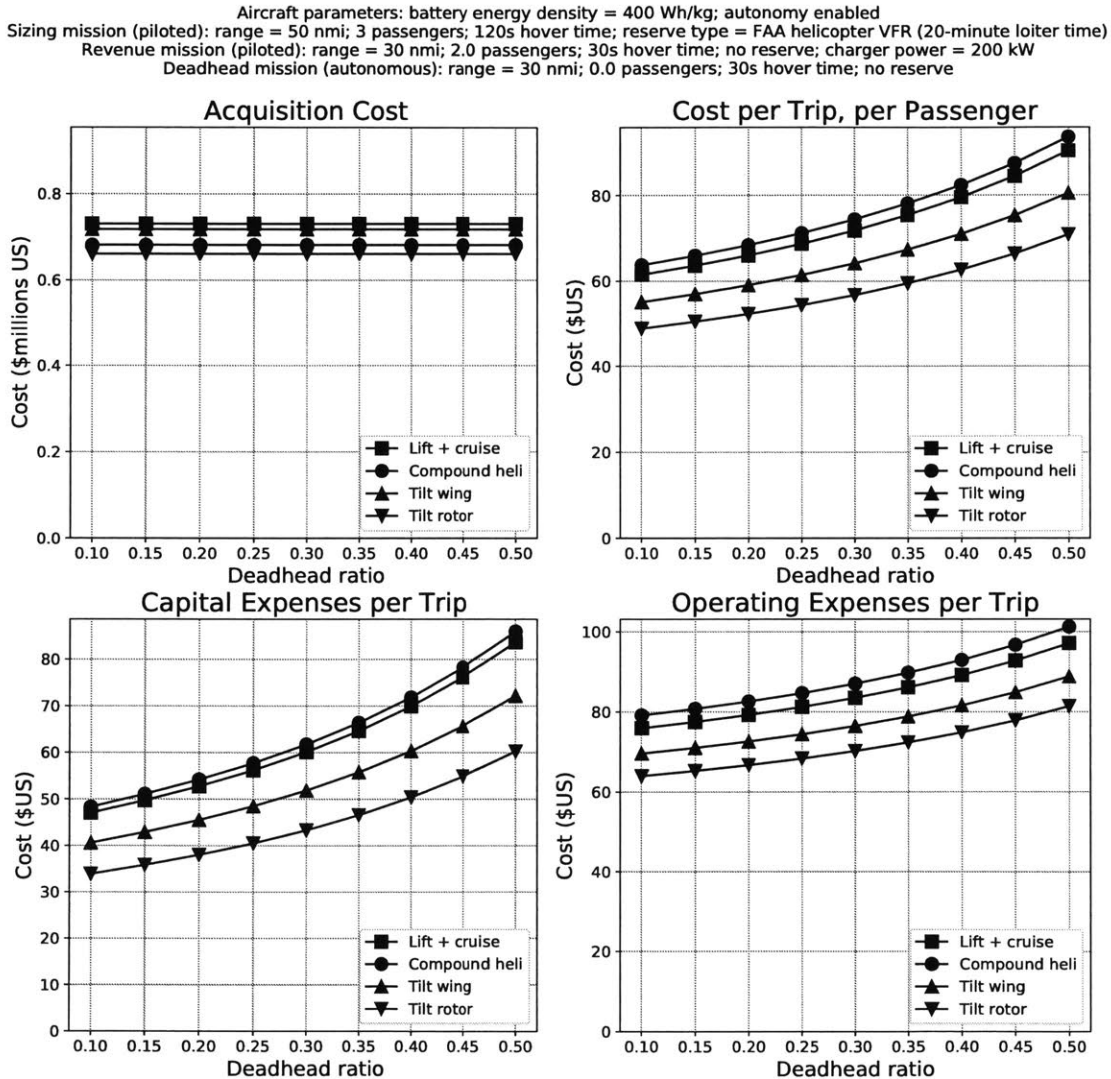


Figure 5-10: Sensitivity to deadhead ratio. Capital expenses, operating expenses, and total costs are per trip; i.e. the effect of deadhead is included.

Figure 5-10 shows that acquisition cost (including vehicle, battery, and avionics cost) is unaffected by deadhead ratio. This is because the deadhead ratio is solely relevant for the purposes of cost calculations; it does not affect vehicle sizing. Vehicle

weight and noise level are similarly unaffected by deadhead ratio, and are therefore not included.

However, cost per trip is affected by deadhead ratio. Capital expenses are affected due to amortization. An increased deadhead ratio means more deadhead missions, so the vehicle can fly fewer revenue missions during its service life. Therefore, although acquisition cost remains constant, capital expenses per trip are increased.

Meanwhile, operating expenses are also affected. The increased number of deadhead missions results in greater pilot, maintenance, and energy costs.

Chapter 6

Future Work

Future work should primarily be focused on vehicle noise. It was shown in Section 4.2 that the 62-dBA Uber noise requirement cannot be met by any vehicle configuration, even with the most generous long-term technological assumptions. Vehicle noise is therefore a critical issue for on-demand aviation.

Noise research can be divided into five main areas. First of all, the noise model should be validated using higher-fidelity methods and/or experimental data. In particular, the value of the leading coefficient K_2 in Equation 2.32 for vortex noise was determined experimentally from helicopter data (see Appendix D.1). K_2 is expected to vary between vehicle configurations. An accurate value for this parameter, for each configuration under examination, is required.

Secondly, it was hypothesized in Section 2.5.4 that blade slap can be avoided by careful selection of approach and departure procedures. While true for helicopters, this hypothesis must be verified for on-demand aircraft. The vortex ring state (which would result in a sudden, dangerous loss of lift) must also be avoided during approach and departure [34].

Thirdly, the results in Section 4.6 hint at the existence at the existence of a Pareto frontier between cost and noise, via the effects of a motor weight model. This tradeoff should be looked at as part of a more detailed multidisciplinary optimization study, incorporating the effect of motor weight.

Fourth, an impartial metric for human annoyance prediction is required. While

experimental evidence suggests that A-weighted SEL and annoyance of UAVs are correlated, the results are preliminary in nature and have not yet been shown to apply to on-demand electric air vehicles (see Section 2.5.7). Also, the correlation between EPNL and annoyance is much weaker than that between A-weighted SEL and annoyance (at least for UAVs) . Despite this, EPNL is currently the standard metric for aircraft noise regulations [44]. A metric for annoyance prediction must be established. This is necessary in order to provide a means by which different vehicle designs can be compared and to establish a regulatory regime for noise that accurately reflects human annoyance.

Finally, a number of design opportunities for reducing noise were discussed in Section 4.3. However, the extent to which these opportunities can be exploited remains uncertain. Studies on rotor structural analysis (needed to limit blade aspect ratio), control margin requirements in hover (needed to limit rotor mean lift coefficient), and rotor blade interference (needed to limit rotor solidity) are required, in order to determine the extent to which noise can be reduced. Additional ideas for reducing noise (ex. ducted rotors, with or without liners; swept, pointed, and/or split rotor blade tips; serrated rotor blade edges; asynchronous blade design; motor digital control synchronization; and asynchronous RPM) should also be explored.

One particularly promising idea for reducing noise is the toroidal propeller. Preliminary experimental evidence suggests that this design offers as much as a 10-dB reduction in noise, relative to conventional propellers [75]. However, due to their unconventional geometry, toroidal propellers cannot be manufactured using conventional techniques. Additive manufacturing must instead be employed. The toroidal propeller is depicted in Figure 6-1.

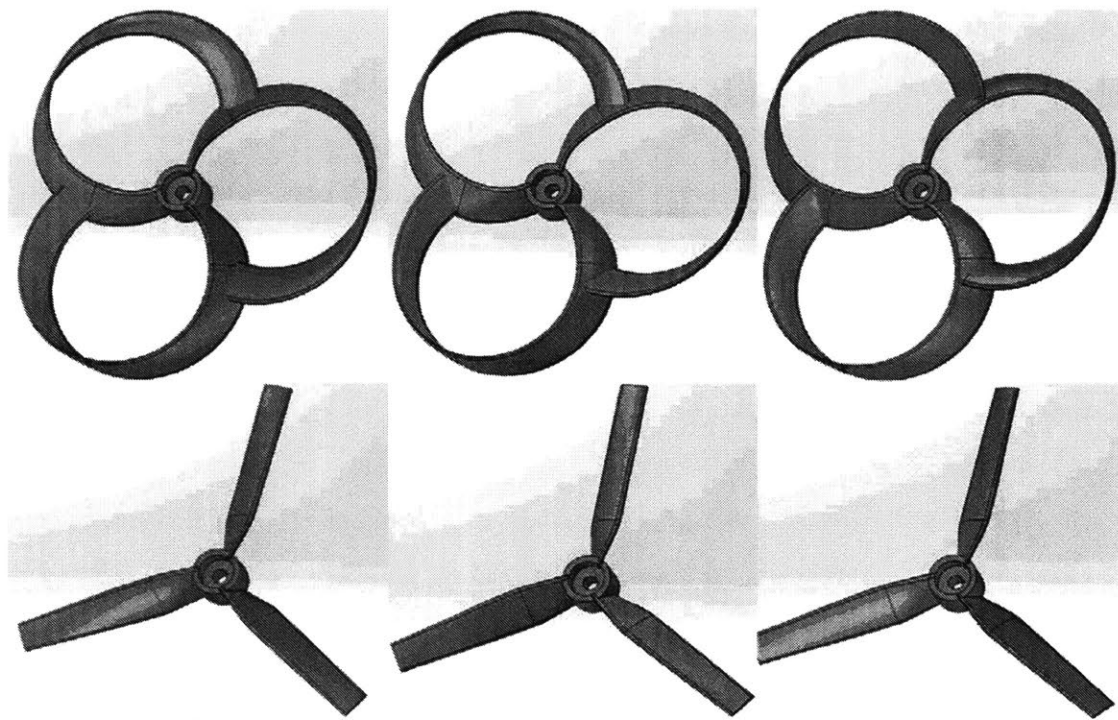


Figure 6-1: Example toroidal propellers, with conventional propellers shown for reference [75].

Chapter 7

Conclusions

A conceptual design and optimization tool for on-demand aviation was developed, using geometric programming. The tool incorporates low-cost aircraft, mission, cost, and noise models. The tool produces results that compare reasonable well with those from more sophisticated analysis techniques. It was used as part of a study on on-demand aviation from a vehicle design perspective.

The configurational trade study showed that on-demand air vehicles are feasible in terms of weight. For the selected mission, only four vehicle configurations are viable: the lift + cruise configuration, the compound helicopter, the tilt wing, and the tilt rotor. These results are contingent on a battery energy density of 400 Wh/kg. While this is significantly greater than the energy density of current batteries, substantial efforts are underway by both industry and government to meet this goal within the next three years.

The two most important costs are pilot salary and battery amortization; the key to lowering the price of an on-demand air service is therefore to implement vehicle autonomy and reduce battery manufacturing costs. Also, currently available charging technology poses a constraint on the cadence of vehicle operations.

An on-demand air service, even in the near term, is far superior in terms of price per trip as compared to current helicopter air taxi operations in New York City. The case study on time frames shows that costs are strongly affected by technological assumptions. In particular, expected improvements in vehicle autonomy and bat-

try manufacturing result in greatly reduced costs. In the long term, on-demand aviation becomes competitive with current car ridesharing services. This indicates the potential for on-demand aviation to become a commute system for the masses, as opposed to merely a high-priced service for the wealthy. However, this result is contingent on the development of fully autonomous air vehicles. While technically feasible, fully autonomous operation will not be possible for many years, owing to a combination of not-yet-overcome engineering challenges, regulatory obstacles, and customer-acceptance issues.

The 62-dBA noise requirement is not met by any vehicle configuration, even with the most generous long-term technological assumptions. While some improvements are possible with careful selection of key design parameters, more significant noise reductions are required. This underscores the necessity of substantial engineering effort to reduce noise.

Carpet plots provide a powerful means of visualizing the design space, as defined by the two most important vehicle sizing parameters: cruise lift-to-drag ratio and hover disk loading. Configurations with a higher lift-to-drag ratio, but a higher disk loading, cost less to operate but are louder. configurations with a lower lift-to-drag ratio, but a lower disk loading, cost more to operate but are quieter.

Sensitivity analysis was conducted with respect to several design requirements and vehicle parameters. Cost per seat mile is minimized at a mission range of about 30 nmi, indicating that on-demand aviation is most cost-competitive with other mobility options at this range. Vehicle designers have several certification options; a decision must consider vehicle sizing implications as well as pilot availability. Finally, a battery energy density of 400 Wh/kg was found to be a critical enabling value for on-demand aviation, a finding in accordance with the wider literature on electric aircraft.

In conclusion, on-demand aviation is feasible from the perspective of a vehicle designer, and may one day become a system for everyday commutes. Sizing plots provide a powerful means of exploring the vehicle design space. However, vehicle noise is a significant problem, requiring substantial engineering effort. Battery technology as well as vehicle autonomy are critical as well.

Appendix A

Noise Definitions

Sound is a pressure wave; it consists of fluctuations in pressure in a medium. In air, pressure waves can be considered as follows [43]:

$$p_{total}(t) = p_0 + p(t) \quad (\text{A.1})$$

$p_{total}(t)$ is the total air pressure, equal to the sum of the static (time-independent) pressure p_0 and the acoustic pressure $p(t)$. $p(t)$ is typically much smaller than p_0 . For example, the standard-sea-level static pressure is approximately 100,000 Pa, while acoustic pressure is typically on the order of ± 1 Pa [43].

Effective sound pressure is the root-mean-square (RMS) value of the acoustic pressure $p(t)$. p is calculated by time-averaging over a period T , as shown in Equation A.2:

$$p = \left[\frac{1}{T} \int_0^T p(t)^2 dt \right]^{1/2} \quad (\text{A.2})$$

Sound pressure level is the most commonly used sound metric, and is abbreviated as SPL. It is calculated using Equation A.3:

$$SPL = 10 \log_{10} \left[\left(\frac{p}{p_{ref}} \right)^2 \right] = 20 \log_{10} \left(\frac{p}{p_{ref}} \right) \quad (\text{A.3})$$

p_{ref} , the reference sound pressure, is typically set to 2×10^{-5} Pa. This represents

the effective sound pressure at which an average adult can hear a 1 kHz tone [43].

Appendix B

Decibel Arithmetic

Obtaining the sum of two different sounds is not as simple as adding their respective sound pressure levels [43]. For example, the sum of two 60-dB sounds is not 120 dB. Instead, the laws of decibel arithmetic must be applied. The sum of n sounds, each with sound pressure level SPL_i , can be computed using Equations B.1 and B.2:

$$\left(\frac{p}{p_{ref}} \right)_i^2 = 10^{SPL_i/10} \quad (\text{B.1})$$

$$SPL = 10 \log_{10} \left[\sum_{i=1}^n \left(\frac{p}{p_{ref}} \right)_i^2 \right] \quad (\text{B.2})$$

Equation B.2 only holds for independent, random sounds, or else sounds with different frequencies [43]. When adding multiple sounds with the same frequency, their relative phase must be considered.

Appendix C

Rotational Noise Derivation

As discussed in Section 2.5.5, rotational noise is divided into loading noise and thickness noise. The root-mean-square (RMS) sound pressures can be predicted using the classical Gutin and Deming formulae (Equations C.1 and C.2 respectively) [76]:

$$p_{m_L} = \frac{mB\Omega}{2\sqrt{2}\pi a(\Delta S)} \int_{hub}^{tip} \left[\frac{dT}{dr} \cos \theta - \frac{dQ}{dr} \frac{a}{\Omega r^2} \right] J_{mB} \left(\frac{mB\Omega}{a} r \sin \theta \right) dr \quad (C.1)$$

$$p_{m_T} = \frac{-\rho(mB\Omega)^2 B}{3\sqrt{2}\pi(\Delta S)} \int_{hub}^{tip} ct J_{mB} \left(\frac{mB\Omega}{a} r \sin \theta \right) dr \quad (C.2)$$

p_{m_L} and p_{m_T} are the RMS sound pressures for loading and thickness noise respectively. m is the harmonic number, B is the number of rotor blades, Ω is the rotor angular velocity, a is the speed of sound, and ΔS is the distance between the rotor and the observer. T is the rotor thrust, Q is the rotor torque, r is the rotor radial location, and θ is the observer azimuthal location (see Figure 2-3). ρ is the air density, c is the blade chord, and t is the blade maximum thickness. J_{mB} is a Bessel function of the first kind of order mB .

The form of the Gutin and Deming formulae given in Equations C.1 and C.2 requires discretized values of rotor radius, thrust and torque. This form is used in Reference [76] in order to employ the outputs from blade-element analysis in acoustic calculations. However, in order to employ the simpler rotor model used in this work,

an equivalent-radius approximation is used. All integrals are evaluated at an effective rotor radius R_e . The resulting alternate forms of the Gutin and Deming formulae are given in Equations C.3 and C.4 respectively:

$$p_{mL} = \frac{mB\Omega}{2\sqrt{2}\pi a(\Delta S)} \left[T \cos \theta - Q \frac{a}{\Omega R_e^2} \right] J_{mB} \left(\frac{mB\Omega}{a} R_e \sin \theta \right) \quad (\text{C.3})$$

$$p_{mT} = \frac{-\rho(mB\Omega)^2 B}{3\sqrt{2}\pi(\Delta S)} ct R_e J_{mB} \left(\frac{mB\Omega}{a} R_e \sin \theta \right) \quad (\text{C.4})$$

Once the loading and thickness pressures are known, sound pressure level SPL can be computed using Equation C.5:

$$SPL = 10 \log_{10} \left[\left(\frac{p_{mL}^2 + p_{mT}^2}{p_{ref}^2} \right) \right] \quad (\text{C.5})$$

p_{ref} is the reference pressure, equal to 2×10^5 Pa.

Equation C.5 only applies to one rotor. If multiple rotors are present, each operating under the same conditions, then Equation B.2 must be employed. Therefore, the square of the pressure ratio is multiplied by the number of rotors N , resulting in Equation C.6:

$$SPL = 10 \log_{10} \left[N \left(\frac{p_{mL}^2 + p_{mT}^2}{p_{ref}^2} \right) \right] \quad (\text{C.6})$$

As discussed in Appendix B, relative phase must technically be considered when adding multiple sounds with the same frequency. The technique used here assumes slightly different frequencies for each rotor; it serves as a reasonable first approximation. The propeller noise prediction method in SAE Standard 1407 [77] uses a similar technique.

Appendix D

Vortex Noise Derivation

D.1 Unweighted Sound Pressure Level

The vortex noise model used in this work was developed from the model in Schlegel et al. [48], as given in Reference [45]. Vortex noise in hover can be estimated using Equation D.1, accurate to within ± 2 dB of experimental data [45]:

$$SPL = 10 \log_{10} (KA_b V_{0.7}^6) + 20 \log_{10} \left(\frac{C_l}{0.4} \right) - 20 \log_{10} \left(\frac{\Delta S}{\Delta S_{ref}} \right) \quad (\text{D.1})$$

SPL is the sound pressure level at an observer distance ΔS from the source. K is a constant, equal to $6.1 \times 10^{-11} \frac{s^6}{ft^8}$. $V_{0.7}$ is the blade velocity at a radial location $r/R = 0.7$ (i.e. 0.7 times the tip speed). C_l is the local blade lift coefficient, referenced to $V_{0.7}$. ΔS_{ref} is equal to 300 ft.

Solve for the square of the pressure ratio using Equation A.3 to obtain Equation D.2:

$$\left(\frac{p}{p_{ref}} \right)^2 = KA_b V_{0.7}^6 \left(\frac{C_l}{0.4} \right)^2 \left(\frac{\Delta S_{ref}}{\Delta S} \right)^2 \quad (\text{D.2})$$

Substitute the expression for blade area ($A_b = BcR$), and let $C_l = \overline{C}_l$. C_l is equal to \overline{C}_l if constant downwash is assumed. This is a reasonable approximation, from

Reference [34].

Once this approximation is made, combine Equation 2.9 (thrust coefficient) and Equation 2.17 (mean lift coefficient) to obtain Equation D.3 for mean lift coefficient:

$$\overline{C}_l = 3 \frac{C_T}{s} = \frac{6T}{\rho s V_T^2 A} \quad (\text{D.3})$$

Substitute Equation D.3 into Equation D.2, substitute for tip speed ($V_{0.7} = 0.7V_T$), rearrange, and cancel terms to obtain Equation D.4:

$$\left(\frac{p}{p_{ref}} \right)^2 = 0.7^6 \left(\frac{6}{0.4} \right)^2 K \left(\frac{\Delta S_{ref}}{\Delta S} \right)^2 V_T^2 \frac{T^2}{\rho^2 A s} \quad (\text{D.4})$$

The next step is to multiply by N, to account for the effect of multiple rotors. As with the rotational noise model (Appendix C), it is assumed that the rotors are operating at slightly different frequencies. Equation B.2 can therefore be employed. We also combine the constants into one term: K_2 .

$$K_2 = \sqrt{0.7^6 \left(\frac{6}{0.4} \right)^2 K (\Delta S_{ref})^2} \quad (\text{D.5})$$

$$\left(\frac{p}{p_{ref}} \right)^2 = K_2^2 \frac{V_T^2 N T^2}{\rho^2 (\Delta S)^2 A s} \quad (\text{D.6})$$

The final result is Equation D.7 for the sound pressure level:

$$SPL = 20 \log_{10} \left[K_2 \frac{V_T}{\rho (\Delta S)} \sqrt{\frac{N T}{s} \left(\frac{T}{A} \right)} \right] \quad (\text{D.7})$$

Equation D.7 was validated using data in Reference [48] for two different helicopter main rotors: the CH-3C and the CH-53A. Results are given in Figure D-1. See Reference [48] for a more detailed description of the experimental setup.

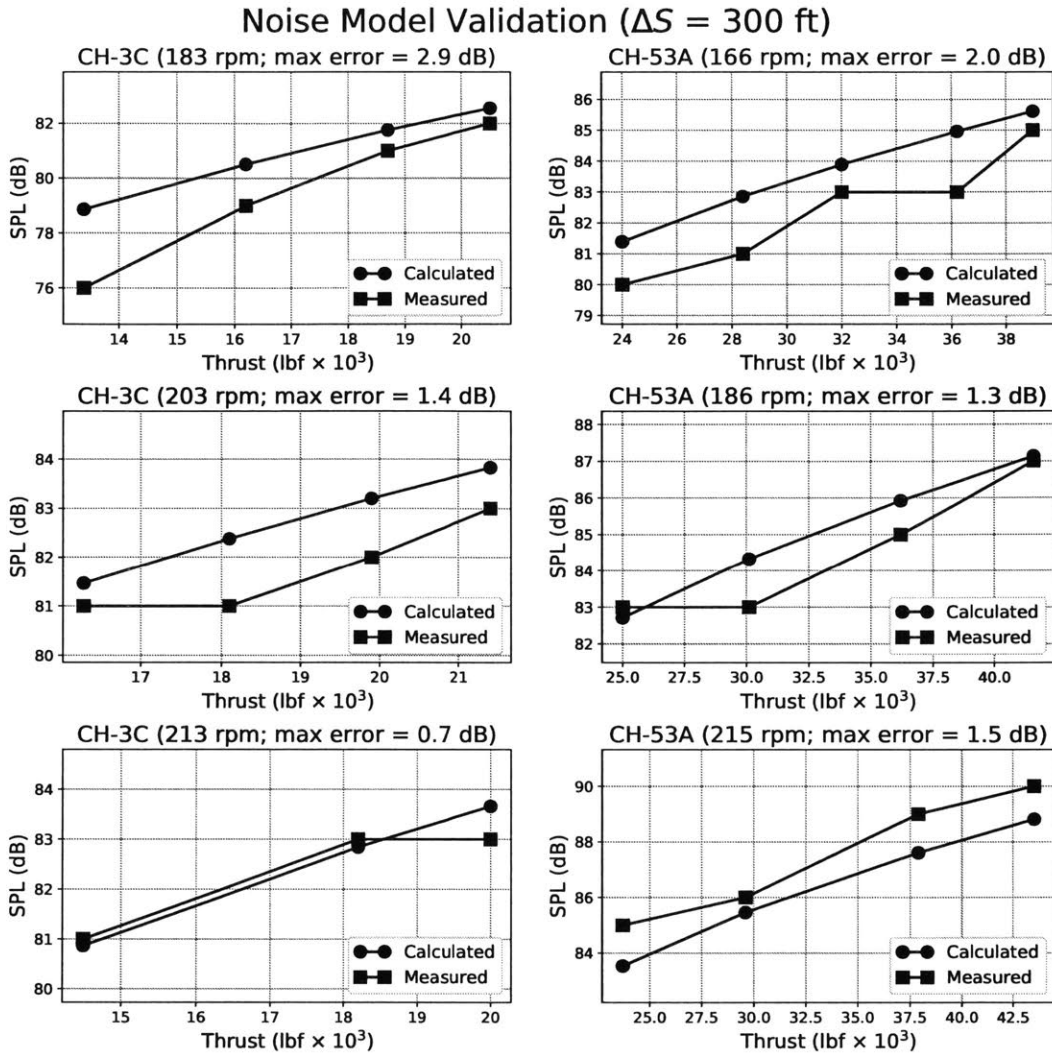


Figure D-1: Validation of the rotor vortex noise model. Note that the experimental data was rounded to the nearest decibel in Reference [48].

Figure D-1 shows that with an (experimentally determined) value of $K_2 = 1.206 \times 10^{-2} \text{ s}^3/\text{ft}^3$, Equation D.7 is accurate to within 3 dB of test data. This is technically only valid for the helicopters under consideration. Therefore, Equation 2.32 serves as a reasonable first approximation, and should also work for predicting noise trends. However, it is recommended in Reference [45] that K_2 be calibrated using higher-fidelity methods and/or experimental data for a given class of vehicle and/or experimental conditions.

D.2 Frequency Spectrum

Although vortex noise is broadband in nature, it has a peak frequency (frequency at which the amplitude is highest). It can be estimated using Equation D.8 [45]:

$$f_{peak} = \frac{(V_{0.7})St}{h} \quad (\text{D.8})$$

f_{peak} is the vortex-noise peak frequency (in Hz), St is the Strouhal number, and h is the projected blade thickness. An estimate of $St = 0.28$ is used; this is a reasonable value for a helicopter [45]. h is computed using Equation D.9:

$$h = t \cos \alpha + c \sin \alpha \quad (\text{D.9})$$

t is the average blade thickness, α is the blade angle of attack (at $r/R = 0.7$), and c is the average blade chord. Two-dimensional airfoil theory is used to approximate the angle of attack:

$$\alpha = \frac{\overline{C_l}}{2\pi} \quad (\text{D.10})$$

The blade chord is estimated using the definition of solidity (Equation 2.14). Since the NACA 0012 airfoil is a traditional choice for helicopter rotor blades [34], the blade thickness is calculated using an assumed thickness-to-chord ratio of 12%.

Once the peak frequency is known, the frequency spectrum can be drawn. Figure D-2 shows the vortex-noise frequency spectrum for an unweighted sound pressure level of 0 dB. This figure was originally Figure 10 from Reference [45].

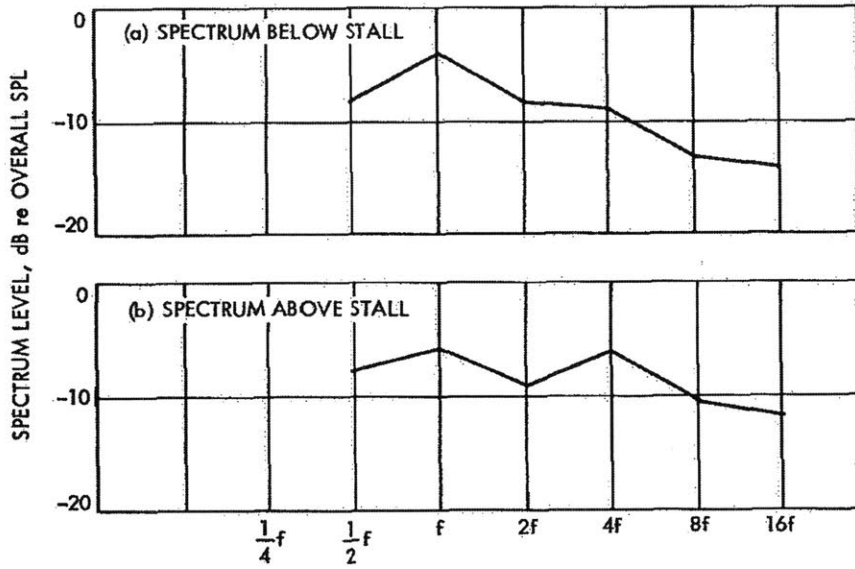


Figure D-2: Plot used to draw the vortex-noise frequency spectrum, obtained from Reference [45].

For each frequency value in Figure D-2, the corresponding sound pressure level weight was obtained. Spectrum (a) is used, since it is assumed that the rotor is below stall. The weights are given in Table D.1.

Table D.1: Frequency spectrum weights.

Frequency	$\frac{1}{2}f_{peak}$	f_{peak}	$2f_{peak}$	$4f_{peak}$	$8f_{peak}$	$16f_{peak}$
SPL weight	7.92	4.17	8.33	8.75	12.92	13.33

The procedure for drawing the frequency spectrum is then as follows. First, calculate the overall SPL and peak frequency, using Equations D.7 and D.8 respectively. Then obtain the sound pressure level for each frequency in Table D.1, by deducting the corresponding weight from the overall SPL. Finally, plot the resulting array of sound pressure level vs. peak frequency. Note that the interpolation between frequencies is only linear if the frequency axis uses a logarithmic scale.

D.3 A-Weighting Procedure

Because the frequency spectrum for vortex noise is continuous rather than discrete, the A-weighting technique for rotational noise discussed in Section 2.5.7 will not work. Instead, the approximate technique developed and used in this work replaces the summation in Equation B.2 with an integral.

Recall from Figure D-2 that the interpolated vortex-noise sound pressure levels are linear in log-space. Therefore, the sound pressure level in the interval between any two f -*SPL* pairs in Table D.1 can be interpolated using Equations D.11, D.12, D.13, and D.14:

$$SPL = C_1 \log_{10}(fr) + C_2 \quad (\text{D.11})$$

$$fr = \frac{f}{f_{peak}} \quad (\text{D.12})$$

$$C_1 = \frac{SPL_2 - SPL_1}{\log_{10}(fr_2) - \log_{10}(fr_1)} \quad (\text{D.13})$$

$$C_2 = SPL_2 - C_1 \log_{10}(fr_2) \quad (\text{D.14})$$

fr is the frequency ratio; it is introduced in order to render the interpolation dimensionless. C_1 and C_2 are interpolation constants, while the pairs (fr_1 , SPL_1) and (fr_2 , SPL_2) represent the frequency-sound pairs defining the upper and lower limits on the interpolation interval under consideration.

According to the laws of decibel arithmetic, adding sounds of different frequencies is analogous to adding the squares of the RMS sound pressure ratios. Therefore, the goal is to obtain the sound pressure ratio, and integrate it over each frequency interval. Writing Equation D.11 in terms of pressure ratio yields Equation D.16:

$$SPL = C_1 \log_{10}(fr) + C_2 = 10 \log_{10} \left[\left(\frac{p}{p_{ref}} \right)^2 \right] \quad (\text{D.15})$$

$$\left(\frac{p}{p_{ref}}\right)^2 = 10^{\frac{C_2}{10}} f r^{\frac{C_1}{10}} \quad (\text{D.16})$$

Integrating over the interval and assuming $C_1 \neq -10$ yields Equation D.17:

$$\int_1^2 \left(\frac{p}{p_{ref}}\right)^2 = 10^{\frac{C_2}{10}} \frac{f r^{\frac{C_1+1}{10}}}{\frac{C_1}{10} + 1} \Big|_{fr_1}^{fr_2} \quad (\text{D.17})$$

Finally, the total sound pressure level over $n - 1$ intervals can be computed using Equation D.18:

$$SPL = 10 \log_{10} \left(\sum_{i=1}^{n-1} \left[\int_1^2 \left(\frac{p}{p_{ref}}\right)^2 \right] \right) \quad (\text{D.18})$$

The procedure for obtaining the A-weighted vortex-noise sound pressure level can be summarized as follows:

1. Obtain the peak frequency and the frequency spectrum array, as described in Appendix D.2.
2. Apply the A-weighting offset function $A(f)$ to each sound pressure level in the frequency spectrum array.
3. For each frequency in the spectrum array, obtain the corresponding frequency ratio using Equation D.12.
4. For each interval in the spectrum array, obtain the constants C_1 and C_2 using Equations D.13 and D.14 respectively.
5. For each interval in the spectrum array, solve for the pressure ratio integral using Equation D.17.
6. Obtain the total A-weighted sound pressure level by adding the pressure ratio integrals using Equation D.18.

Ideally, if step 2 is skipped (i.e. if A-weighting is not applied), then the resulting sound pressure level should be identical to that obtained from Equation D.7. However,

due to the approximations made in drawing the frequency spectrum, the obtained answer is approximately 1.3 dB higher than that predicted by Equation D.7. This technique is therefore somewhat conservative.

Appendix E

Code API

E.1 Overview

All of the optimization results documented in this thesis were obtained using a set of open-source codes, available online at [27]. The codes are written in Python 2. All optimization solutions were obtained using GPkit [28], with MOSEK as the backend solver.

E.2 Class Definitions

A typical study defines five objects, each based on a different class. All classes are defined in the file `aircraft_models.py`. Using the configuration trade study (executed using the script `config_tradeStudy.py`) as an example, the five objects are listed below. Boolean inputs have been omitted for clarity.

- `Aircraft = OnDemandAircraft()` (representing the aircraft)
- `SizingMission = OnDemandSizingMission(Aircraft)` (representing the sizing mission)
- `RevenueMission = OnDemandRevenueMission(Aircraft)` (representing the revenue mission)

- `DeadheadMission = OnDemandDeadheadMission(Aircraft)` (representing the deadhead mission)
- `MissionCost = OnDemandMissionCost(Aircraft, RevenueMission, DeadheadMission)` (representing the mission cost model)

Note that `OnDemandSizingMission`, `OnDemandRevenueMission`, and `OnDemandDeadheadMission` all require an `Aircraft` object as an input. Meanwhile, `OnDemandMissionCost` requires an `Aircraft` object, a `RevenueMission` object, and a `DeadheadMission` object. A `SizingMission` object is not required. This is as expected, since the sizing mission does not influence cost.

All of these models contain sub-models as well as top-level parameters, which together make up the complete model. For example, `OnDemandMissionCost` contains top-level parameters like `cpt_seat_mile` (cost per trip, per seat mile), as well as sub-models like `RevenueMissionCost` and `DeadheadMissionCost`. These sub-models are further decomposed into `CapitalExpenses` and `OperatingExpenses`, and so forth. For further details, see the file `aircraft_models.py`

E.3 Inputs

Most of the input parameters for a given study are contained in the file `study_input_data.py`. This file contains two dictionaries: `generic_data`, which contains input parameters used by all configurations; and `configuration_data`, which contains data specific to a given configuration. These dictionaries are then imported into a given study.

The most common way to provide a parameter as an input for a given study is via substitution. However, three other inputs are available. They are called when the objects listed in Section E.2 are instantiated:

- `autonomousEnabled` (input to the `OnDemandAircraft` class)
- `mission_type` (input to the `SizingMission`, `RevenueMission`, and `DeadheadMission` classes)

- `reserve_type` (input to the `SizingMission` class)

`autonomousEnabled` (a Boolean) can be set to `True` or `False`; it determines whether the vehicle includes an autopilot. If set to `True`, the avionics cost per aircraft is included, as described in Section 2.4.1.

`mission_type` (a string) determines the type of mission to be flown. It can be set to either "`piloted`" (the default) or "`autonomous`". Crew weight and cost models are applied corresponding to either option, as discussed in Sections 2.3 and 2.4.2 respectively.

Finally, three options for `reserve_type` (a string) are available: "`FAA_heli`" (the default), "`FAA_aircraft`", and "`Uber`". If either of the first two options are selected, the loiter flight segment time is set to 20 minutes and 30 minutes respectively (see Section 2.3). Also, the loiter speed and lift-to-drag ratio adjustments in Equations 2.20 and 2.21 are used. If the "`Uber`" reserve option is selected, the loiter flight segment distance is set to 2 nmi, and the loiter speed and lift-to-drag ratio adjustments are not used.

E.4 Solutions

Once the problem has been set up, the next steps are to select an objective function, assemble the models, insert the substitutions, and solve:

```
problem = Model(MissionCost["cost_per_trip"], [Aircraft, ...
    SizingMission, RevenueMission, DeadheadMission, MissionCost])
problem.substitutions.update(problem_subDict)
solution = problem.solve(verbosity=0)
```

In this case, cost per trip is the objective function; other choices are possible. `problem_subDict` is a dictionary contains all of the parameter substitutions, while `solution` is an object containing all of the output data.

Noise analysis is then completed, using the data from `solution` and functional implementations of the noise models in Appendices C and D. These noise functions are contained in the file `noise_models.py`.

E.5 Tips & Tricks

On rare occasions, a model will fail to converge at seemingly random intervals. For instance, after 50 successful consecutive solves with no changes to the code, the model will fail to converge on the 51st, then converge on the 52nd. This is believed to be caused by the tail-rotor power fractions.

Recall from Table 3.4 (Section 3.1) that the conventional and compound helicopters require power for their tail rotors, during both hover and cruise. This is controlled by the parameters `tailRotor_power_fraction_hover` and `tailRotor_power_fraction_levelFlight` respectively. Both are given, by configuration, in the file `study_input_data.py`

The values in Table 3.4 are used for the conventional and compound helicopter. For the other configurations, a value of 0 should theoretically be used. However, GPkit is incapable of handling zeros in a product, and so values of 0.001 are used for the other configurations.

Sometimes, this practice leads to convergence issues. For example, the random failures described above become much more common if a value of 0.0001 is used instead. If convergence issues reappear, try setting the tail-rotor power fractions to a higher value, such as 0.005.

Bibliography

- [1] M. D. Moore and B. Fredericks, “Misconceptions of Electric Propulsion Aircraft and Their Emergent Aviation Markets,” AIAA SciTech, Conference Paper, Jan. 2014.
- [2] P. Jackson, *Jane’s All the World’s Aircraft: Development and Production, 2017-2018*. IHS, 2017.
- [3] *ALPHA Trainer - Overview*, <http://www.pipistrel-usa.com/models/alpha-trainer.html>, 2018.
- [4] C. Brooks and S. Salgueiro, “Design Space Investigation for a Small Electric General Aviation Airplane,” 2017 AIAA Aerospace Sciences Meeting, AIAA SciTech Forum, Grapevine, TX, Conference Paper, Jan. 2017.
- [5] H. J. Price, *Fact Sheet - Leaded Aviation Fuel and the Environment*, https://www.faa.gov/news/fact_sheets/news_story.cfm?newsId=14754, 2013.
- [6] R. W. Moorman, *Noise In the Cities - Revisited*, Vertiflite, Nov. 2016.
- [7] M. Lowson and J. Ollerhead, “A Theoretical Study of Helicopter Rotor Noise,” *Journal of Sound and Vibration*, vol. 9, no. 2, pp. 197–222, Mar. 1969.
- [8] *NASA Armstrong Fact Sheet: NASA X-57 Maxwell*, <https://www.nasa.gov/centers/armstrong/news/FactSheets/FS-109.html>, 2017.
- [9] N. K. Borer, M. D. Patterson, J. K. Viken, *et al.*, “Design and Performance of the NASA SCEPTOR Distributed Electric Propulsion Flight Demonstrator,” 16th AIAA Aviation Technology, Integration, and Operations Conference, Washington, D.C., Conference Paper, Jun. 2016.

- [10] *SolidEnergy - The World's Lightest Rechargeable Cells*, <http://www.solidenergysystems.com/>, 2018.
- [11] "Revision of Airworthiness Standards for Normal, Utility, Acrobatic, and Commuter Category Airplanes," FAA, Report, Dec. 2016.
- [12] P. Bergqvist, *Electric Aircraft Developers Hail Part 23 Rewrite*, <https://www.flyingmag.com/electric-aircraft-developers-hail-part-23-rewrite>, Feb. 2017.
- [13] *eCFR - Code of Federal Regulations*, <https://www.ecfr.gov/cgi-bin/text-idx?rgn=div8&node=14:1.0.1.1.0.1.1>, Apr. 2018.
- [14] M. D. Moore, "Concept of Operations for Highly Autonomous Electric Zip Aviation," 14th AIAA Aviation Technology et al., Conference Paper, Sep. 2012.
- [15] J. Holden and N. Goel, "Fast-Forwarding to a Future of On-Demand Urban Air Transportation," Uber, White Paper, Oct. 2016.
- [16] *Uber Elevate: Fast-Forwarding to the Future of On-Demand, Urban Air Transportation*, <https://www.uber.com/info/elevate/summit/>, Apr. 2017.
- [17] *From the Ground Up: Uber Elevate in 2020*, <http://evtol.news/2017/08/22/uber2020/>, 2017.
- [18] *Uber Elevate Joins NASA, Los Angeles*, <http://evtol.news/2017/12/22/uber-elevate-joins-nasa-los-angeles/>, 2017.
- [19] *Voom*, <https://www.voom.flights/en>, 2018.
- [20] T. Osborne and G. Warwick, *On-Demand Helicopter Experience Feeds Into Airbus Air Taxi Design*, <http://aviationweek.com/commercial-aviation/demand-helicopter-experience-feeds-airbus-air-taxi-design>, Feb. 2018.
- [21] P. Jackson, *Jane's All the World's Aircraft: Unmanned, 2014-2015*. IHS, 2014.
- [22] *Unmanned Aircraft Systems Sense and Avoid System Certification Obstacles*, <https://www.faa.gov/uas/research/reports/media/UAS-SAA-System-Certification-Obstacles.pdf>, 2018.

- [23] G. Warwick, *Demo Makes Autonomous Resupply Look Deceptively Easy*, <http://aviationweek.com/future-aerospace/demo-makes-autonomous-resupply-look-deceptively-easy>, 2018.
- [24] D. Nelms, *Thinking Outside the Box Is Inside the Box at Aurora Flight Sciences*, <http://evtol.news/2018/04/19/thinking-outside-the-box-is-inside-the-box-at-aurora-flight-sciences/>, May 2018.
- [25] V. C. Nneji, M. L. Cummings, A. J. Stimpson, *et al.*, “Functional Requirements for Remotely Managing Fleets of On-Demand Passenger Aircraft,” 2018 AIAA Aerospace Sciences Meeting, AIAA SciTech Forum, Kissimmee, FL, Conference Paper, Jan. 2018.
- [26] R. McDonald and B. German, *eVTOL Stored Energy Overview*, Presentation Slides, Uber Elevate summit, Apr. 2017.
- [27] *GitHub - convexengineering/eVTOL: Codes related to the analysis, design, and optimization of on-demand, electric vertical-takeoff-and-landing aircraft.* <https://github.com/convexengineering/eVTOL>, 2018.
- [28] *Table of contents - gpkit 0.7.0 documentation*, <http://gpkit.readthedocs.io/en/latest/>, 2018.
- [29] W. Hoburg and P. Abbeel, “Geometric Programming for Aircraft Design Optimization,” *AIAA Journal*, vol. 52, no. 11, pp. 2414–2426, Nov. 2014.
- [30] P. G. Kirschen and W. W. Hoburg, “The Power of Log Transformation: A Comparison of Geometric and Signomial Programming with General Nonlinear Programming Techniques for Aircraft Design Optimization,” AIAA SciTech Forum, Kissimmee, FL, Conference Paper, Jan. 2018.
- [31] M. J. Burton and W. W. Hoburg, “Solar-Electric and Gas Powered Long-Endurance Unmanned Aircraft Sizing via Geometric Programming,” *Journal of Aircraft*, vol. 55, no. 1, pp. 212–225, Jan. 2018.
- [32] J. D. Anderson, *Introduction to Flight, 6th Edition*. McGraw-Hill, 2008.

- [33] P. G. Kirschen, M. A. York, B. Ozturk, *et al.*, *Application of Signomial Programming to Aircraft Design*, Journal of Aircraft (preprint), 2017.
- [34] J. Seddon and S. Newman, *Basic Helicopter Aerodynamics*, 3rd ed. John Wiley & Sons, 2011.
- [35] A. Bagai and J. G. Leishman, “Experimental Study of Rotor Wake/Body Interactions in Hover,” *Journal of the American Helicopter Society*, vol. 37, no. 4, pp. 48–57, Oct. 1992.
- [36] J. G. Leishman, *Principles of Helicopter Aerodynamics*, 2nd ed. New York, NY: Cambridge University Press, 2006.
- [37] FAA, *14 CFR 91.151 - Fuel requirements for flight in VFR conditions*. <https://www.law.cornell.edu/cfr/text/14/91.151>, 2017.
- [38] D. P. Raymer, *Aircraft Design: A Conceptual Approach*, 5th Edition. AIAA, 2012.
- [39] B. German, M. Daskilewicz, T. K. Hamilton, *et al.*, “Cargo Delivery by Passenger eVTOL Aircraft: A Case Study in the San Francisco Bay Area,” 2018 AIAA Aerospace Sciences Meeting, AIAA SciTech Forum, Kissimmee, FL, Conference Paper, Jan. 2018.
- [40] S. Gudmundsson, *General Aviation Aircraft Design: Applied Methods and Procedures*. Butterworth-Heinemann, 2013.
- [41] M. Woolhouse, *Officials will study plane noise after complaints about Logan*, <https://www.bostonglobe.com/business/2016/10/07/faa-massport-agree-study-airplane-noise-after-rising-complaints/hIVSjqJnk5vWv6gAHzk0eI/story.html>, 2016.
- [42] S. Choi, J. J. Alonso, and I. M. Kroo, “Multifidelity Design Optimization of Low-Boom Supersonic Jets,” *Journal of Aircraft*, vol. 45, no. 1, pp. 106–118, Feb. 2008.
- [43] F. Fahy and D. Thompson, *Fundamentals of Sound and Vibration*, 2nd ed. Boca Raton, FL: CRC Press, Taylor & Francis Group, 2015.

- [44] O. Zaporozhets, V. Tokarev, and K. Attenborough, *Aircraft Noise: Assessment, Prediction, and Control*. Boca Raton, FL: CRC Press, Taylor & Francis Group, 2011.
- [45] J. E. Marte and D. W. Kurtz, “A Review of Aerodynamic Noise from Propellers, Rotors, and Lift Fans,” Jet Propulsion Laboratory, Pasadena, CA, Technical Report 32-1462, Jan. 1970.
- [46] “Fly Neighborly Guide,” Helicopter Association International, Alexandria, VA, Technical Report, May 2013.
- [47] W. Johnson, *Helicopter Theory*. New York, NY: Dover Publications, 1994.
- [48] R. Schlegel, R. King, and H. Muli, “Helicopter Rotor Noise Generation and Propagation,” US Army Aviation Material Laboratories, Fort Eustis, VA, Technical Report, Oct. 1966.
- [49] A. Christian and R. Cabell, “Initial Investigation into the Psychoacoustic Properties of Small Unmanned Aerial System Noise,” AIAA Aviation Technology, Integration, and Operations Conference, Conference Paper, Jun. 2016.
- [50] *Urban Air Mobility: Can It Ever Be Safe Enough?* <http://aviationweek.com/technology/urban-air-mobility-can-it-ever-be-safe-enough>, 2017.
- [51] M. J. Duffy, S. R. Wakayama, R. Hupp, *et al.*, “A Study in Reducing the Cost of Vertical Flight with Electric Propulsion,” 17th AIAA Aviation Technology, Integration, and Operations Conference, Denver, CO, Conference Paper, Jun. 2017.
- [52] *Aurora Flight Sciences Showcases New eVTOL Aircraft*, <http://www.auvsi.org/blogs/auvsi-news/2017/04/25/aurora-flight-sciences-showcases-new-evtol-aircraft>, 2017.
- [53] *Carter partners with Mooney for Uber Elevate air taxi concept*, <https://www.verticalmag.com/press-releases/carter-partners-mooney-uber-elevate-air-taxi-concept/>, Apr. 2017.

- [54] *Airbus has a secret flying-car project called Vahana*, <https://www.theverge.com/2016/10/21/13357690/airbus-flying-car-vahana-a-cubed-autonomous-taxi>, Oct. 2016.
- [55] *Joby S2*, <http://www.jobyaviation.com/S2/>, 2016.
- [56] *R44 Raven Series*, http://www.robinsonheli.com/rhc_r44_raven_series.html, 2016.
- [57] *Kamov Ka32*, <https://barrieaircraft.com/kamov-ka32.html>, 2017.
- [58] J. Bennett, *EHang Wants You to Fly in Their Autonomous Drone*, <http://www.popularmechanics.com/flight/drones/a18865/ehang-184-fly-in-autonomous-drone/>, Jan. 2017.
- [59] *M-16 Tandem Trainer*, <http://www.magnigyro.com/models/m16.html>, 2017.
- [60] *Lilium Aviation*, <https://lifeboat.com/blog/2016/05/lilium-aviation>, 2016.
- [61] *Lift Where You Need It*, <http://evtol.news/2016/11/01/lift-where-you-need-it-nov-1-2016/>, 2016.
- [62] *BLADE - The Sharpest Way to Fly*, <https://www.flyblade.com/>, 2017.
- [63] *New York City Helicopter Tours*, <https://www.newyorkhelicopter.com/>, 2017.
- [64] *SkyVector: Flight Planning / Aeronautical Charts*, <https://skyvector.com/>, 2017.
- [65] P. D. Vascik and R. J. Hansman, “Evaluation of Key Operational Constraints Affecting On-Demand Mobility for Aviation in the Los Angeles Basin: Ground Infrastructure, Air Traffic Control and Noise,” 17th AIAA Aviation Technology, Integration, and Operations Conference, AIAA AVIATION Forum, Denver, CO, Conference Paper, Jun. 2017.
- [66] M. Campbell, *Patent filings detail Retina MacBook Pro's quiet asymmetric fans*, <http://appleinsider.com/articles/12/12/20/patent-filings-detail-retina-macbook-pros-quiet-asymmetric-fans>, 2012.

- [67] A. M. Stoll, J. Bevirt, P. P. Pei, *et al.*, “Conceptual Design of the Joby S2 Electric VTOL PAV,” AIAA Aviation, Technology, Integration, and Operations Conference, Atlanta, GA, Conference Paper, Jun. 2014.
- [68] NASA, *OpenVSP*, <http://www.openvsp.org/>, 2017.
- [69] A. M. Stoll and G. V. Mikic, “Design Studies of Thin-Haul Electric Aircraft with Distributed Electric Propulsion,” AIAA Aviation Technology, Integration, and Operations Conference, Conference Paper, Jun. 2016.
- [70] FAA, *U.S. Civil Airmen Statistics*, https://www.faa.gov/data_research/aviation_data_statistics/civil_airmen_statistics/, 2016.
- [71] M. Kamlet, *X-57 Battery System Survives Flight-Condition, Thermal Runaway Testing*, <https://www.nasa.gov/centers/armstrong/feature/X-57-battery-major-milestone.html>, Dec. 2017.
- [72] *Battery500 Consortium to Spark EV Innovations: Pacific Northwest National Laboratory-led, 5-year \$50M effort seeks to almost triple energy stored in electric car batteries*, <https://www.energy.gov/technologytransitions/articles/battery500-consortium-spark-ev-innovations-pacific-northwest-national>, Jul. 2016.
- [73] T. Christen and M. W. Carlen, “Theory of Ragone plots,” *Journal of Power Sources*, vol. 91, no. 2, pp. 210–216, Mar. 2000.
- [74] L. W. Traub, “Range and Endurance Estimates for Battery-Powered Aircraft,” *Journal of Aircraft*, vol. 48, no. 2, pp. 703–707, Mar. 2011.
- [75] T. Sebastian, “Toroidal Propeller Description for Technology Disclosure,” MIT Lincoln Laboratories, Memo, Aug. 2017.
- [76] M. K. Herniczek, D. Feszty, S.-A. Meslioui, *et al.*, “Applicability of Early Acoustic Theory for Modern Propeller Design,” 23rd AIAA/CEAS Aeroacoustics Conference, AIAA AVIATION Forum, Denver, CO, Conference Paper, Jun. 2017.

- [77] "Prediction Procedure for Near-Field and Far-Field Propeller Noise," Society of Automotive Engineers, Technical Standard AIR1407, May 1977.